

PERFORMANCE ASSESSMENT OF A HOLLOW FIBER MEMBRANE
CONTACTOR REACTOR FOR REACTIVE EXTRACTION IN BIODIESEL
PRODUCTION

Nevardo Bello Yaya

Tese de Doutorado apresentada ao Programa de Pós-graduação em Engenharia Química, COPPE, da Universidade Federal do Rio de Janeiro, como parte dos requisitos necessários à obtenção do título de Doutor em Engenharia Química.

Orientadores: Alberto Claudio Habert
 Frederico de Araujo Kronemberger

Rio de Janeiro
Fevereiro de 2025

PERFORMANCE ASSESSMENT OF A HOLLOW FIBER MEMBRANE
CONTACTOR REACTOR FOR REACTIVE EXTRACTION IN BIODIESEL
PRODUCTION

Nevardo Bello Yaya

TESE SUBMETIDA AO CORPO DOCENTE DO INSTITUTO ALBERTO LUIZ
COIMBRA DE PÓS-GRADUAÇÃO E PESQUISA DE ENGENHARIA DA
UNIVERSIDADE FEDERAL DO RIO DE JANEIRO COMO PARTE DOS
REQUISITOS NECESSÁRIOS PARA A OBTENÇÃO DO GRAU DE DOUTOR EM
CIÊNCIAS EM ENGENHARIA QUÍMICA.

Orientadores: Alberto Claudio Habert
 Frederico de Araujo Kronemberger

Aprovada por: Prof. Alberto Claudio Habert
 Prof. Frederico de Araujo Kronemberger
 Prof. Cristiano Piacsek Borges
 Prof. Yordanka Reyes Cruz
 Dra. Lourdes Maria Correa Cabral
 Prof. Paulo César Narváez Rincón

RIO DE JANEIRO, RJ - BRASIL

FEVEREIRO DE 2025

Bello Yaya, Nevardo

Performance Assessment of a Hollow Fiber Membrane Contactor Reactor for Reactive Extraction in Biodiesel Production / Nevardo Bello Yaya. – Rio de Janeiro: UFRJ/COPPE, 2025.

XIX, 110 p.: il.; 29,7 cm.

Orientadores: Alberto Claudio Habert

Frederico de Araujo Kronemberger

Tese (doutorado) – UFRJ/ COPPE/ Programa de Engenharia Química, 2025.

Referências Bibliográficas: p. 99-110.

1. Hollow fiber membrane contactor reactor. 2. Process Intensification. 4. Reactive Extraction. 5. HFMCR Modeling I. Habert, Alberto Claudio *et al.* II. Universidade Federal do Rio de Janeiro, COPPE, Programa de Engenharia Química. III. Título.

*Porque dele, e por Ele, e para Ele são todas as coisas;
glória, pois, a Ele eternamente.
Rom. 11:36*

Acknowledgments

O desenvolvimento de um trabalho de tese de doutorado seria impossível sem a colaboração de muitas pessoas, muitas delas de forma aparentemente invisível, mas não menos importantes.

Quero começar expressando minha profunda gratidão ao meu orientador, professor Alberto Claudio Habert, que foi a pessoa que me convidou, ao final do meu mestrado na Colômbia, para iniciar essa jornada transformadora que é o doutorado. Foi ele quem me recebeu no aeroporto e tem me acompanhado ao longo de todos esses anos, inclusive durante o período da pandemia de COVID-19, quando estive internado. Sempre serei grato por ter tido o privilégio de caminhar ao seu lado durante esses anos de doutorado. O aprendizado foi muito além dos processos de separação com membranas. Gostaria também de expressar minha profunda gratidão ao meu orientador, Frederico de Araujo Kronemberger, pela sua dedicação, paciência e pela visão enriquecedora que trouxe ao longo de todo esse processo. Foi em uma das suas aulas de Tecnologia de Membranas no Tratamento de Efluentes que surgiu a ideia que se desenvolveu ao longo deste trabalho de doutorado. Agradeço por sempre estar disposto a me ouvir e por se demonstrar genuinamente interessado em propor ideias que contribuíram de forma significativa para o bom andamento do meu trabalho. Sou imensamente grato pelo tempo de aprendizado compartilhado e pela sincera atenção dedicada às minhas ideias.

Agradeço também ao corpo docente e administrativo do Programa de Engenharia Química da COPPE/UFRJ, especialmente ao professor Cristiano Piacsek, pelo valioso aprendizado proporcionado em suas aulas. Agradeço ainda às secretárias Vera Cruz e Luciana dos Santos, que sempre estiveram dispostas a me auxiliar na resolução de todos os assuntos burocráticos durante meu tempo como estudante de doutorado. Ao pessoal do Laboratório de Processos de Separação com Membranas e Polímeros – PAM, pela parceria e companhia nas longas jornadas de experimentação. Ao pessoal do Laboratório de Desenvolvimento e Otimização de Processos Orgânicos, especialmente à sua diretora, professora Érika Chrisman, que me acolheram durante meu período como docente da Escola de Química e me forneceram as ferramentas necessárias para as análises por cromatografia gasosa, fundamentais para o desenvolvimento deste trabalho. Agradeço

também às agências de fomento CAPES e FAPERJ pelo apoio por meio das bolsas de pesquisa.

Sem dúvida, um dos melhores resultados do doutorado foram as amizades que fiz ao longo desses anos. Amizades que se fortaleceram nas noites de estudo e no compartilhamento das nossas experiências diárias como doutorandos. Agradeço a Carol de Sá, Sérgio Castaño, Leonardo Dantas e Rafael Marinho, amigos que se tornaram irmãos. Deus me abençoou com a oportunidade de tê-los como parte da minha família no Brasil. Agradeço pelas aulas de forró, pelos almoços e pelas viagens juntos. Sem dúvida, o doutorado foi muito mais leve graças a cada um de vocês.

Sou grato também aos meus irmãos da Primeira Igreja Batista Bíblica do Rio de Janeiro, pelo carinho, companhia e apoio ao longo desses anos. Ter vocês por perto me faz sentir em casa. À minha amiga Paola Andréa Borda, pelo apoio e parceria durante todo esse tempo. Ao meu irmão adotivo Roberto Abrantes, por me receber em sua família, sempre disposto a me ouvir, me aturar e me acolher em sua casa. Sua amizade é, sem dúvida, um presente de Deus! Ao meu colega de lutas Carlos Ortiz Bravo, pela amizade e parceria. Admiro muito você e sou imensamente grato por tê-lo por perto. À minha querida Johanna Diez, insisto que me faz falta beber uma cerveja e jogar conversa fora com você, mas mesmo à distância, você fez parte de tudo isso. Saudade!

Agradeço à minha família pelo apoio incondicional durante todo esse tempo. Estar longe é difícil e o caminho tem sido longo, mas vocês sempre foram meu porto seguro. Graças a vocês, tenho a certeza de que sempre terei na Colômbia um lugar para chamar de lar. Agradeço à minha esposa, Girlene, pelo apoio e paciência durante esses meses de escrita da tese. Pelo carinho, cuidado e por ficar no sofá apenas para estar ao meu lado nas longas noites do verão carioca enquanto eu trabalhava na tese, mesmo grávida do nosso Nathan. Te amo infinitamente!

Finalmente quero expressar minha gratidão ao Senhor, pela sua fidelidade, bondade e graça durante todos esses anos. Mesmo no vale da sombra da morte Ele me sustentou. Sempre sou surpreendido pelas coisas que Ele faz e pela enorme graça concedida a mim. Que este trabalho honre o nome de Cristo, porque dele por Ele e para Ele são todas as coisas!

Resumo da Tese apresentada à COPPE/UFRJ como parte dos requisitos necessários para a obtenção do grau de Doutor em Ciências (D.Sc.)

AVALIAÇÃO DO DESEMPENHO DE UM REATOR DE CONTATOR COM MEMBRANAS DE FIBRA OCA PARA EXTRAÇÃO REATIVA NA PRODUÇÃO DE BIODIESEL

Nevardo Bello Yaya

Fevereiro/2025

Orientadores: Alberto Claudio Habert
 Frederico de Araujo Kronemberger

Programa: Engenharia Química

Esta tese de doutorado avalia o desempenho de um reator contactor de membranas de fibra oca (HFMCR) na extração reativa para a produção de biodiesel por transesterificação de óleo de soja com metanol, catalisada por álcali. Foram investigados os efeitos das principais variáveis do processo — como o caudal de óleo (OFR), a razão molar metanol/óleo (MR) e a fração de empacotamento (PF) — na conversão e no rendimento. Os resultados demonstram a eficácia do HFMCR em promover o contacto entre as fases e permitir a extração reativa de glicerol com metanol, resultando em uma baixa concentração de glicerina de apenas 0,06% p/p no biodiesel final. Adicionalmente, foi desenvolvido e validado um modelo com base em dados experimentais, que representa com precisão o processo no HFMCR. Os melhores resultados — 35% de conversão e 20% de rendimento — foram alcançados com um PF de 30%, uma razão molar de 4:1 e um OFR de 0,4 L/h. A integração da extração reativa no sistema de contactor de membrana apresenta um método de produção de biodiesel mais rentável e ambientalmente sustentável, reduzindo o tempo de processamento e simplificando a purificação a jusante ao eliminar a necessidade de etapas de separação do glicerol.

Abstract of Thesis presented to COPPE/UFRJ as a partial fulfillment of the requirements for the degree of Doctor of Science (D.Sc.)

PERFORMANCE ASSESSMENT OF A HOLLOW FIBER MEMBRANE
CONTACTOR REACTOR FOR REACTIVE EXTRACTION IN BIODIESEL
PRODUCTION

Nevardo Bello Yaya

February/2025

Advisors: Alberto Claudio Habert
 Frederico de Araujo Kronemberger

Department: Chemical Engineering

This doctoral thesis assesses the performance of a hollow fiber membrane contactor reactor (HFMCr) for reactive extraction in the production of biodiesel through the alkali-catalyzed transesterification of soybean oil with methanol. The study investigates the effects of key process variables—such as oil flow rate (OFR), methanol-to-oil molar ratio (MR), and packing fraction (PF)—on conversion and yield. The results demonstrate the efficiency of the HFMCr in promoting phase contact and enabling the reactive extraction of glycerol with methanol, leading to a low glycerol concentration of just 0.06% wt in the final biodiesel. Additionally, a model was developed and validated using experimental data, accurately representing the process within the HFMCr. The best results—35% conversion and 20% yield—were obtained at a PF of 30%, a MR of 4:1, and an OFR of 0.4 L/h. The integration of reactive extraction into the membrane contactor system offers a cost-effective, environmentally sustainable biodiesel production method, reducing processing time and simplifying downstream purification by eliminating glycerol separation.

Contents

Chapter 1 - Introduction	1
1.1. Relevance and motivation	1
1.2. Objectives	2
1.2.1. General.....	2
1.2.2. Specific	3
1.3. Document Structure	3
1.4. Publications	4
1.4.1. Publications in Indexed Journals	4
1.4.2. Conference Papers	5
Chapter 2 - Literature Review	6
2.1. Membrane Contactors.....	6
2.1.1. Membranes Properties	9
2.1.2. Hollow Fiber Membrane Modules	10
2.1.2.1. Module Components	11
2.1.2.2. Module Characteristics and Operating Conditions.....	12
2.1.3. Mass Transport Mechanism.....	13
2.1.4. Membrane Contactor Reactors	16
2.2. Biodiesel	20
2.2.1. World and Brazilian Context	20
2.2.2. Feedstocks	22
2.2.2.1. Triglycerides	22
2.2.2.2. Alcohol Short Carbon Chain	24
2.2.3. Main Variables in the Biodiesel Production	25
2.2.3.1. Temperature	25
2.2.3.2. Water Content	25
2.2.3.3. Free Fatty Acids Concentration (Acidity)	26
2.2.3.4. Catalyst	26
2.2.3.5. Methanol-to-oil Molar Ratio (MR).....	27
2.2.4. Transesterification Reaction	27
2.2.5. Current Status in Biodiesel Production Processes	30
2.3. Membrane Processes in Biodiesel Production	33
2.3.1. Membrane Separators	35
2.3.2. Membranes Reactors	38
2.3.3. Catalytic Membranes Reactors	40
2.4. Concluding Remarks	42

Chapter 3 - Design and Construction of the Reaction System	43
3.1. Methodology.....	43
3.2. Design Considerations	44
3.3. Hollow Fiber Membrane Module: Materials Selection.....	45
3.3.1. Literature Review	45
3.3.2. Chemical Resistance Test	45
3.4. Initial Modeling: PFR.....	50
3.5. Hollow Fiber Membrane Module Fabrication.....	53
3.6. Hollow Fiber Membrane Contactor Reactor Laboratory Scale System	57
3.7. Concluding Remarks	58
Chapter 4 - Experimental Preliminary Evaluation	59
4.1. Experimental.....	59
4.1.1. Materials	59
4.1.2. Experimental design	60
4.1.3. Procedure	61
4.2. Characterization and sample analysis.....	61
4.3. Results and Discussion	62
4.3.1. Influence of the Oil Flow Rate (OFR).....	64
4.3.2. Influence of the methanol to oil molar ratio (MR)	65
4.3.3. Methanol and Glycerol Content in the FAME-rich phase	66
4.3.4. Operation of a HFMCR for Biodiesel Production in a Countercurrent Setup	68
4.4. Final Remarks.....	69
Chapter 5 - Modeling and Validation of HFMCR Performance in Biodiesel Production	71
5.1. Model Development	71
5.1.1. Batch-in-series Modeling.....	72
5.1.2. Shell-side (phase α) Mass Transfer Coefficient	75
5.1.3. Lumen-side (phase β) Global Mass Transfer Coefficient	76
5.1.4. Model Solution.....	77
5.1.5. Estimation of Parameters for the Shell-Side Sherwood General Correlation	77
5.2. Model Validation	79
5.2.1. Experimental Design	79
5.2.2. Materials	80
5.2.3. Characterization and Sample Analysis	81
5.3. Results and Discussion	81
5.3.1. Model Validation	81
5.3.2. Estimation of Parameters for the Shell-side Sherwood General Correlation	83

5.3.3.	Response Surfaces	87
5.4.	Effect of the hydrophilicity of the membrane: Mass transfer coefficient inside the membrane	92
5.5.	Model-based design of membrane contactor	93
5.6.	Final Remarks.....	94
Conclusions and Recommendations		96
References		99

Figure List

Figure 2.1. Operating scheme of a HFM contactor module in countercurrent setup	7
Figure 2.2. Hollow fiber membrane module	11
Figure 2.3. Concentration profile for L-L extraction in a membrane contactor using a hydrophobic membrane	13
Figure 2.4. Model of resistances in series	14
Figure 2.5. Biodiesel production 2013 - 2023	21
Figure 2.6. World oil feedstocks for biodiesel production	23
Figure 2.7. Transesterification of a triglyceride	28
Figure 2.8. Typical concentration profiles for TG and FAME in batch transesterification of TG.....	29
Figure 2.9. Schematic transesterification reaction of triglycerides	29
Figure 2.10. Conventional process flow diagram for biodiesel production	30
Figure 2.11. Membrane processes in the production of biodiesel	35
Figure 3.1. SEM images Sample M2 (PP Membrane) after the test.....	48
Figure 3.2. SEM images Sample M3 (PTFE Membrane) after the test.	48
Figure 3.3. Results for gravimetry test of resin DION6694	49
Figure 3.4. Images of the PP HFM – Membrane P80 Zena Membranes.....	50
Figure 3.5. Conversion and Yield profiles for the PFR model	52
Figure 3.7. Hollow fiber membrane module housing - Construction Datasheet.....	54
Figure 3.7. HFM module Potting. (a) Cross-section (b) Schematic diagram.....	56
Figure 3.8. Laboratory-scale setup of the HFMCr system.....	57
Figure 3.9. HFMCr laboratory scale system – PAM Laboratory PEQ/COPPE/UFRJ..	58
Figure 4.1. Obtained products. a) FAME-rich phase; b) Alcohol phase	63
Figure 4.2. FAME-rich phase sample chromatogram.....	63
Figure 4.3. Effect of the OFR on reacted triglyceride mol rate.....	64
Figure 4.4. Effect of the OFR on produced FAME mol rate	64
Figure 4.5. Effect of the MR on reacted triglyceride mol rate	66
Figure 4.6. Effect of the MR on produced FAME mol rate.....	66
Figure 4.7. Total produced glycerol mass partitioning in both phases	67
Figure 4.8. Total fed methanol mass partitioning in both phases	67

Figure 4.9. Schematic diagram of phase contacts and reaction path at the microporous membrane wall for the FAME production in an HFMCr operating in countercurrent flow..	68
Figure 4.10. Qualitative schematic representation of the concentration profiles in the HFMCr operation, based on the experimental results obtained.	69
Figure 5.1. Hollow fiber membrane contactor reactor counter-current setup	72
Figure 5.2. Batch-in series modelling for HFMCr in counter-current	73
Figure 5.3. Batch reactor model	74
Figure 5.4. Algorithm for model solution.....	77
Figure 5.5. Algorithm for the estimation of parameters for shell-side Sherwood general correlation.....	78
Figure 5.6. Predicted vs. Experimental results for conversion.....	82
Figure 5.7. Predicted vs. Experimental results for yield	82
Figure 5.8. Sensitivity analysis for parameters of the shell-side Sherwood general correlation.....	83
Figure 5.9. Adjusted Correlation: Predicted vs. Experimental results for conversion ...	86
Figure 5.10. Adjusted Correlation: Predicted vs. Experimental results for yield.....	87
Figure 5.11. Effect of OFR and PF on the TG conversion. MR = 4:1.....	87
Figure 5.12. Effect of OFR and MR on the TG conversion. PF = 30%.	88
Figure 5.13. Effect of PF and MR on the TG conversion. OFR = 0.4 L h ⁻¹	88
Figure 5.14. Effect of OFR and PF on the yield to FAME. MR = 9:1	89
Figure 5.15. Effect of OFR and MR on the yield to FAME. PF = 30%	89
Figure 5.16. Effect of MR and PF on the yield to FAME. OFR = 0.4 L h ⁻¹	90
Figure 5.17. Effect of the shell-side mass transfer resistance on conversion and yield.	92
Figure 5.18. Profile of conversion and yield for the HFMR	94
Figure 5.19. Molar flow rate profile for the HFMR	94

Table List

Table 2.1. Membrane contactor processes, alternative to common separation devices ...	7
Table 2.2. Specific surface areas of different contactor devices.....	8
Table 2.3. Empirical correlations for shell-side mass transfer in parallel flow for liquid-liquid systems in handmade, randomly-packed modules.	17
Table 2.4. Oil feedstocks for biodiesel production	23
Table 2.5. National and international limits for common biodiesel impurities	31
Table 2.6 Some intensified processes for biodiesel production.....	34
Table 3.1. Material selection for membrane contactor: Chemical resistance chart	45
Table 3.2. Membranes tested for chemical resistance according to ASTM D543-14	46
Table 3.3. Results for chemical resistance test of the membranes	47
Table 3.4. Specifications for PP HFM – Membrane P80 Zena Membranes.....	50
Table 3.5. Reaction Rate for each chemical species.....	51
Table 3.6. Conditions for the solution of the ODEs	51
Table 3.7. Detailed parameters for membrane contactors.	53
Table 3.8. Potting process description	55
Table 4.1. Soybean oil specifications	59
Table 4.2. Selected variables for the evaluation of soybean oil transesterification in a HFMCR.	60
Table 4.3. Set of experiments performed.....	61
Table 5.1. Reaction Rate for each chemical species.....	75
Table 5.2. Selected variables for the evaluation of soybean oil transesterification in a HFMCR	79
Table 5.3. Set of experiments performed.....	80
Table 5.4. Soybean oil specifications	80
Table 5.5. Parameters estimated for TG and FAME to empirical Sh correlation.....	84
Table 5.6. Empirical correlations for shell-side mass transfer for liquid-liquid systems, handmade, parallel flow, and randomly-packed modules	85

Abbreviations List

ANP	: Brazilian National Agency of Petroleum, Natural Gas, and Biofuels
ASTM	: American Society for Testing and Materials
BP	: Bubble point
BSTFA	: Derivatization agent N,O-bis(trimethylsilyl) trifluoroacetamide
BzH	: Benzaldehyde
BzOH	: Benzyl alcohol
CA	: Contact angle measurements
CCS	: Centrifugal contact separator
CFD	: Computational fluid dynamics
CNPE	: Brazilian National Council for Energy Policy
DG	: Diglycerides
DMAc	: Dimethylacetamide
DMF	: Dimethylformamide
EU	: European Union
FAAs	: Free fatty acids
FAEE	: Fatty acid ethyl esters
FAME	: Fatty acid methyl esters (Biodiesel)
FID	: Flame ionization detector
FTIR	: Fourier transform infrared spectroscopy
G	: Glycerol
GC	: Gas chromatography
HDPE	: High density polyethylene
HFM	: Hollow fiber membrane
HFM	: Hollow fiber membrane
HFMCR	: Hollow fiber membrane contactor reactor
HPO	: Hydrogenated/refined palm oil
HT	: Hydrotalcite
ILUC	: Indirect land-use changes
IS	: Internal standard
LDPE	: Low density polyethylene
LEP	: Liquid entry pressure
LLE	: Liquid-liquid extraction

M	: Methanol
MCR	: Membrane contactor reactor
MD	: Membrane distillation
ME	: FAME
MEK	: Methyl ethyl ketone
MF	: Microfiltration
MG	: Monoglycerides
MR	: Methanol-to-oil molar ratio
MWCO	: Molecular weight cut-off
ODE	: Ordinary differential equation
OFR	: Soybean oil flow rate
PAM	: Membrane Process Laboratory – PEQ/COPPE/UFRJ
PAN	: Polyacrylonitrile
PF	: Packing fraction
PDMS	: Polydimethylsiloxane
PES	: Polyether sulfone
PFD	: Process flow diagram
PFD	: Process flow diagram
PFR	: Plug Flow Reactor
PFR	: Plug flow reactor
phr	: Parts per hundred resin
PID	: Proportional–integral–derivative controller
PP	: Polypropylene
PTFE	: Polytetrafluoroethylene
PTSA	: Paratoluenesulphonic acid
PVA	: Polyvinyl alcohol
PVDF	: Polyvinylidene fluoride
RBDPO	: Bleached and deodorized palm oil
RED	: European Renewable Energy Directive
SA	: Succinic acid
SEM	: Scanning electron microscopy
SRUF	: Solvent-resistant ultrafiltration polymer
TEP	: Triethyl phosphate
TG	: Triglycerides
TMP	: Transmembrane pressures

TOA	:	Trioctylamine
TPA	:	Tripropylamine
UF	:	Ultrafiltration
WVOs	:	Waste vegetable oils

Symbols List

$C_{i p}$: Concentration of i at the bulk of phase p
$v_{0 p}$: Volume flow rate at the inlet of phase p
A_{CS}	: Cross section area of the reactor
$A_{CS p}$: Cross section area of the phase p
A_{ms}	: Surface membrane area
C_{TG}	: Conversion of TG
C_i^*	: Concentration of i at the reaction layer
C_{i0}	: Solute concentration in the organic phase
C_{iw}	: Solute concentration in the aqueous phase
D_{iM}	: Diffusivity of i in the mixture
$FAME_p$: Produced FAME
F_i	: Molar flow of i
G_z	: Graetz number
J_{iz}	: Molar flux of i
K_i	: Mass transfer coefficient of i
N_i	: Mass of i [mol]
$V_{\Delta z}$: Volume of the reaction layer
V_p	: Volume of phase p
Y_{FAME}	: Yield to FAME
d_h	: Hydraulic diameter [m]
$d_{H.in}$: HFM Housing inner diameter
d_{im}	: Hollow fiber membrane inner diameter
d_{out}	: Hollow fiber membrane outer diameter
d_p	: Pore diameter [m]
k_O	: Mass-transfer coefficient for the organic phase
k_{iw}	: Alcohol-rich phase mass transfer coefficient
k_j	: Kinetic constant
k_m	: Mass-transfer coefficient for the membrane
k_w	: Mass-transfer coefficient for the aqueous phase
l_R	: Reactor length
m_i	: Distribution coefficient

n_m	: Number of hollow fiber membranes
r_i	: Reaction rate of i
γ_t	: Interfacial tension
δ_m	: Membrane thickness
θ_t	: Contact angle
$\bar{\tau}$: Membrane tortuosity
τ_{Av}	: Average residence time
τ_p	: Residence time of phase p
$[i]$: Concentration of i
ΔC	: Concentration gradient (driving the mass transfer)
ΔP	: Breakthrough pressure
Δz	: Differential length
K	: Overall mass-transfer coefficient
Re	: Reynolds number
Sh	: Sherwood number
Sc	: Schmidt number
TG_R	: Reacted triglycerides
TG_{in}	: Molar flow rate of triglycerides in the oil phase at the reactor inlet
TG_{out}	: Molar flow of triglycerides in the oil phase at the reactor outlet
$f(g)$: Function of geometry
l	: Active length [m]
t	: Time
z	: Length
α	: FAME-rich phase (oil phase)
β	: Alcohol-rich phase (alcohol phase)
γ	: Parameter for the hydraulic ratio
δ	: Parameter for Re
ε	: Membrane porosity
η	: Dynamic viscosity
θ	: Parameter for Sc
ρ	: Mass density
ω	: Parameter for the free fraction
ϕ	: Packing fraction

Chapter 1 - Introduction

1.1. Relevance and motivation

The current trend in industrial processes focuses on maximizing profit while minimizing emissions and energy consumption through improved energy efficiency. As a result, processes that enhance existing industrial practices present an excellent opportunity for research and development [1]. In line with this trend, Process Intensification aims to drive advancements in chemical engineering that result in smaller, cleaner, and more energy-efficient technologies. This approach targets two key areas: innovative equipment, such as novel reactors and heat and mass transfer devices, and methods, which include the integration of reaction and separation stages, membrane processes, alternative energy sources, and advanced process control techniques [2].

In addition to the conventional membrane processes, the use of hollow fiber membrane contactors in intensified processes, such as reactive extraction in gas-liquid and liquid-liquid systems, has gained significant relevance in the last years [3,4,5,6]. Membrane contactors are devices that promote continuous, non-dispersive contact between two phases. In these processes, the membrane acts as a barrier, enhancing the surface area for mass transfer between the phases [7]. As a result, separation in membrane contactors is governed by phase equilibrium principles rather than membrane selectivity [8]. The potential advantages of membrane contactors were previously explored and demonstrated in the Membrane Separation Processes Laboratory (PAM/COPPE/UFRJ), where this research was conducted [9,10,11,12,13,14]. This investigation presented an additional challenge for innovation in biodiesel production. When a hollow fiber membrane contactor is used for reactive extraction, it is referred to as a hollow fiber membrane contactor reactor (HFMCr).

The production processes for biodiesel could benefit from the application of HFMCR technology. Conventional biodiesel production processes face several challenges which have been the focus of research over the past decade [15,16,17,18]. These include the high cost of biodiesel, driven largely by the expense of feedstocks like vegetable oil, which account for 70–85% of production costs [19]. This highlights the need to optimize processes to utilize cheaper, lower-quality feedstocks. Additionally, since transesterification is a reversible reaction, the chemical equilibrium limits both conversion and yield, demanding multiple reaction-separation stages to achieve the required quality [20,21]. The use of alkaline catalysts can lead to the formation of soaps and gels that hinder downstream separation and purification stages[17]. Moreover, the immiscibility of vegetable oils and methanol creates mass transfer limitations, typically addressed by using stirred reactors, which come with associated energy costs [22]. Environmental concerns are also significant, as current purification methods generate substantial waste—wet purification uses water to wash impurities, resulting in effluent, while dry purification generates solid waste contaminated with soaps, catalysts, and biodiesel, all of which must be properly treated [17,23].

This research aims to harness the characteristics of hollow fiber membrane contactor reactors (HFMCR) to address some of the key challenges in the biodiesel industry. It is expected to design, assemble, and operate an HFMCR that promotes non-dispersive contact between reactive phases, thereby reducing energy consumption. Additionally, it is expected to overcome the limitations of chemical equilibrium of by enabling the simultaneous extraction of glycerol using methanol as the extractant solvent, facilitating a reactive extraction process. Soybean oil serves as the feedstock, with sodium hydroxide acting as the catalyst during the reaction.

1.2. Objectives

1.2.1. General

To develop a reactive extraction process for the continuous production of biodiesel using a hollow fiber membrane contactor reactor (HFMCR).

1.2.2. Specific

- To fabricate a hollow fiber membrane module suitable for operation under reaction conditions.
- To evaluate the impact of various operational parameters—such as oil flow rate, methanol-to-oil molar ratio, and packing fraction—on the transesterification conversion and biodiesel yield.
- To develop a mathematical model that represents the behavior of the hollow fiber membrane contactor reactor for reactive extraction in biodiesel production.

1.3. Document Structure

This doctoral thesis is organized into five chapters, which are structured as follows:

Chapter One lays the groundwork for the thesis by emphasizing the significance and motivation of the research. It articulates both the general and specific objectives of the study, presents a comprehensive overview of the document's structure, and includes a list of publications resulting from the research.

Chapter Two provides an overview of the key themes in the thesis, starting with membrane contactors, their features, advantages, and the concept of hollow fiber membrane modules, along with the resistance-in-series model for mass transport, focusing on reactive extraction. It then introduces biodiesel, discussing its global and Brazilian context, feedstocks, production trends, and transesterification reaction kinetics. The chapter concludes by highlighting current biodiesel production methods, with an emphasis on intensified processes and the role of membrane processes in biodiesel production, covering reaction, separation, and catalytic membranes.

Chapter Three outlines the design of a laboratory-scale system for evaluating Fatty Acid Methyl Esters (FAME) production. It includes defining parameters for the hollow fiber module (HFM), selecting materials, and fabricating the HFM. Key process variables such as oil flow rate, methanol-to-oil molar ratio, and packing fraction were defined, and peripheral equipment like pumps, heating devices, and control systems were specified.

Chapter Four corresponds with a paper published as described in Section 1.4.1. The chapter describes initial tests evaluating the hollow fiber membrane contactor reactor (HFMCr) for reactive extraction in FAME (biodiesel) production. The experiments, using a laboratory-scale system, assessed the effects of oil flow rate (OFR) and methanol-to-oil molar ratio (MR) on triglyceride reaction rates and FAME production. It also estimated glycerol and methanol content in the FAME-rich phase for each condition.

Chapter Five corresponds with a paper in preparation for submission as described in Section 1.4.1. The chapter outlined the development of a mathematical model to predict the behavior of a hollow fiber membrane contactor reactor (HFMCr) for FAME production. The model includes estimating parameters for an empirical correlation to calculate the Sherwood number. Its accuracy was validated with experimental data from a laboratory system, examining the impact of key variables—oil flow rate (OFR), methanol-to-oil molar ratio (MR), and packing fraction (PF)—on triglyceride conversion and FAME yield.

The concluding chapter summarizes the principal findings of the research, presenting the results of the performance evaluation of the HFMCr in biodiesel production while emphasizing the most significant outcomes. It also summarizes the main contributions of the study and proposes potential avenues for future research grounded in the observed results.

1.4. Publications

This section presents an overview of the academic products developed during this doctoral research, published in peer-reviewed journals, and presented at academic conferences. These works provide the basis for the methodologies and results presented in this thesis, demonstrating their relevance, validation, and application for the academic research community.

1.4.1. Publications in Indexed Journals

- ♦ BELLO YAYA, N.; HABERT, A. C.; KRONEMBERGER, F. D. A. **Evaluation of a hollow fiber membrane contactor reactor for reactive extraction in biodiesel**

production. Chemical Engineering and Processing - Process Intensification, v. 194, p. 109574, 2023. DOI: <https://doi.org/10.1016/j.cep.2023.109574>

- ♦ BELLO YAYA, N.; HABERT, A. C.; KRONEMBERGER, F. D. A. **Mass-transfer-based modeling and experimental validation of reactive extraction in a hollow fiber membrane contactor reactor for biodiesel production.** *In preparation for submission to Journal Fuel.* <https://www.sciencedirect.com/journal/fuel>

1.4.2. Conference Papers

- ♦ KRONEMBERGER, F. D. A.; BELLO YAYA, N.; HABERT, A. C. **Evaluation of hollow fiber membrane contactor reactor in reactive extraction for biodiesel production.** North American Membrane Society 2025 Annual Meeting. Energy and Sustainability. *Submitted on 02/2025.*

Chapter 2 - Literature Review

This chapter provides a comprehensive review of the central themes explored in this doctoral thesis. It begins by defining membrane contactors and outlining their characteristics, as well as their advantages and disadvantages. The properties of membranes and the concept of hollow fiber membrane modules are also examined in detail. Furthermore, the chapter addresses the resistance-in-series model for mass transport in membrane contactors and concludes this section with a concise overview of the application of membrane contactors in reactive processes. The second section introduces key concepts related to biodiesel, presenting an overview of its global context, with particular emphasis on the Brazilian scenario. It discusses the various feedstocks used in biodiesel production, current trends, and critical variables influencing the production process. The subsequent section delves into the kinetics of the transesterification reaction and provides an updated analysis of current biodiesel production methods, with a specific focus on production intensification techniques. The chapter concludes by summarizing the role of membrane processes in biodiesel production, encompassing the reaction phase, separation and purification stages, and the use of catalytic membranes.

2.1. Membrane Contactors

Membrane contactors are devices that promote a continuous nondispersive contact between two phases. In this kind of process, the primary function of the membrane is to act as a barrier, enhancing the surface area for mass transfer exchange between the two phases [7]. Consequently, separation in membrane contactors is based on phase equilibrium principles rather than membrane selectivity [8]. Transport across the membrane occurs through its pores, driven by concentration (or partial pressure) differences and/or temperature gradients as the main driving forces [7,24,25,26].

Typically, membrane contactors are designed as shell-and-tube devices, utilizing microporous hollow fiber membranes (HFM) (Figure 2.1) [7,27,4].

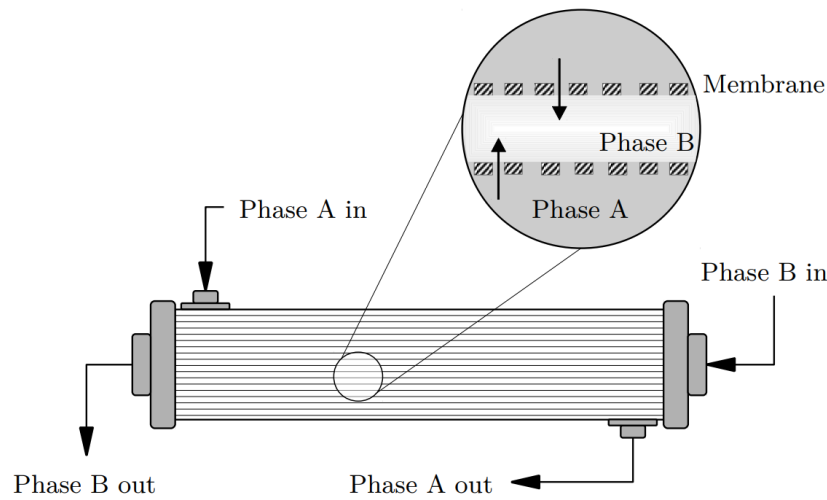


Figure 2.1. Operating scheme of a HFM contactor module operating in countercurrent setup

Currently, membrane contactors are employed in industrial processes as an alternative to conventional separation devices, as outlined in Table 2.1 [26,27].

Table 2.1. Membrane contactor processes as an alternative to common separation devices

Common Separator	Membrane Contactor Process
Absorption/stripping	Gas-Liquid contactors
Extraction (two immiscible liquids)	Liquid-Liquid contactor
Extraction (two miscible liquids)	Membrane distillation (MD) and crystallization

This technology offers several advantages over traditional contactor devices, including enhanced mass transfer efficiency, compact design, greater operational flexibility, and improved process control [7,24,25,26,27,28]:

- i. High interfacial area per volume unit. The HFM provides a controlled and known high interfacial area, making it possible to obtain smaller and lighter equipment. Table 2.2 compares the specific contact area of membrane contactor devices [27].
- ii. No dispersion occurs between the phases, preventing the formation of emulsions and foaming

Table 2.2. Specific surface areas of different contactor devices

Contactor Device	Surface area per volume unit [cm cm ⁻³]
Free dispersion columns	0.03 – 0.3
Packed/trayed columns	0.3 – 3
Mechanically agitated columns	2 – 5
Membranes	10 – 50

- iii. The surface area is well-defined and remains constant, independent of the flow rate ratio between the phases. This ensures that the available surface area remains undisturbed, eliminating common issues such as flooding at high flow rates or unloading at low flow rates.
- iv. Enables operation in a countercurrent flow configuration.
- v. There is no need for a density difference between the fluids, and downstream separation is not required.

Similarly, membrane contactors also have some drawbacks, including the following [7,24,26]:

- i. Additional resistance to transport due to the inherent membrane resistance.
- ii. Channeling and bypassing of fluids occur when the operating pressure exceeds the breakthrough pressure, thereby limiting the maximum operating pressure.
- iii. Fouling, which, while generally smaller than in pressure-driven processes, can still affect the performance of membrane contactors.
- iv. The potting resin, used to secure the fiber bundle to the tube sheet, must have high chemical resistance to the fluids in contact.
- v. Membrane lifetime, with the need to consider the costs of periodic membrane replacement and the required chemical resistance.

2.1.1. Membranes Properties

Pore size

Pore size in membranes refers to the average diameter of the small openings that facilitate the selective passage of substances. It determines the permeability of the membrane, with pore sizes typically measured in micrometers or nanometers. Most membrane contactors employ microfiltration membranes, characterized by pore sizes ranging from 5 to 0.1 μm . Larger pore sizes increase the mass transfer flux, but they also result in lower breakthrough pressures [24,26]. Additionally, the pore sizes must be small enough to prevent capillary forces from driving direct phase mixing [27].

Morphology: Porosity, Thickness, and Tortuosity

Porosity refers to the fraction of the membrane surface occupied by pores (voids). An increase in porosity enhances flux but may also result in bubble coalescence during gas-liquid operations. Thickness denotes the distance between the two surfaces of the membrane, influencing its permeability and overall performance in membrane processes. A thinner membrane reduces mass transfer resistance; however, in membrane distillation, it may also increase heat loss through conduction. Tortuosity describes the degree of deviation in the path that fluid molecules must travel through the porous structure, thereby impacting mass transport resistance. A lower tortuosity improves flux by reducing the mass transfer resistance imposed by the membrane [26].

Chemical Stability

Long-term exposure to solvents, solutions, or process conditions can alter the morphology of polymeric membranes, potentially causing significant changes in their transport properties. Therefore, polymeric membranes must be chemically inert to both solvents and chemicals, as well as physically stable under operating conditions [26].

Hydrophobicity

The hydrophobicity of a membrane is related to the physicochemical properties of both the membrane and the solvent. The interface between a liquid and a solid substrate can be characterized by measuring the contact angle. For water, a contact angle of less than 90° indicates strong interactions between the substrate and the liquid, causing the liquid

to wet the substrate (hydrophilic). In contrast, when the contact angle is greater than 90°, the liquid does not tend to wet the surface, indicating hydrophobic behavior [4].

Breakthrough Pressure

The breakthrough pressure is the minimum pressure required for a non-wetting fluid to pass through the membrane pores to the other side. This pressure can be estimated using the Young-Laplace equation (Equation 2.1), assuming the pores are ideal cylinders [7,8,24,27]. The equation involves the interfacial tension (γ), the contact angle (θ), and the pore diameter (d_p). A higher contact angle results in a lower breakthrough pressure.

$$\Delta P = \frac{4 \gamma_t \cos \theta_t}{d_p} \quad \text{Equation 2.1}$$

Membrane Matrix Material

Most commercial membranes are polymeric (organic-based). Polypropylene (PP), polyvinylidene fluoride (PVDF), polytetrafluoroethylene (PTFE), and perfluoropolymers are commonly used in the preparation of membrane contactors. Isotactic PP offers excellent solvent resistance and high crystallinity. PTFE membranes are highly crystalline, with very good thermal stability and chemical resistance, making them highly resistant to most common solvents. PVDF, while soluble in aprotic solvents such as dimethylformamide (DMF), dimethylacetamide (DMAc), and triethyl phosphate (TEP), also demonstrate good thermal and chemical resistance [24,8,26,4].

2.1.2. Hollow Fiber Membrane Modules

The performance of a hollow fiber membrane module is determined by both the intrinsic transport properties of the membrane and the fluid hydrodynamics within the module. Ideally, the performance of the membrane within the module should correspond to that of individual fibers, as assessed before the construction of the module, as described in Section 2.1.1. To achieve this, the module design must minimize hydrodynamic pressure losses and concentration polarization, while maximizing the effective membrane surface area [28,29,30].

Designing and fabricating hollow fiber modules demands a multidisciplinary approach due to the wide range of application requirements and the lack of a one-size-fits-all

design. The evolution of module design has been shaped by a combination of prior knowledge, practical experience, and advancements in computational fluid dynamics (CFD). Although module design is critical to achieving efficient separation, the available literature on the subject remains sparse, as much of the expertise is kept as trade secrets, with a greater focus placed on membrane materials [28,29,31].

2.1.2.1. Module Components

A hollow fiber module consists of three key parts: the hollow fiber membrane bundle, the housing, and the potting, as illustrated in Figure 2.2. The bundle, which serves as the functional component of the module, contains numerous membranes typically arranged in parallel. These membranes divide the module into two compartments: the lumen side, which is the space enclosed by the membranes, and the shell-side, which is the space between the outer surfaces of the membranes and the housing. The housing is generally a lengthened tubular structure with a uniform circular cross-section [27,30,32,33].

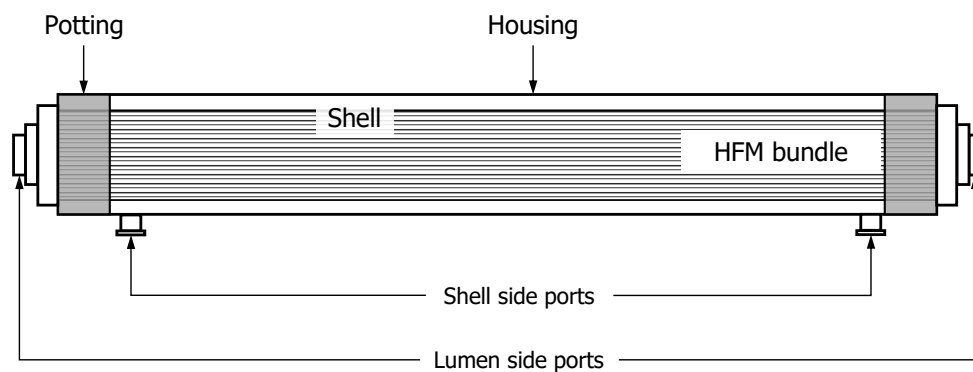


Figure 2.2. Hollow fiber membrane module

The potting material in the module plays a critical role in forming a fluid-tight seal between the fibers, preventing fluid mixing between the lumen and shell-sides. This seal is created by injecting a liquid potting material into a mold, where it solidifies. Potting materials must have adequate mechanical strength, chemical resistance, and compatibility with other module components. Common materials include cements, waxes, and resins. A key property of potting materials is low viscosity, which allows them to self-level and fully penetrate the fiber bundle. However, if the viscosity is too low, unwanted capillary flow into the fiber bundle can occur, which may impair the performance of the module [29,30,31].

2.1.2.2. Module Characteristics and Operating Conditions

Flow Rates

High flow rates reduce the thickness of boundary layers, thereby decreasing mass and heat transport resistances. This flow condition also helps prevent stagnant zones and channeling inside the module, enhancing the performance of the process. However, high flow rates can also increase stream pressures, potentially exceeding the breakthrough pressure [24,34].

Operating Pressure

The interfacial area must be kept constant by controlling the operating pressure of the two phases. Typically, the phase that does not wet the pores should be maintained at a slightly higher pressure than the other phase to prevent exceeding the breakthrough pressure [7,26].

Feeding

Streams with high viscosity or containing larger particles should preferably be directed to the shell-side of the module. The fluid with a higher affinity for the species to be transferred should fill the membrane pores, as this helps reduce the mass transfer resistance of the membrane [26].

Packing Fraction (PF)

The packing fraction (ϕ) in a hollow fiber membrane module refers to the ratio of the total volume occupied by the hollow fibers themselves, excluding the space between them, to the total volume of the membrane module. It is a measure of how efficiently the module's volume is utilized by the fibers, compared to the space dedicated to feed channels. This relationship is mathematically expressed in Equation 2.2.

$$\phi = n_m \left(\frac{d_{out}}{d_{H.in}} \right)^2 \quad \text{Equation 2.2}$$

Where, d_{out} is the outer diameter of the hollow fiber and $d_{H.in}$ is the inner diameter of the housing of the module.

A higher packing fraction indicates that the fibers occupy a larger portion of the total volume of the module, which improves space efficiency but may lead to challenges such as increased pressure drops or uneven flow distribution. Conversely, a lower packing fraction provides better fluid dynamics but can reduce the total surface area available for mass transfer. Ensuring uniform packing is crucial for maintaining a consistent flow pattern on the shell-side, preventing channeling, bypassing, and stagnant areas, all of which can significantly impair the performance of the system [24,26,27]. Gas separation modules typically have higher packing densities than liquid separation modules, as overly high packing densities can result in excessive resistance to flow and undesirable pressure drops [27,33].

2.1.3. Mass Transport Mechanism

The mass transport in a typical membrane contactor is often described using the film model, which assumes a sequence of three steps: mass transport from the bulk to the membrane surface, diffusion through the liquid within the membrane pores, and transport from the membrane surface into the stripping solution [25]. Mass transfer occurs exclusively through diffusion across the immobilized phase inside the pores and is driven by the solute concentration (chemical potential) difference between the phases in contact [7,27,4]. Figure 2.3 illustrates a typical operation for liquid/liquid extraction in a membrane contactor using a hydrophobic membrane.

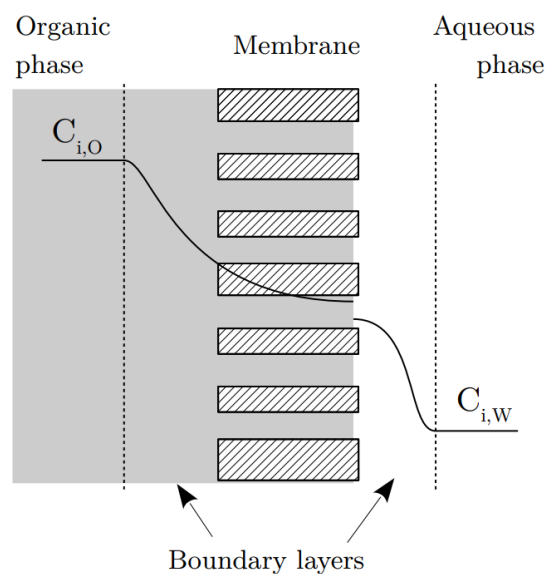


Figure 2.3. Concentration profile for liquid-liquid extraction in a membrane contactor using a hydrophobic membrane

The concentration profile is discontinuous at the interface, following the equilibrium relationship described in Equation 2.3, where C_{i0} and C_{iw} are the solute concentrations in the organic and aqueous phases, and m_i is the distribution coefficient.

$$C_{i0} = m_i C_{iw} \quad \text{Equation 2.3}$$

A general mathematical expression for mass transport depends on the flow configuration and the interface location. When a species is transferred from an aqueous phase to an organic phase, the global mass transport coefficient can be expressed as a sum of three resistances in series: the organic phase boundary layer, the membrane, and the aqueous phase boundary layer (Figure 2.4) [24,25,26]. Equation 2.4 describes the resistance-in-series model without chemical reaction, where K denotes the overall mass-transfer coefficient, k_o and k_m are the individual mass-transfer coefficients for the organic phase and the membrane, respectively, and k_w refers to the aqueous phase mass-transfer coefficient, and m_i represents the distribution coefficient [24,4,27,35].

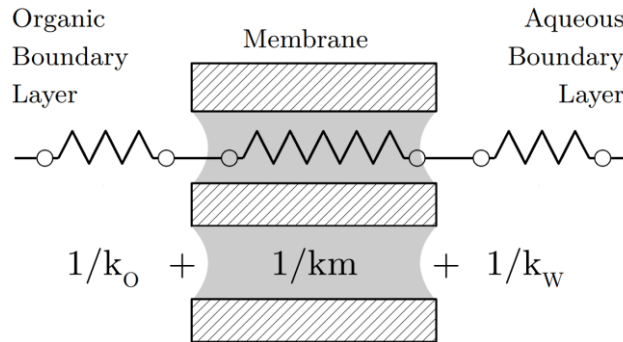


Figure 2.4. Model of resistances in series

$$\frac{1}{K} = \frac{1}{k_o} + \frac{1}{k_m} + \frac{m_i}{k_w} \quad \text{Equation 2.4}$$

Correlations for estimating mass transfer coefficients are essential in membrane contactors. However, general equations derived from mathematical analysis are often insufficient due to the random geometry of most membrane contactors. Equation 2.5 provides the general form for the empirical estimation of mass transfer coefficients for the shell-side and the lumen side [24,26,35,36,37]. In this context, Sh denotes the Sherwood number, Re represents the Reynolds number, and Sc is the Schmidt number,

while $f(g)$ is a function dependent on the geometry, hydraulic diameter, and length. Likewise, δ and θ are parameters within the empirical correlation.

$$Sh = \frac{k_i d_h}{D_{iM}} = f(g) Re^\delta Sc^\theta \quad \text{Equation 2.5}$$

The L  v  que correlation (Equation 2.6) is widely used to determine the tube side mass transfer coefficient. This correlation is applicable under laminar flow conditions for systems with a Graetz number (G_z) greater than 6 [36].

$$Sh = \frac{k_{iw} d_{im}}{D_{iM}} = 1.62 \cdot \left(\frac{d_h}{l}\right)^{0.33} \cdot Re^{0.33} \cdot Sc^{0.33} \quad \text{Equation 2.6}$$

Where k_{iw} is the tube side mass transfer coefficient, d_{im} represents the inner diameter of the hollow fiber membrane, D_{iM} is the diffusivity of component i in the mixture, dh refers to the hydraulic diameter, and l denotes the active length of the membrane module.

A general correlation for calculating the mass transfer coefficient on the shell-side is not readily available, as it depends on specific module characteristics such as packing fraction, fiber arrangement, and flow configuration (parallel or crossflow) [3,25]. Table 2.3 summarizes various empirical correlations based on Equation 2.5 for predicting shell-side mass transfer coefficients in parallel flow for liquid-liquid systems in handmade, randomly-packed modules [38,39].

The mass transfer coefficient for a membrane was estimated using the methods outlined by Prasad and Sirkar, which depend on key membrane properties such as porosity, tortuosity, and thickness. This estimation specifically applies to unhindered diffusion through organic fluid-filled pores, as shown in (Equation 2.7) [24,34,35]. The variables include D_{iM} , the diffusivity of species i in the mixture through the membrane; ε , membrane porosity; $\bar{\tau}$, membrane tortuosity; δ_m , membrane thickness.

$$k_{i|m} = \frac{\varepsilon \cdot D_{iM}}{\bar{\tau} \delta_m} \quad \text{Equation 2.7}$$

2.1.4. Membrane Contactor Reactors

Membrane contactor reactors (MCR) are useful for intensifying the interaction between non-miscible reactants or enabling the extraction of one of the products within the same device. This extractive capacity helps overcome chemical equilibrium limitations in reversible reactions. In a MCR, the membrane can function in two main ways: as an interfacial contactor or a forced flow-through contactor. In the interfacial contactor setup, the membrane acts as a barrier between two fluid phases (gas-liquid or liquid-liquid), allowing the reaction to occur in the membrane pores. The products will preferentially migrate to one or both phases, and the membrane can either be catalytically active or hold the catalyst within the feed solution. In contrast, the forced flow-through contactor involves pushing the fluid phase containing the reagents through the membrane pores, where it reacts with the catalyst. The membrane in this case is always catalytically active, facilitating the reaction on the catalytic sites within its structure [7].

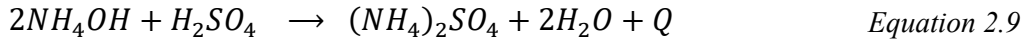
Buonomenna and Drioli [40] studied a catalytic process for the selective oxidation of benzyl alcohol (BzOH) to benzaldehyde (BzH) using hydrogen peroxide in a flat microporous membrane contactor reactor (Equation 2.8). They examined the effects of temperature, membrane type, catalyst type, and hydrogen peroxide addition mode on BzOH conversion and BzH selectivity. The organic phase, containing the substrate and product, and the aqueous phase with the oxidant were fed into a two-compartment cell with a flat sheet membrane ($4.91 \times 10^{-4} \text{ m}^2$ surface area). The phases were stirred at constant temperatures of 60°C, 70°C, and 80°C. Three different membranes based on hydrophobic polyvinylidene fluoride (PVDF) were prepared and characterized. The catalysts used were ammonium molybdate, $(\text{NH}_4)_6\text{Mo}_7\text{O}_{24}$, and sodium tungstate, Na_2WO_4 . The results demonstrated that BzOH could be selectively oxidized to BzH with hydrogen peroxide as the oxidant. The best results showed 99% selectivity and 74% BzOH conversion at 353 K, using ammonium molybdate as the catalyst and a PVDF microporous membrane (30 μm thickness, 0.9 μm pore radius, 0.55 overall porosity, 170 tortuosity).



Table 2.3. Empirical correlations for shell-side mass transfer in parallel flow for liquid-liquid systems in handmade, randomly-packed modules.

Author	Correlation	Conditions	OD/ID [μm]	Ref.
Dahuron and Cussler	$Sh = 8.8 \left(Re \frac{d_h}{l} \right) Sc^{1/3}$	Laminar flow $\phi = 0.15$	300/240	[41]
Prasad and Sirkar	$Sh = 5.85(1 - \phi) \left(\frac{d_h}{l} \right) Re^{0.60} Sc^{1/3}$	$0 < Re < 500$ $0.04 < \phi < 0.4$	290/240	[35]
Basu et al.	$Sh = 17.4(1 - \phi) \left(\frac{d_h}{l} \right) Re^{0.60} Sc^{1/3}$	$1 < Re < 100$ $0.25 < \phi < 0.48$	290/240 1,000/600 150/100	[42]
Gawronski et al.	$Sh = 0.09(1 - \phi) Re^{(0.8-0.16\phi)} Sc^{1/3}$	$0 < Re < 100$ $0.21 < \phi < 0.80$	650/350 1,032/1,000 630/300 1,000/600	[25]
Koo et al.	$Sh = 1.89 f(\phi) \left(\frac{d_h}{l} \right)^{1/3} Re^{1/3} Sc^{1/3}$ $f(\phi) = (0.42 + 0.90\phi) (1 - \phi)^{1/3}$	Laminar flow $0.05 < \phi < 0.45$	<i>Mathematical development based on previously published data</i>	[43]
Asimakopoulou et al.	$Sh = 1.615 (0.6 + 1.7\phi) \left(\frac{d_h}{l} \right)^{1/3} Re^{1/3} Sc^{1/3}$	$3 < Re < 78$ $0.05 < \phi < 0.45$	300/220	[44]

The ammonia removal from aqueous solutions using a polypropylene (PP) hollow fiber membrane contactor reactor (HFMCr) was studied by Ashrafizadeh and Khorasani [45]. They investigated the impact of various factors on ammonia removal, including the concentrations of ammonia and sulfuric acid solutions, the pH of the ammonia feed, the velocity of the feed streams, and the presence of excess ions in the ammonia feed solution. A membrane contactor from Liqui-Cel Company was used, with specifications of a 0.03 μm pore diameter, 0.40 porosity, and 0.60 packing fraction. The ammonia feed solution was pumped through the lumen of the HFMCr, while a dilute sulfuric acid solution, used as a stripping solution, was pumped into the module shell-side. Both solutions were recycled to their respective reservoirs. Since the reaction between NH_4OH and H_2SO_4 (Equation 2.9) is exothermic, a cooling water system was employed to maintain the temperature at 20°C. The ammonia in the raw solution decreased due to the reaction, forming ammonium salt in the acid solution. Under optimized conditions, ammonia removal exceeded 99%, demonstrating the effectiveness of PP-HFMCr for ammonia removal. Furthermore, higher pH values (up to 10) in the ammonia feed significantly improved ammonia removal. Increasing the ammonia feed velocity enhanced the overall mass transfer coefficient and, consequently, ammonia removal, while the velocity and concentration of the stripping solution had negligible effects on the process.



Agrahari et al. [46] explored the use of a HFMCr for liquid-liquid extraction, specifically for removing dissolved CO_2 from water. The membrane contactor utilized hydrophobic polypropylene (PP) microporous hollow fibers, with experiments conducted to assess CO_2 removal from the feed water passing through the fiber lumens. The dissolved CO_2 , present at concentrations ranging from 300 to 1200 ppm, was extracted using an aqueous diethanolamine solution flowing on the shell-side of the contactor. A mathematical model was developed to simulate the process, incorporating radial and axial diffusion of CO_2 in the lumen and its permeation through the membrane pores. This model was solved numerically using the alternate direction implicit technique to predict CO_2 concentration profiles and understand its transport behavior. The permeation coefficient of CO_2 through the hollow fiber membrane was consistent with literature values, and the experimental data revealed an average permeating flux of $3.7 \times 10^{-5} \text{ mol m}^{-2} \text{ s}^{-1}$. The HFMC performance, measured by CO_2 recovery, improved with decreasing feed flow rates,

although steady-state conditions took time to reach. The predictive model aligned well with the data, particularly at the adjusted permeation coefficient of $20 \times 10^{-9} \text{ mol m}^{-2} \text{ s}^{-1}$ for CO₂ through PP at 30°C.

In another study, Agrahari et al. [5] focused on removing dissolved succinic acid (SA) from aqueous streams using a polypropylene HFMCR and extractant solutions of tripropylamine (TPA) in 1-octanol. The HFMCR, was operated in the liquid-liquid extraction (LLE) mode with aqueous SA as the feed solution. The feed was prepared by dissolving SA in deionized water, with concentrations ranging from 5,000 to 59,000 ppm. Two organic extractant solutions were tested: one consisting of 30% TPA in 1-octanol and the other a mixture of 30% trioctylamine (TOA) and TPA in a 2:8 ratio, also dissolved in 1-octanol. The aqueous feed was circulated through the lumen of the hollow fibers, while the extractant solution flowed through the shell-side of the module, with both liquids moving counter-currently and being recirculated. Operating variables such as SA-water flow rate, organic phase flow rate, and initial SA concentration were varied. A complexation reaction between SA and the amine occurred at the aqueous–organic interface, with the complex diffusing through the membrane pores filled with the organic phase and being carried away by the organic liquid. The HFMC exhibited high efficiency, achieving removal efficiencies of over 95%, with some cases reaching 99%. Mathematical simulations of SA transport were conducted and showed good agreement with experimental results.

Zhu et al. [47] studied the production of glycolic acid via the carbonylation of formaldehyde using a high-temperature, high-pressure poly(tetrafluoroethylene) (PTFE) HFMCR for both batch and continuous synthesis. The results showed a significant improvement in glycolic acid yield with the membrane contactor system compared to a conventional stirred tank reactor. At a reaction temperature of 120 °C and pressure of 5.0 MPa, the glycolic acid yield reached over 90% after 1 hour, while it was only around 45% in the stirred tank reactor. This enhanced yield was attributed to the improved mass transfer and dispersion of CO within the membrane contactor system, which offered a larger gas-liquid contact area and shorter mass transfer distance. Additionally, the stability of the PTFE hollow fiber membranes was examined using techniques like Fourier transform infrared (FTIR) spectroscopy, scanning electron microscopy (SEM), liquid entry pressure (LEP), bubble point (BP), and contact angle (CA) measurements. These

characterizations showed that the PTFE membranes maintained excellent chemical and thermal stability under the experimental conditions. The study highlighted the potential of PTFE membrane contactors in the carbonylation of formaldehyde and similar gas-liquid reactions, providing a new approach for improving mass transfer and yield in such processes.

2.2. Biodiesel

The standard ASTM D6751 defines biodiesel as a mixture of mono-alkyl esters of long-chain fatty acids derived from renewable raw materials such as vegetable oils, animal fats, and microalgae oils [20,48,49,50]. Biodiesel is widely accepted in the energy market as a biofuel due to its physicochemical properties, which closely resemble those of conventional diesel fuel, making it a viable substitute for petroleum diesel [51,52,53]. These properties include a higher cetane number, the absence of sulfur, inherent lubricity, a higher flash point, and compatibility with both the existing fuel distribution infrastructure and current diesel automotive systems [20,19,54]. In addition to its role as a biofuel, biodiesel can be used as a feedstock for producing higher value-added chemical specialties. Derivatives such as free fatty acids (FFAs), fatty alcohols, sulfonated methyl esters, metallic soaps, and fatty amines and amides can be obtained from biodiesel. These oleochemicals play a crucial role in the manufacturing of a wide range of products, including surfactants, greases, lubricants, explosives, agrochemicals, pharmaceuticals, coatings, inks, solvents, adhesives, and more [55]. Almost all biodiesel produced industrially today is synthesized through the transesterification of triglycerides with a short-chain alcohol in the presence of a catalyst [54].

2.2.1. World and Brazilian Context

Global biodiesel production increased by 17.5% between 2021 and 2023, reaching 62.4 billion liters in 2023. Looking forward, demand is expected to grow by 41% between 2023 and 2028. The European Union is the largest producer, followed by the United States, Indonesia, and Brazil (Figure 2.5) [56,57].

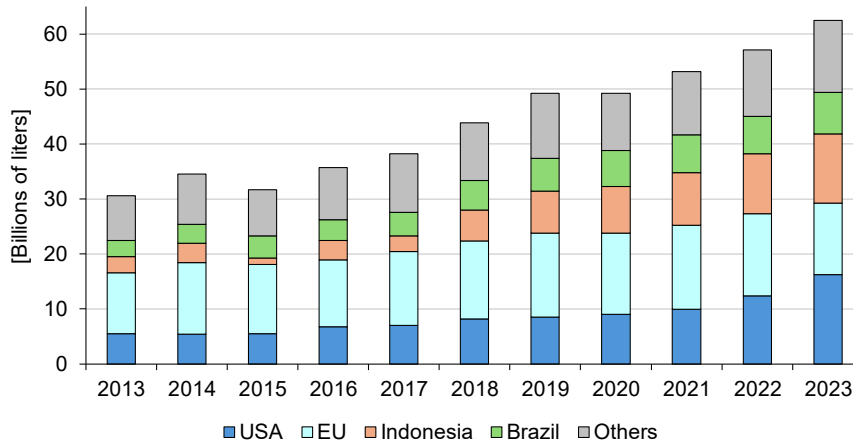


Figure 2.5. Biodiesel production 2013 - 2023

All major biodiesel-producing countries have implemented mandates to stimulate the industry. These policies are typically accompanied by additional incentives, such as tax credits and subsidies, to support biodiesel producers. Without such financial assistance, the industry remains unprofitable, even during periods of low feedstock prices (Irwin, 2017 in Naylor e Higgins) [58].

Brazil is the third-largest producer of biodiesel, generating 7.5 billion liters in 2023, which represents 12.1% of the world's total production. The use of biodiesel in Brazil is mandatory, and in January 2024, the CNPE (National Council for Energy Policy) increased the blending mandate from 12% (B12) to 14% (B14), effective March 1, 2024. Additionally, the CNPE decided to implement a B15 blending requirement starting in 2025, advancing the timeline from the originally planned 2026 [59].

Biodiesel constitutes a critical sector within Brazil's economy. Estimates indicate that by 2023, the industry sustained approximately 403,700 jobs, representing a substantial increase from the revised figure of 284,700 positions reported in the preceding year [60]. In 2024, Brazil reported 68 biodiesel plants across 15 states and all five regions of the country: 32 plants in the Center-West, 5 in the Northeast, 7 in the North, 8 in the Southeast, and 16 in the South. These plants have a total installed capacity of 14.6 billion liters per year, according to the National Agency of Petroleum, Natural Gas, and Biofuels (ANP) [61].

2.2.2. Feedstocks

2.2.2.1. Triglycerides

The primary raw material for biodiesel production is a source of long-chain fatty acids, found in high concentrations as glycerol esters (triglycerides - TG) in vegetable oils, animal fats, and microalgae oils [51]. Domestic oil crops are typically the main feedstock, although in regions like the European Union (EU) and Brazil, recycled vegetable oils and animal fats also make significant contributions to feedstock supplies [53,58].

In the biodiesel industry, vegetable oil feedstock accounts for approximately 77% of the total production cost, regardless of the technology used in the process [53,19,58,62,63]. The literature emphasizes the need to increase the use of cheaper feedstock alternatives, such as non-edible oil plants, waste vegetable oil, and animal fats. However, these low-cost feedstocks require additional pretreatment and product separation-purification steps due to higher levels of impurities, primarily free fatty acids (FFA) and water content, which ultimately increases the total manufacturing cost [63,19]. Similarly, microalgae oils are a promising feedstock due to their high growth rate, low freshwater requirements, high oil content compared to crops, and the lack of need for arable land. However, large-scale algal oil productivity remains quite low, making it impractical for industrial-scale oil production [64,65]. Table 2.4 summarizes the main feedstocks reported for biodiesel production.

In 2023, the global feedstocks for biodiesel production were primarily composed of edible oils, representing 61% of the total (Figure 2.6) [56]. The widespread use of edible oil crops has prompted socio-political discussions regarding food prices, food security, and indirect land-use changes (ILUC) [20,66]. These concerns have led to a substantial reduction in incentives for first-generation¹ biodiesel production, particularly in developed nations. In December 2018, the European Union adopted the revised Renewable Energy Directive (RED II), which imposed stricter limitations on high ILUC-risk biofuels, capping their usage and mandating a phased reduction by 2030. This marked a critical step in promoting more sustainable renewable energy sources within the European Union (EU) [67]. Similarly, Norway also prohibited the use of palm-based

¹Biofuels made from edible crops grown on arable land.

biodiesel due to the environmental and social costs associated with large-scale palm oil production, including deforestation, greenhouse gas emissions, and land conflicts [58].

Table 2.4. Oil feedstocks for biodiesel production [52,53,65]

Edible Oils	Non-edible oils	Microalgae	Other Sources
Soybean	Jatropha curcas	Spirulina platensis	WVO
Peanut	Pongamia glabra (Karanja)	Chlorella protothecoides	Animal fats
Rapeseed	Madhuca indica (Mahua)	Nannochloropsis oculata	Beef tallow
Palm	Salvadora oleoides (Pilu)	Phaeodactylum tricornutum	Poultry fat
Rice bran	Cottonseed	Scenedesmus dimorphus	Fish oil
Corn	Tobacco	Chlorella emersonii	
Coconut	Calophyllum inophyllum	Chlorella salina	
Olive	Eruca Sativa Gars	Chlorella vulgaris	
Safflower	Terebinth	Chlorella zofingiensis	
Castor	Rubber seed	Schizochytrium lima- cinum	
Linseed oil	Jjoba		
Canola	Neem		
Mustard	Eucalyptus		
	Polanga		

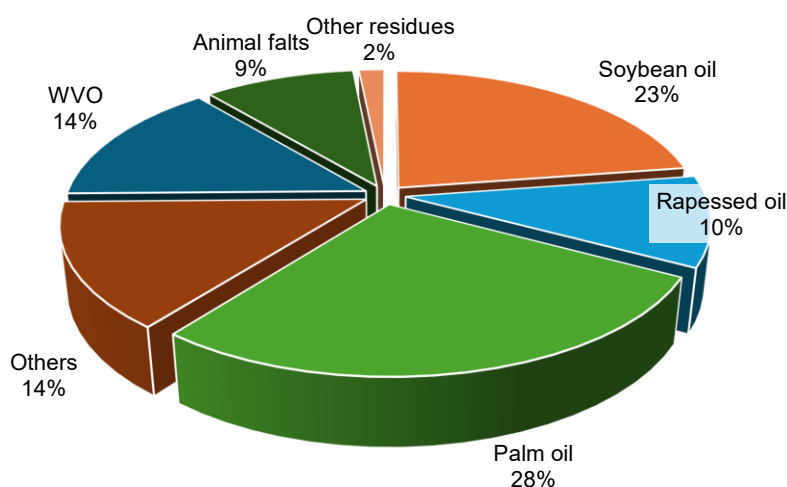


Figure 2.6. World oil feedstocks for biodiesel production

Nearly all biodiesel production in Brazil comes from soybean (69%) and animal fats (8%), with other feedstocks accounting for 19%. These include waste vegetable oils (WVOs), palm, sunflower, cottonseed, jatropha, babassu, and macaúba, among others [68,69].

2.2.2.2. Alcohol Short Carbon Chain

The transesterification of vegetable oils and animal fats is typically facilitated by primary or secondary monohydric aliphatic alcohols with 1-8 carbon atoms [70]. Although methanol and ethanol are the most commonly used, literature reports biodiesel production using higher molecular weight alcohols such as butanol, propanol, and isopropanol [70,71,72,73]. Industrially, nearly all biodiesel produced globally uses methanol as the alcohol feedstock, though the use of ethanol has seen an increase in recent years [74,75,20,63]. The use of methanol yields fatty acid methyl esters (FAME), while ethanol results in fatty acid ethyl esters (FAEE).

Ethanol, derived from renewable and locally sourced feedstocks, has lower toxicity and utilizes well-established production technologies [52]. However, the transesterification of vegetable oils and fats with ethanol proceeds at a slower rate compared to methanol, as the reactivity decreases with the increasing carbon chain length of the alcohol [75]. Additionally, ethanol tends to form more stable emulsions and gels, which significantly complicates the separation and purification stages of esters [76,51]. On the other hand, methanol is more cost-effective, and homogeneous catalysts are more soluble in methanol than in ethanol [70]. Furthermore, renewable methanol (bio-methanol) has been produced since 2015, using sustainable biomass or carbon dioxide and green hydrogen. For instance, the Canadian biochemical company Enerkem uses gasification technology to produce methanol from non-recyclable and non-compostable waste. They operate a facility in Alberta that converts 100,000 metric tons of bio-methanol annually. Additionally, the company is constructing a new plant in Varennes, Quebec, Canada, which will convert residual biomass and non-recyclable waste into 125 million liters of bio and circular methanol through gasification. To enhance the facility's performance, it will utilize hydrogen and oxygen from a co-located 90 MW electrolysis facility, projected to begin operation in 2026. Other projects under construction include the Ecoplanta in El Morell, Spain, which is expected to process 400,000 tons of non-recyclable waste annually and produce 240,000 tons of methanol by 2029 [77,78].

2.2.3. Main Variables in the Biodiesel Production

A review of the literature indicates that the yield of biodiesel, produced by the transesterification route, is influenced not only by the type of feedstock but also by several key factors. These include the process temperature, water content (moisture), FFA content (acidity), the alcohol-to-oil molar ratio, and the type and amount of catalyst used [51,54,55,79].

2.2.3.1. Temperature

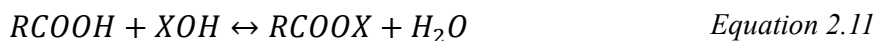
The temperature of the transesterification directly impacts the yield of biodiesel. Increasing the temperature accelerates the reaction, leading to a higher yield [80]. However, as the temperature rises further, side reactions, such as the hydrolysis of FAME to FFA and methanol, become more prevalent, which can ultimately reduce the biodiesel yield [52]. Industrially, the temperature is limited by the boiling point of the selected alcohol at the operating pressure. Higher temperatures may cause the alcohol to evaporate, increasing the risk of flammable vapors and potential intoxication from staff exposure.

Freedman et al. investigated the effect of temperature on the reaction rate by conducting tests at 32°C, 45°C, and 60°C, using NaOH as a catalyst and a methanol-to-oil ratio (MR) of 6:1. The results indicated that after 0.1 hours of reaction, the methyl ester content was 64%, 87%, and 94% at 32°C, 45°C, and 60°C, respectively. However, after one hour of reaction, the methyl ester content remained the same for the 60°C and 45°C tests, with a slight decrease observed at 32°C [81]. To minimize residence times in reaction equipment, the transesterification of fatty compounds is typically conducted at temperatures just below the boiling point of methanol, which represents the highest feasible temperature under atmospheric pressure conditions [82,55,63].

2.2.3.2. Water Content

Water can enter the reaction medium through the feedstock as moisture, be generated during the methoxide formation process (Equation 2.10), or result from the neutralization of free fatty acids with the alkaline catalyst (Equation 2.11) [63]. Even a small amount of

water, as little as 1 g kg⁻¹, can reduce the biodiesel yield, and the reaction is completely inhibited at 50 g kg⁻¹ [55,70,74].



Where: $X = Na$ or K

2.2.3.3. Free Fatty Acids Concentration (Acidity)

The raw materials used as triglyceride feedstock may contain varying concentrations of free fatty acids (FFAs), primarily produced by hydrolysis. In base-catalyzed transesterification, the FFAs are neutralized by the alkaline catalyst, forming soaps that reduce the concentration of available catalysts in the reaction system [83]. These soaps can also emulsify the glycerin-rich phase within the biodiesel-rich phase, leading to product loss and complicating the separation and purification processes, while increasing the pollutant load of byproduct glycerol [74,79]. Literature suggests that the feedstock should have an acid number lower than 1 mg KOH g⁻¹ and recommends that biodiesel should be as free from FFAs as possible, as they can cause corrosion and increase the melting point of the final product [63,72].

2.2.3.4. Catalyst

Catalysis for the transesterification reaction can be alkaline (homogeneous or heterogeneous), acidic (homogeneous or heterogeneous), or enzymatic. Homogeneous alkaline catalysts are preferred in the industry due to their faster reaction rates compared to acid-catalyzed processes, milder temperature and pressure conditions, lower alcohol-to-oil molar ratio, and relatively low costs [83,84]. The most commonly studied alkaline catalysts for transesterification are potassium and sodium alkoxides and hydroxides [74,79,83,85]. In industrial processes, potassium and sodium hydroxide dissolved in methanol are commonly used due to their lower cost and reduced corrosive effects, despite slightly lower catalytic activity. The amount of catalyst typically used ranges from 0.5 wt% to 1.0 wt% based on the mass of oil, achieving yields between 94% and 99% for methyl esters. However, using catalyst concentrations above 1.0wt% can complicate separation operations due to the formation of gels in the glycerol-rich phase [52,55,72,80].

Enzymatic processes, primarily carried out by lipases, are capable of catalyzing both esterification and transesterification reactions, offering advantages such as the ability to handle feedstocks with high FFA and moisture content. Furthermore, enzyme-based processes simplify purification since they do not require neutralization and washing steps. However, lipases are highly sensitive to alcohols, especially methanol, and can quickly lose their catalytic activity. To mitigate this, cosolvents are often added, or acetates are used in place of alcohols [86]. Additionally, the high cost, low yields, and long reaction times of current enzymatic processes limit their potential to replace conventional industrial methods [63,15,87].

2.2.3.5. Methanol-to-oil Molar Ratio (MR)

One of the key characteristics of transesterification reactions is their reversibility. As a result, large amounts of alcohol are required to shift the reaction in the forward direction [51,80,52]. As the methanol-to-oil molar ratio increases, the concentration of intermediate species decreases, leading to an enhanced production of FAME. However, an excessively high molar ratio can reduce the yield, as excess methanol can cause the emulsification of glycerol and FAME. This emulsification can drive the reaction backward, ultimately lowering the yield [52]. Ma e Hanna [79] established that the practical range for the methanol to oil molar ratio is between 3.3:1 and 5.25:1. Molar ratios greater than 5.25:1 do not improve the concentration of methyl esters. This is consistent with the work of other researchers who established that relationships higher than 6:1, do not increase production, but do hinder separation and purification stages [51,88].

2.2.4. Transesterification Reaction

The transesterification of a triglyceride (Figure 2.7) is the result of three consecutive and reversible reactions: the partial transesterification of the triglyceride (TG) to form the diglyceride (DG), the partial transesterification of the DG to form the monoglyceride (MG), and the partial transesterification of the MG to form glycerol (G) [72,80]. In each stage, a FAME molecule is formed. Since alcohol and triglycerides are immiscible under typical process conditions of temperature and pressure, it is necessary to promote contact between the phases. Mechanical mixing is commonly employed to enhance the interaction between the reactants, increasing the mass transfer rate and enabling the reaction to proceed according to intrinsic kinetics [82,89]. To avoid transport phenomena

from affecting the reaction time, the alcohol is dispersed throughout the oil as small droplets. The triglycerides in the oil then transfer across the interface with the alcohol droplets, where the reaction occurs. As the reaction progresses, the alcohol droplets become smaller, while the concentration of glycerol in the interphase increases. Since glycerol has low solubility in the oil and FAME mixture, it is almost entirely transferred to the alcoholic phase [80,90].

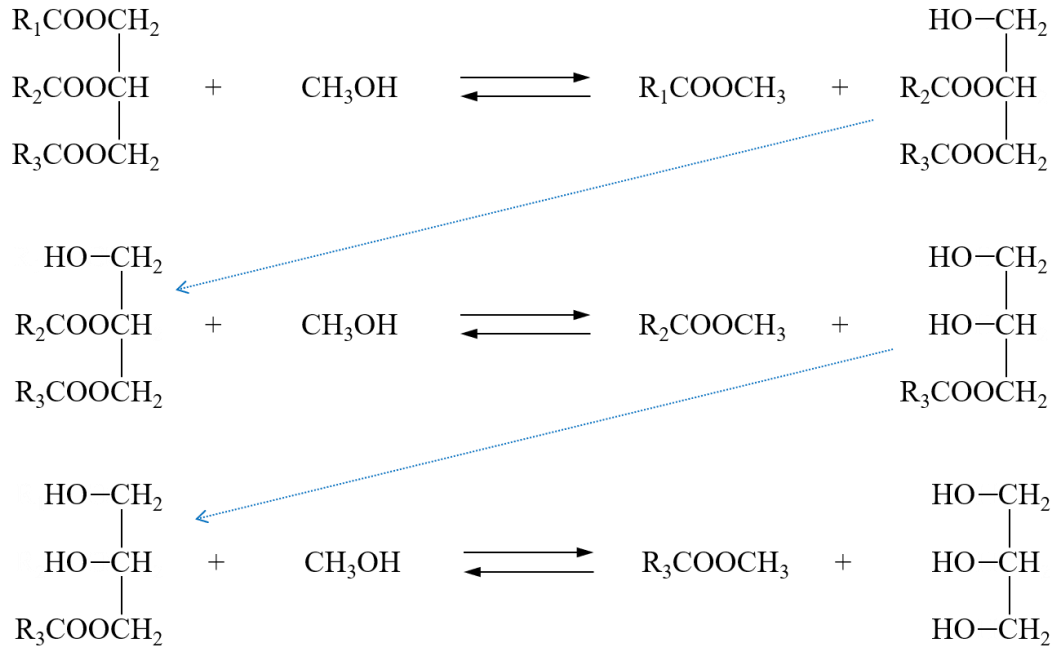


Figure 2.7. Transesterification of a triglyceride [72]

Typically, the concentration of TG and FAME as a function of time follows a sigmoidal curve (Figure 2.8). This pattern indicates a slow reaction at the beginning, which is mass transfer-controlled, followed by a sharp increase in the kinetically controlled region, and finally, a slow rate phase as chemical equilibrium is approached [82].

The kinetics of transesterification, represented in Figure 2.9, have been modeled by different authors as a differential molar balance, represented by six differential equations (Equation 2.12 to Equation 2.17), with six reaction rates (k_i) [80,82,88,91].

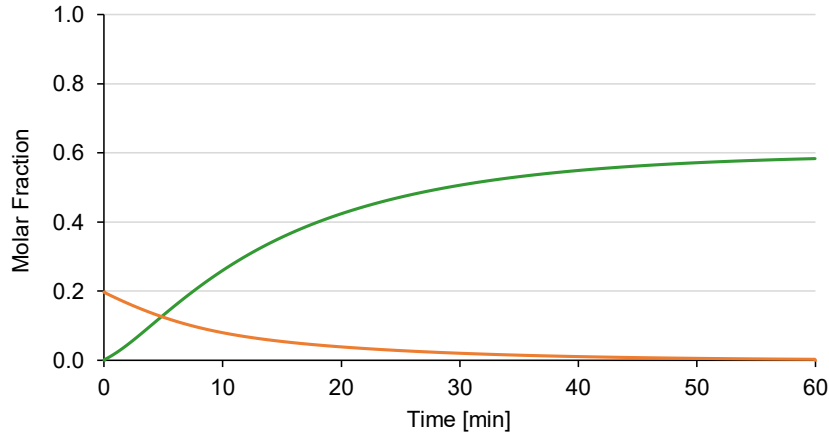


Figure 2.8. Typical concentration profiles for TG (orange) and FAME (green).
Batch transesterification of TG

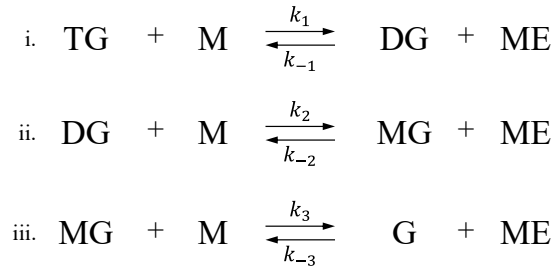


Figure 2.9. Schematic transesterification reaction of triglycerides. Triglyceride (TG); Methanol (M); Diglyceride (DG); Monoglyceride (MG); Glycerol (G); Fatty Acid Methyl Ester (ME)

$$\frac{d[\text{TG}]}{dt} = -k_1[\text{TG}][\text{M}] + k_{-1}[\text{DG}][\text{ME}] \quad \text{Equation 2.12}$$

$$\frac{d[\text{DG}]}{dt} = k_1[\text{TG}][\text{M}] - k_{-1}[\text{DG}][\text{ME}] - k_2[\text{DG}][\text{M}] + k_{-2}[\text{MG}][\text{ME}] \quad \text{Equation 2.13}$$

$$\frac{d[\text{MG}]}{dt} = k_2[\text{DG}][\text{M}] - k_{-2}[\text{MG}][\text{ME}] - k_3[\text{MG}][\text{M}] + k_{-3}[\text{G}][\text{ME}] \quad \text{Equation 2.14}$$

$$\begin{aligned} \frac{d[\text{ME}]}{dt} = & k_1[\text{TG}][\text{M}] - k_{-1}[\text{DG}][\text{ME}] + k_2[\text{DG}][\text{M}] - k_{-2}[\text{MG}][\text{ME}] \\ & + k_3[\text{MG}][\text{M}] - k_{-3}[\text{G}][\text{ME}] \end{aligned} \quad \text{Equation 2.15}$$

$$\frac{d[\text{G}]}{dt} = k_3[\text{MG}][\text{M}] + k_{-3}[\text{G}][\text{ME}] \quad \text{Equation 2.16}$$

$$\frac{d[\text{M}]}{dt} = \frac{-d[\text{ME}]}{dt} \quad \text{Equation 2.17}$$

Where, TG: triglycerides; DG: diglycerides; MG: monoglycerides; M: methanol and ME: FAME.

2.2.5. Current Status in Biodiesel Production Processes

2.2.5.1. Conventional Process

Most biodiesel plants operate using conventional homogeneous alkali-based transesterification technology [16]. The main stages of conventional industrial processes for biodiesel production are outlined in Figure 2.10. The process begins with mixing a catalyst with methanol in stirred tanks equipped with temperature control systems. A pre-treatment stage for the fatty compound may also be included to reduce the content of FFA and moisture. Common pre-treatment methods include chemical refining, physical refining, or an esterification stage for the FFA, aimed at minimizing product losses and reducing impurities upstream. Following this, the methanol/catalyst and pre-treated fatty compound streams are fed into a reactor and processed for approximately 1 hour at 60°C. Smaller plants typically use batch reactors, while continuous flow processes are recommended for plants with production capacities exceeding 4 million liters per year [74,92,93,94,17].

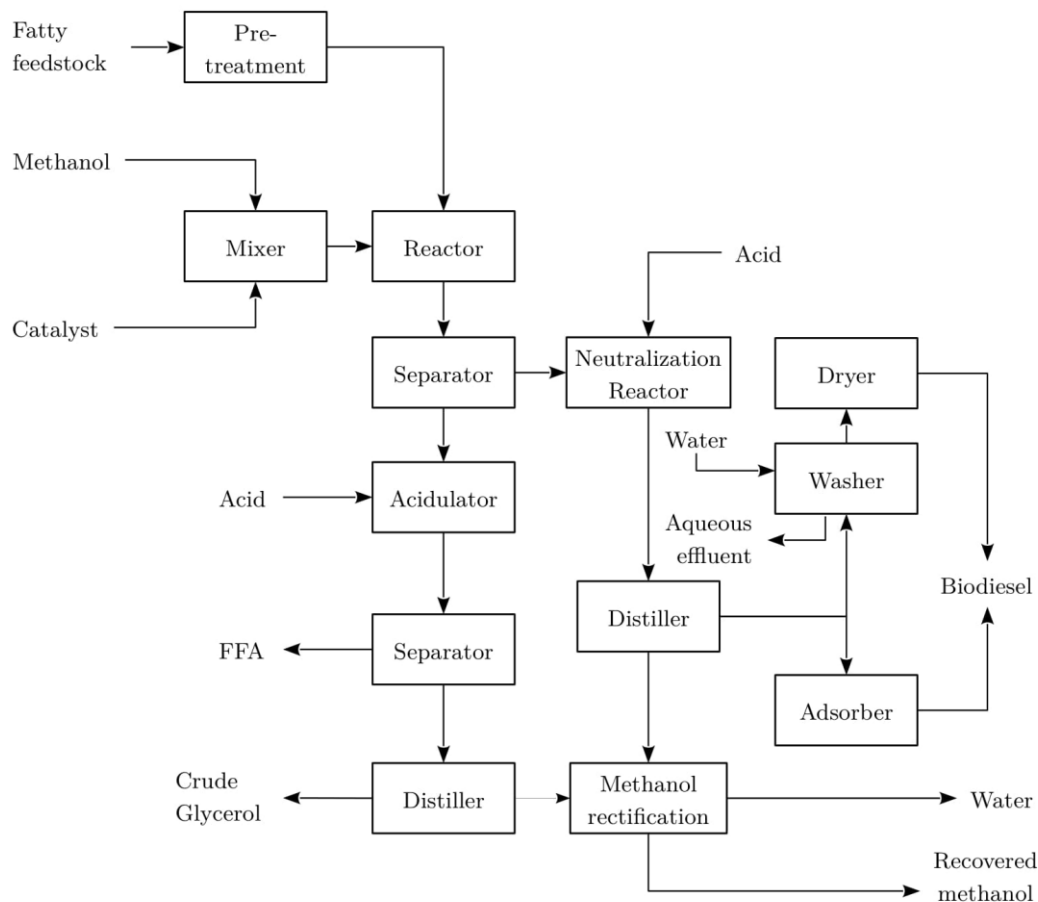


Figure 2.10. Conventional process flow diagram for biodiesel production

The reactor effluent mixture is sent to biphasic separators or centrifuges, where it separates into an alcoholic phase (rich in glycerol) and an oil phase (rich in biodiesel). Each phase is then directed to a catalyst neutralization stage before being distilled to remove excess methanol. The biodiesel-rich phase can be purified using either a wet or dry process. In the wet process, the biodiesel is washed with pure or slightly acidic water to remove salts, soaps, and other polar impurities. The resulting aqueous phase, a byproduct of the washing, is sent to effluent treatment, while the organic phase (rich in biodiesel) is dried.

In the dry purification process, adsorbents are used to capture neutralized catalysts, soaps, glycerol, MG, DG. Commonly used adsorbents in this process include Magnesol®, TriSyl®, Siliporite®, Tonsil®, and Sorbead®, among others. Similarly, ion-exchange resins such as Purolite® PD206, Amberlite™ BD10Dry, Lewatit® GF 202, Thermax Tulsion®, and DudaLite® DW-R10 are also employed to efficiently remove these impurities. At the end of the process, purified biodiesel and solid waste are obtained. This solid waste typically contains between 0.5 wt% and 2 wt% biodiesel and must be handled appropriately [80,95,96]. All these processes ensure the quality of biodiesel in compliance with national specifications set by ANP Resolution No. 920/2023 [97], as well as international standards ASTM D6751 [50] and EN 14214 [98], which are summarized in Table 2.5.

Table 2.5. National and international limits for common biodiesel impurities

Impurities	ANP N° 920/2023	ASTM D6751	EN 14214
Water, max [mg/kg]	200	-	500
Methanol/Ethanol, max [%wt]	0.20	0.2	0.20
Total glycerol, max [%wt]	0.20	0.240	0.25
Free glycerol, max [%wt]	0.02	0.020	0.02
Diglycerides, max [%wt]	0.20	-	0.20
Monoglycerides, max [%wt]	0.50	0.40	0.70
Triglycerides, max [%wt]	0.20	-	0.20

Current industrial biodiesel production processes face several challenges, which have been the focus of research in recent years [15,16,17,18]. These challenges are primarily based on the following five factors:

- i. High cost of biodiesel: The high cost of biodiesel remains a significant barrier to commercialization, especially when compared to petroleum-based diesel fuel. Feedstock costs, mainly vegetable oil, account for 70–85% of total biodiesel production costs. Therefore, biodiesel industrial processes must be optimized to process cheaper, lower-quality feedstocks.
- ii. Incomplete conversion and yield: Since transesterification is a reversible reaction, achieving complete conversion and high yield in a single-step process is challenging. Multiple reaction-separation stages are necessary, including glycerol removal, to improve overall efficiency.
- iii. Formation of soaps and gels: The use of an alkaline catalyst can lead to the formation of soaps and gels during the reaction, which hinders the separation and purification stages, complicating the overall process.
- iv. The immiscibility of vegetable oils and methanol: Due to the immiscibility of oils and methanol, it is essential to disperse the alcoholic phase in the oil phase to reduce mass transfer limitations and improve reaction kinetics.
- v. Environmental impact: Environmental concerns are significant in current biodiesel production processes. The wet purification method consumes large amounts of water (approximately 20 kg of water per ton of biodiesel) for washing, generating substantial effluent that requires treatment. Similarly, dry purification produces solid waste contaminated with soaps, catalysts, and biodiesel, which must also be properly handled.

2.2.5.2. Intensified Processes

Process intensification, as defined by Stankiewicz et al., refers to any chemical engineering advancement that results in significantly smaller, cleaner, and more energy-efficient technologies. These improvements focus on two key areas: equipment—such as novel reactors and heat and mass transfer devices—and methods, including the integration of reaction and separation stages, membrane processes, alternative energy sources, and advanced process control techniques [16,2].

Extensive research, particularly in process intensification, has been dedicated to enhancing biodiesel production processes by optimizing the reaction stage and improving the efficiency of the separation and purification steps. Non-conventional reactors, including static mixers, ultrasonic, microwave, hydrodynamic cavitation, rotary, falling film, and microreactors, as well as advanced technologies like plasma and supercritical processes, have been explored as alternatives to traditional stirred reactors. These approaches aim to reduce reaction time, enhance reagent mixing with lower energy consumption, and minimize catalyst usage [15,99,100,101,102,103,104].

For the separation and purification stages, membrane processes have emerged as a prominent alternative. Studies on micro and ultrafiltration for biodiesel/glycerol separation indicate that the final product can meet required quality standards with reduced energy consumption and environmental impact due to less water use and decreased solid waste generation [99,105,106,23].

Additionally, simultaneous reaction/separation processes, such as reactive distillation, reactive extraction, and membrane reactors, have been investigated to further optimize biodiesel production. These intensified processes combine reaction and separation stages within a single unit, boosting overall productivity by reducing equipment size, energy consumption, and processing time while easing the load on downstream separation units [15,99,105,107,22,108]. A summary of some intensified processes is provided in Table 2.6, excluding membrane processes, which are discussed separately.

2.3. Membrane Processes in Biodiesel Production

In recent years, the application of membrane technology in biodiesel production has attracted significant attention. Membrane separators are increasingly being employed to purify the biodiesel-rich phase stream, offering a promising alternative to conventional wet and dry purification methods. Additionally, the use of membrane reactors facilitates the simultaneous reaction and separation within a single unit, allowing for the continuous removal of products, which shifts the chemical equilibrium and results in higher yields. The literature emphasizes the potential of membrane processes to produce biodiesel of high purity and quality through highly selective separation techniques [15,17,18,105,107,109]. Figure 2.11 illustrates the operational diagrams for these two primary applications of membrane technology.

Table 2.6 Selected intensified processes for biodiesel production

Intensified process	Catalyst Type	Catalyst Load wt%	MR	Temperature [°C]	Special Conditions	Yield	Ref.
Microchannel reactors	NaOH, KOH, H ₂ SO ₄	0.6 – 4.5	6:1 – 12:1	55 – 70	Use of WVO 30 min.	Max. 98% Min. 89%	[110,111]
Ultrasound reactors	Homogeneous base	0.5 – 2.0	2:1 – 12:1	20 – 60	1 – 50 min 20 - 611 kHz	Max. 99% Min. 89%	[112]
	Heterogeneous base	1 – 10	4:1 – 16:1	60 – 75	15 – 120 min 20 – 40 kHz	Max. 98% Min. 80%	[113]
	Heterogeneous acid	2.9 – 30	16:1 – 25:1	-	15 – 40 min 20 – 37 kHz	Max. 98% Min. 84%	[114]
Microwave reactors	Heterogeneous - SrO	1.85	6:1	80	40 – 180 s	Max. 99% Min. 93%	[115]
Reactive extraction	Supercritical fluids	-	-	175 – 325	2.3 – 30 MPa 5 min. - 8 h	Max. 100% Min. 51%	[116]
Reactive distillation	Heterogeneous base	1.0 - 1.5	4:1 – 9:1	65 – 78	3 - 6 min	Max. 99%	[15]
	Heterogeneous acid		67.9:1	30 – 65		Min. 94%	[117]
Centrifugal contact separator (CCS)	Sodium methoxide	1.1	6:1	60 – 75	30 min	Max. 96%	[16]
Oil reactive extraction	Lipase			200 – 300	Needs solvent 45 – 80 min	Max. 99.9% Min. 86.1%	[15]
Hydrodynamic and Ultrasonic cavitation reactors	NaOH, KOH	1	6:1	60	Use WVO 5 – 30 s	Max. 99% Min. 98%	[118,119]
Falling film liquid reactor	NaOH	1	8:1 – 10:1	60	5 min	Max. 97.2%	[95,120]

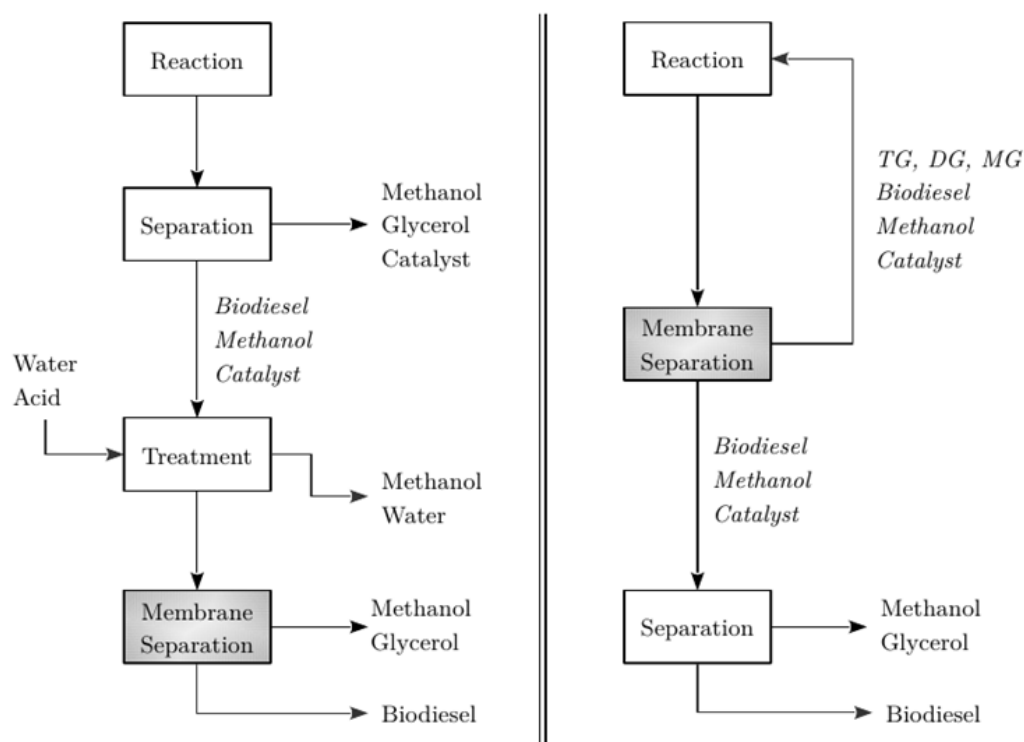


Figure 2.11. Membrane processes in the production of biodiesel
Separation stage (left), reaction/separation stage (right)

2.3.1. Membrane Separators

Membrane separators used in purification stages are extensively reported in the literature. In this setup, the stream exiting the first separation stage undergoes additional processing before entering the membrane separator. This pre-treatment may include adding water to enhance glycerol separation or acid to neutralize the mixture, aiding in the removal of residual catalysts, as sodium salts are insoluble in biodiesel [17,18,105,109].

Wang et al. [121] evaluated the refining of crude biodiesel from palm oil using ceramic microfiltration (MF) membranes. The study investigated pore sizes of 0.6, 0.2, and 0.1 μm , with transmembrane pressures (TMP) ranging from 0.5 to 2.0 bar and temperatures between 30°C and 70°C. The best results were achieved using a 0.1 μm pore size membrane, operating at 1.5 bar and 60°C. In this test, the membrane flux was maintained at 300 $\text{L m}^{-2} \text{h}^{-1}$, with a retentate-to-permeate volume ratio of 4:1. The residual glycerol in the permeate, estimated by water extraction, was 0.0108 wt.%, demonstrating the process's ability to effectively remove free glycerol from the product stream.

Gomes et al. [23] investigated the efficiency of biodiesel-glycerol separation from a mixture using batch microfiltration (MF) modules in a tangential filtration configuration. The experiments utilized a tubular ceramic membrane ($\alpha\text{Al}_2\text{O}_3/\text{TiO}_2$) with average pore sizes of 0.2, 0.4, and 0.8 μm , and a filtration area of $5.0 \times 10^{-3} \text{ m}^2$. The feed mixture consisted of 80% biodiesel, 10% glycerol, and 10% anhydrous ethanol, processed at 60°C under pressures of 1.0, 2.0, and 3.0 bar. The study evaluated the membrane's ability to retain glycerol and the permeate flux. The best performance was observed with the 0.2 μm pore size membrane at 2.0 bar. Subsequently, the influence of ethanol concentration in the feed was assessed, achieving glycerol retention of 99.6% with a 5% ethanol solution.

Biodiesel from canola oil and methanol was purified by Saleh et al. [122] using ultrafiltration (UF) membranes. Their study focused on the effects of methanol, soaps, and water on the final glycerol separation stage. A modified polyacrylonitrile (PAN) membrane with a molecular weight cut-off (MWCO) of 100 kDa was used in all experiments, operating at 25°C and 5.52 bar. The results highlighted the significant impact of water concentration on glycerol removal. The authors proposed a mechanism for free glycerol separation involving the removal of ultrafine glycerol droplets present in crude biodiesel. As water concentration increased, the size of the glycerol droplets also grew. Optimal results were obtained using 2.0 g of water per liter of biodiesel (0.225 wt.%).

Othman et al. [123] explored the potential of solvent-resistant ultrafiltration polymer (SRUF) membranes in the biodiesel purification process. They evaluated eight commercial membranes: Solsep 030705, Solsep 030306F, Starmem 240, and Starmem 120 (polyimide type); Desal-DL and Desal-DK (polyamide type); and MPF-34 and MPF-44 (polydimethylsiloxane, PDMS type). These membranes were chosen for their ability to separate methyl esters from mixtures containing homogeneous basic catalysts, free glycerol, and methanol. The tests were conducted using membranes with an active area of $1.52 \times 10^{-3} \text{ m}^2$, transmembrane pressures (TMP) between 6.0 and 30.0 bar, and a temperature of 40°C. The composition of the streams was analyzed by gas chromatography, and membrane morphology changes were examined using scanning electron microscopy (SEM) and Fourier transform infrared spectroscopy (FTIR). The best separation performance and chemical resistance were observed with the Solsep 030705

membrane, operating at 10.0 bar. This membrane demonstrated high rejection rates for triglycerides (99.80%), diglycerides (97.16%), monoglycerides (40.65%), free glycerol (75.24%), methanol (74.98%), and methyl esters (25.37%). The PDMS and polyamide membranes exhibited structural damage that adversely affected their permeation performance.

Ultrafiltration (UF) membranes for pre-treated palm biodiesel purification were studied by Atadashi et al. (Atadashi 2012). The membrane used was a tubular multi-channel type made of $\text{Al}_2\text{O}_3/\text{TiO}_2$ with a pore size of 0.02 μm . The pre-treatment involved methanol distillation, followed by the addition of acidified water to neutralize the catalyst (KOH). The separator operated with an effective membrane area of $3.1 \times 10^{-2} \text{ m}^2$, at transmembrane pressures (TMP) ranging from 1 to 3 bar, temperatures between 30°C and 50°C, and feed flow rates from 60 to 150 L min^{-1} . The best results reduced the glycerol and potassium concentrations to 0.007 wt.% and 0.297 mg L^{-1} , respectively, both below the limits specified in ASTM D6751 (see Table 2.5). These results were achieved with the system operating at 2 bar, 40°C, and a feed flow of 150 L min^{-1} , corresponding to a permeate flow of 9.08 $\text{kg m}^{-2} \text{ h}^{-1}$.

Alves et al. [124] evaluated microfiltration (MF) and ultrafiltration (UF) for the purification of crude biodiesel produced from soybean oil and methanol, using KOH as a catalyst. The output stream was first distilled to remove light components (methanol and water) and then allowed to separate in a decanter for 12 hours. The biodiesel-rich phase was subsequently treated using MF cellulose ester membranes with pore sizes of 0.22 and 0.30 μm , and UF polyethersulfone (PES) membranes with molecular weight cut-offs (MWCO) of 10 and 30 kDa. Operating pressures were set at 1–2 bar for microfiltration and 4 bar for ultrafiltration. The results showed that the 10 kDa PES membrane reduced the glycerol concentration in the refined biodiesel to less than 0.02% while operating at a flux of 55 $\text{kg m}^{-2} \text{ h}^{-1}$. Additional tests revealed that increasing the water content improved glycerol separation efficiency.

Bello et al. [107] evaluated the use of poly(ether sulfone) (PES) hollow fiber membranes for biodiesel production in a liquid-liquid film reactor integrated with membranes (LLFRM). This device combines the advantages of both technologies: the high productivity of the liquid-liquid film reactor (LLFR) and the continuous removal of products through the hollow fiber membranes. The intensified process was assessed to

address challenges associated with limitations in chemical equilibrium. The LLFRM effectively selectively removed the glycerol-methanol mixture. The maximum conversion and yield in the reactor were 85% and 63%, respectively, using a reaction-separation zone of 30% (Membrane Length / Maximum Length) at a methanol-to-oil molar ratio of 9:1.

Biodiesel and glycerol-rich phase separation was experimentally assessed using poly(ether sulfone) hollow fiber membranes (PES-HFM) by Noriega et al. [125]. Biodiesel was produced through an alkali-catalyzed transesterification reaction in a bench-scale system. The study investigated the effects of pressure difference, feed composition, and biodiesel-rich phase mass fraction on permeability and permeate composition. A mathematical model, based on the Hagen–Poiseuille transport equation for ultrafiltration, was proposed, correlated, and experimentally validated. Experimental results showed that only the glycerol-rich phase permeated through the membrane, following liquid-liquid equilibrium (LLE). The highest permeability ($33.2 \text{ kg bar}^{-1} \text{ h}^{-1} \text{ m}^{-2}$) occurred at 66% methanol content, with an 18:1 methanol-to-oil molar ratio. The model accurately predicted flux changes with temperature and methanol content.

2.3.2. Membranes Reactors

The use of membrane reactors in biodiesel production enables simultaneous reaction and product separation, resulting in higher yields while reducing the number and volume of upstream separation stages. The process operates as a closed-loop system, where reagents are first introduced into a conventional reactor and then directed to the membrane separator. Methyl esters, glycerol, and the majority of the methanol permeate through the membrane, while unreacted triglycerides (TG), diglycerides (DG), and monoglycerides (MG) are retained within the system and recirculated back into the reactor. The permeate stream is then subjected to separation and purification operations to produce biodiesel that meets quality specifications.

Dubé et al. [126] investigated the production of biodiesel from canola oil and methanol in a reactor equipped with membranes. The study was conducted in two phases. The first phase examined the impact of temperature and acid catalyst concentration on conversion rates, while the second phase focused on the influence of the methanol-catalyst mixture flow rate on the same variable. The experiments were performed in a semi-batch operation, with the reactor initially charged with 100g of oil, followed by the controlled

feeding of the methanol-catalyst mixture at a specified flow rate. A microfiltration carbon membrane (0.05 μm pore size) was used for the separation stage at a transmembrane pressure (TMP) of 1.38 bar. The temperatures were varied at 60°C, 65°C, and 70°C, with acid catalyst concentrations of 0.5, 2.0, 4.0, and 6.0 wt.%. The methanol-catalyst mixture flow rates were 2.5, 3.2, and 6.1 ml min^{-1} , with a 1 wt.% catalyst concentration, using both H_2SO_4 and NaOH as catalysts. The optimal results were achieved with basic catalysis, showing a 96% conversion at a methanol-catalyst mixture flow rate of 3.2 ml min^{-1} and 65°C. However, the authors noted a reduction in the concentration of FAME in the permeate as the reaction progressed, due to the depletion of triglycerides in the reactive mixture.

Biodiesel production in a semi-continuous reactor coupled with a membrane-based separation system was studied by Cao et al. [127]. Various triglyceride sources were tested, including soybean oil, canola oil, a 25:75 mixture of hydrogenated/refined palm oil and bleached and deodorized palm oil (HPO/RBDPO), used cooking oil (10 wt.% free fatty acids, FFA), and fats recovered from effluents (17 wt.% FFA). The transesterification process was carried out for 1 hour at 65°C, using a methanol-to-oil molar ratio of 23.9:1. NaOH, at a concentration of 0.5 wt.%, was used as the catalyst, while feedstocks containing FFA were neutralized with the same base. A titanium oxide (alumina-free) multi-channel tubular ultrafiltration (UF) membrane with a 300 kDa molecular weight cut-off was employed at 0.4 bar and a reactive mixture flow rate of 19.2 g min^{-1} . The results demonstrated that the levels of free glycerol and total glycerol were below the ASTM D6751 requirements (see Table 2.5) when canola oil, soybean oil, and palm oil were used. Furthermore, all triglyceride sources achieved 100% conversion, and the resulting product was free of monoglycerides (MG).

Biodiesel production from soybean and ethanol using a membrane contactor reactor (MCR) was studied by Maia Filho et al. [128]. The transesterification process was conducted in a flat-sheet membrane contactor, with compartments of 0.4 L separated by a microporous membrane. The reaction took place in one of the compartments, while the other was used for the extracting phase. Both compartments were stirred and heated to the desired reaction temperature. The study investigated the effects of membrane hydrophobicity, catalyst type, temperature, and extractant on conversion and glycerol removal capacity. Nylon (hydrophilic) and PTFE (hydrophobic) microporous membranes

with a pore size of 0.22 μm and a thickness of 150 μm were tested. Ion-exchange resins were used as catalysts, including cationic (AmberlystTM A15) and anionic (AmberlystTM A26 and AmberliteTM IRA 410) types. The reaction temperature was varied from 298 to 343 K, catalyst loading from 1.0 to 10.0 wt.%, and the ethanol-to-soybean molar ratio from 6:1 to 9:1. Water and ethanol were used as the extraction phase. The mass transfer coefficients of the reactive mixture were estimated using a synthetic reaction medium with different extraction phases. The results showed that triglyceride conversion increased by 18% when AmberlystTM A26 (an anionic resin) was used with ethanol as the extracting phase. A simplified mass transfer model was developed and applied to simulate the coupled system. The simulated results indicated that a membrane area-to-reactor volume ratio of 2.2 cm^2/cm^3 resulted in a 97.3% reduction in glycerol content in the medium. These findings highlighted the potential of coupling transesterification with a membrane contactor to shift the reaction equilibrium and reduce the purification steps of the biodiesel production process.

2.3.3. Catalytic Membranes Reactors

The use of catalytic membranes in biodiesel production aims to combine the advantages of membrane reactor processes while overcoming the challenges associated with the use of homogeneous catalysts, particularly those related to free fatty acid (FFA) and water content in the oil feedstock. This approach offers a more efficient and sustainable method by addressing the limitations of traditional catalytic systems.

Guerreiro et al. [129] studied the catalytic activity and yield of the transesterification reaction in a membrane reactor. The researchers used an active membrane made of polyvinyl alcohol (PVA) with hydrotalcite (HT) dispersed in the polymeric matrix. The catalytic activity was evaluated by modifying the membrane's hydrophilic properties in seven samples, which were treated with varying proportions of acetic acid and succinic anhydride. The reaction was carried out at 60°C in a reactor equipped with magnetic stirring, using soybean oil and methanol (molar ratio 1:283) as feedstocks. The results showed that the HT-supported membrane exhibited catalytic activity 20 times higher than the unsupported HT. Moreover, after seven runs, the supported HT membrane still maintained three times the catalytic activity of the unsupported one. Additionally, an increase in the membrane's hydrophilicity led to an increase in catalytic activity, but a decrease in the process yield. Conversely, reducing the hydrophilicity improved the

membrane's reaction performance. The best results were obtained with the untreated PVA membrane, which achieved yields greater than 90%, although its catalytic activity was about nine times lower than that of the more hydrophobic membrane.

Production of palm biodiesel in a tubular reactor with microporous TiO₂/Al₂O₃ membranes was evaluated by Baroutian et al. [130]. The membrane, packed with potassium hydroxide supported on palm shell activated carbon, had an active area of $2.01 \times 10^{-2} \text{ m}^2$ and a pore size of 0.05 μm . All experiments were conducted with a transmembrane pressure (TMP) of 1 bar. The study examined the effects of temperature (50–70°C), catalyst amount (37.5–250.0 mg cm^{-3}), and cross-flow velocities (0.179–0.212 cm s^{-1}) on conversion rates. The highest conversion of palm oil was 94%, achieved at 70°C, with a catalyst concentration of 157.04 g cm^{-3} (catalyst per unit volume of the reactor) and a cross-flow velocity of 0.21 cm s^{-1} . The biodiesel produced met the requirements of the ASTM D6751 standard, without the need for washing or additional purification stages.

Xu et al. [131] studied another type of reactor with catalytically active membranes, evaluating the effects of temperature, catalyst amount, and flow rate on the transesterification of soybean oil. The membrane used was a tubular microfiltration ceramic membrane packed with paratoluenesulphonic acid (PTSA) supported on MCM-41. The study assessed the impact of temperature (60–80°C), catalyst amount (0.09 and 0.27 g ml^{-1}), and flow rate (2.8–4.8 ml min^{-1}), with a transmembrane pressure (TMP) of 0.8 bar and a methanol-to-oil molar ratio (MR) of 24:1. The optimal operating conditions were found to be 80°C, 0.27 g ml^{-1} of catalyst per unit reactor volume, and a flow rate of 4.15 ml min^{-1} , achieving a reaction efficiency of 84.1%.

To summarize, the state-of-the-art overview highlights key research opportunities in biodiesel production, particularly focusing on process intensification and the use of alternative low-cost fatty feedstocks. These opportunities point to equipment that can shift chemical equilibrium by simultaneously separating products with lower energy consumption. It emphasizes the need for non-dispersive phase contact to prevent emulsions, which complicate separation stages. Additionally, opportunities exist in developing cost-effective processes that purify fatty feedstocks before they enter the reaction stage. The state-of-the-art also underscores the features of Membrane Contactor Reactors (MCRs), including their ability to facilitate simultaneous separation and reaction

while maintaining independent flows for each phase. These characteristics position MCRs as a promising alternative for continuous biodiesel production.

2.4. Concluding Remarks

This chapter has reviewed the literature on membrane contactors, focusing on their key characteristics, advantages, and disadvantages, as well as some empirical models for mass transfer phenomena. It also explored the application of hollow fiber membrane contactor reactors (HFMCRs) in liquid-liquid reactions, highlighting their potential as effective alternatives to conventional stirred reactors. By leveraging the ability of HFMCRs to maintain independent phase flows, these devices show promising potential for facilitating the simultaneous separation and reaction through reactive extraction, offering opportunities to improve processes limited by chemical equilibria, such as esterification and transesterification.

The review also explores the latest advancements in biodiesel production, with a particular focus on the increasing interest in process intensification over the past two decades. While membrane processes have predominantly been investigated for separation and purification in biodiesel technologies, there is considerable potential for further research into integrating both reaction and separation stages within a single device. Despite a decline in recent publications on biodiesel technologies, driven by the growing interest in green diesel from vegetable oil hydrotreating, biodiesel's industrial development remains highly relevant, especially in Brazil, where production is projected to rise in the coming years.

In this context, HFMCRs present a promising technology for biodiesel production. Their operational characteristics could enhance the process by shifting chemical equilibrium through reactive extraction. The non-dispersive contact within the system also helps prevent emulsion formation, simplifying the separation stages. These features position MCRs as an attractive alternative for continuous biodiesel production, offering opportunities to develop more cost-effective processes.

Chapter 3 - Design and Construction of the Reaction System

The objective of the reaction system is to produce FAME, or biodiesel, from refined soybean oil transesterification with methanol, using sodium hydroxide as a catalyst in a laboratory-scale hollow fiber membrane contactor reactor (HFMCr). The system is composed of two main components: the hollow fiber membrane module (HFM) and peripheral equipment. This chapter outlines the design of the laboratory-scale reaction system developed to evaluate FAME production within the reactor. The design process included defining the hollow fiber module parameters, selecting appropriate materials, and fabricating the HFM. The construction was necessary because commercial modules lacked sufficient chemical resistance, particularly to methanol and sodium hydroxide. Additionally, the key process variables—such as oil flow rate, methanol-to-oil molar ratio, and packing fraction—were defined. Peripheral equipment, including pumps, heating devices, and control systems, was also specified.

3.1. Methodology

The design considerations mark the starting point for the development of the reaction system. The operational ranges for key parameters, including soybean oil flow rate (OFR), methanol-to-oil molar ratio (MR), packing fraction (PF), catalyst proportion, and process temperature, were determined through a combination of literature review and the prior experience of the author.

To select suitable materials for the module construction (housing, membranes, and potting), a literature review was conducted to identify materials with high chemical resistance to methanol, soybean oil, and caustic environments, while also considering their commercial availability. Based on the findings, selected materials for the membranes and potting were tested for chemical resistance to biodiesel and a mixture of methanol

and sodium hydroxide (NaOH). The tests were performed following the ASTM D543-14 standard.

With these parameters established, a Plug Flow Reactor (PFR) model was developed and solved to determine the flow configuration, either cocurrent or countercurrent. The reactor length was deliberately designed to prevent complete conversion, thus ensuring no interference with the analysis of key variables in the study. If conversion and yield within the reactor were to reach 100%, critical data regarding mass transfer effects could be compromised, hindering the accurate evaluation of these phenomena.

Finally, the hollow fiber contactor was successfully assembled and tested for leaks, utilizing the extensive expertise of the Membrane Process Laboratory (PAM/COPPE/UFRJ) in manually assembling hollow fiber membrane modules. Additional equipment was integrated to complete the laboratory-scale system, ensuring that operational variables stayed within the specified parameters. This included components such as pumps, a heating system, and control systems. A datasheet documenting the module construction and a process flow diagram (PFD) were also developed.

3.2. Design Considerations

The reaction system was designed for laboratory-scale operation to minimize chemical residue generation during experiments. Accordingly, the soybean oil flow rate (OFR) was set between 0.4 and 0.8 L h⁻¹, while the methanol-to-oil molar ratio (MR) was established between 4:1 and 9:1. This MR range was selected based on studies identifying an optimal ratio around 6:1 [79,51,88]. The lower MR value exceeds the stoichiometric requirement to ensure sufficient methanol availability as the extractant for glycerol. The packing fraction (PF) was set between 10% and 30%, with the upper value based on commercial hollow fiber membrane modules with similar fiber diameters. Sodium hydroxide was employed as the catalyst, with a concentration of 0.75 wt% relative to the weight of soybean oil maintained across all experiments.[132,107]. To minimize safety and health risks associated with methanol handling, particularly evaporation, the system operated at 55°C [133].

3.3. Hollow Fiber Membrane Module: Materials Selection

3.3.1. Literature Review

As outlined in Section 2.1.2.1, a hollow fiber membrane (HFM) module consists of three main components: the housing, the hollow fiber membrane bundle, and the potting. To ensure the appropriate selection of materials for each component, chemical resistance charts from various suppliers of materials commonly used in membrane fabrication, industrial pipelines, and commercial resins were reviewed. A list of potential materials was compiled based on their resistance to methanol, soybean oil, and NaOH solutions, as well as their commercial availability in Brazil. The findings of this review are summarized in Table 3.1.

Table 3.1. Material selection for membrane contactor: Chemical resistance chart

Material	Housing	Membrane	Potting	Chemical Resistance			References
				Methanol	NaOH	Soybean Oil	
Stainless Steel 316	X			A	B	A	[134,135]
PTFE	X	X		A	A	A	[136,137,138]
PP	X	X		A	A	A	[137,139]
Nylon	X	X		A	A	A	[140,138]
HDPE / LDPE		X		A	A	B	[141,137]
PVDF		X		A	B	A	[142,143,138]
PES		X		A	A	A	[144,138]
Polyester resin			X	A	A	A	[145,146]

A - Excellent; B – Good

3.3.2. Chemical Resistance Test

The selection of membrane and potting materials was an additional step to ensure chemical resistance and prevent any morphological changes that could affect the experimental stage. This was particularly important given the variability in the properties of commercial polymers, even those known for excellent chemical resistance.

Materials

Membranes were selected from the potential materials identified in the review, as outlined in Table 3.2. For the potting resin, test samples of bisphenol fumarate polyester resin (Rechold™ DION6694) were prepared and cured according to the guidelines of the manufacturers, using a 6% cobalt octoate solution as a catalyst and methyl ethyl ketone (MEK) as initiator.

Table 3.2. Membranes tested for chemical resistance according to ASTM D543-14

Sample	Manufacturer	Material	Specification
M1	Microdyn Nadir	PES	Nadir PM UP020
M2	Microdyn Nadir	PP	Tube 0,2µm
M3	Millipore	PTFE	UF Type FH 0,50µm
M4	PAM Laboratory	PVDF	Hollow fiber membrane

The biodiesel was prepared from food-grade soybean oil in the PAM laboratory, with a FAME concentration of 96.8% wt. Analytical grade methanol was purchased from Isofar Ltda. (Duque de Caxias – RJ, Brazil), and sodium hydroxide was sourced from Neon Comercial Ltda. (Suzano – SP, Brazil).

Methodology

The chemical resistance tests followed the ASTM D543-14 standard [147]. Samples of the membranes and resin DION6694 were immersed in two different solutions: Biodiesel and an 8 wt% NaOH/methanol solution. The NaOH solution concentration corresponded to a stoichiometric molar ratio (MR) of 3:1, representing the highest concentration condition for transesterification. The temperature was maintained at 60°C ±0.1°C in sealed flasks for 48 hours. Afterward, the membrane samples were carefully washed with distilled water and dried for 24 hours at 40°C. To ensure the reliability and reproducibility of the results, the experiment was conducted in triplicate.

The effect on the membranes was evaluated by assessing changes in mechanical properties, such as flexibility, in comparison with a control (blank) sample. The morphology of membranes that exhibited minimal or no changes was further characterized using Scanning Electron Microscopy (SEM). For the resin, the visual integrity of the samples was inspected, and any changes in the color of the solution were

noted to assess alterations in the resin. Additionally, a gravimetric analysis was performed to determine any mass variations resulting from swelling or chemical degradation.

Results

The results of the chemical resistance of the tested membranes are summarized in Table 3.3. After immersion in Biodiesel, all samples remained flexible and did not break when bent. For membranes M1 and M4, the Biodiesel became opaque and lost its brightness, indicating some effect on the membranes. In contrast, membranes M2 and M3 showed no visible change in the appearance of the Biodiesel. After exposure to the NaOH solution, sample M1 lost its flexibility and became brittle. Sample M4 turned brown immediately upon contact with the solution, and after the test, a white precipitate formed. When attempting to remove the membrane, it broke apart completely.

Table 3.3. Results for chemical resistance test of the membranes

Sample	Biodiesel	NaOH/Methanol	Result
M1	Suitable	Not Suitable	Not Suitable
M2	Suitable	Suitable	Suitable
M3	Suitable	Suitable	Suitable
M4	Suitable	Not Suitable	Not Suitable

Membranes M2 and M3 retained their flexibility, and the solution maintained its original appearance, which aligns with the well-established chemical resistance of polypropylene to a broad spectrum of chemicals, including acids, bases, solvents, and oils, without any degradation or loss of structural integrity. However, its resistance to alcohols, esters, and ketones is limited, particularly at elevated temperatures [139]. Similarly, PTFE is renowned for its exceptional chemical resistance, especially in aggressive chemical environments. It exhibits high resistance to most acids, bases, solvents, and gases, even at elevated temperatures, making it unmatched in many industrial sectors [136].

Figure 3.1 and Figure 3.2 present the membrane morphology through SEM micrographs for samples M2 and M3, respectively, after the testing process.

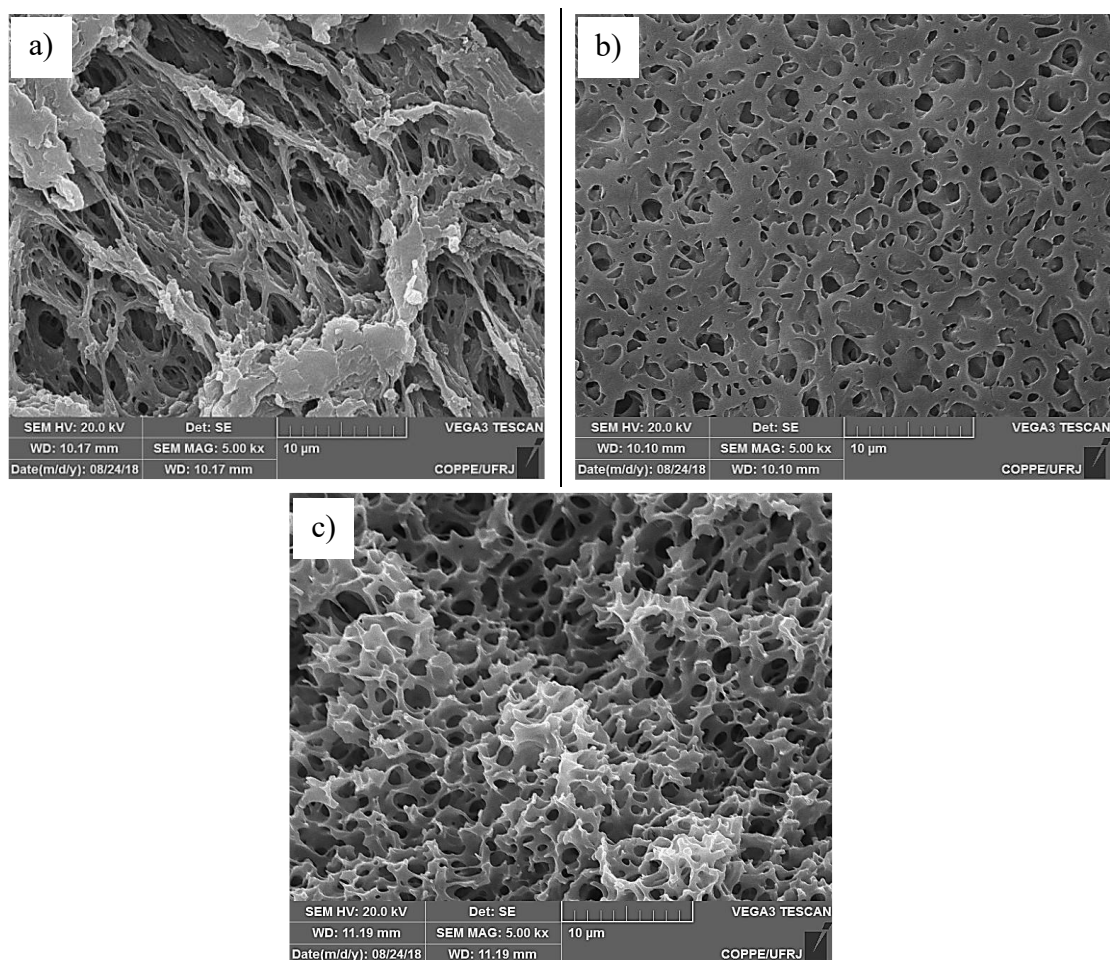


Figure 3.1. SEM images Sample M2 (PP Membrane) after the test. a) External Surface; b) Internal Surface; c) Cross-section.

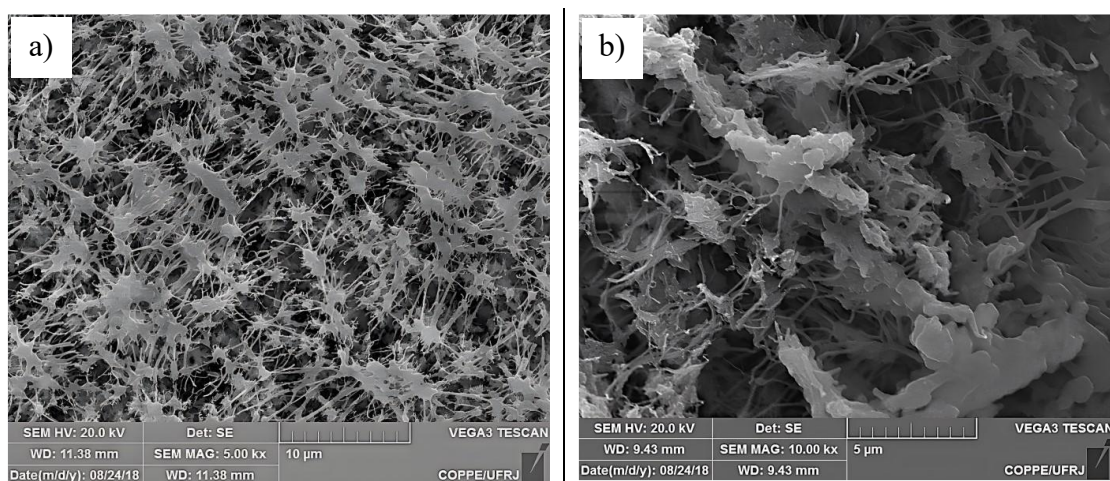


Figure 3.2. SEM images Sample M3 (PTFE Membrane) after the test. a) Surface; b) Cross-section.

The results of the gravimetric analysis for resin DION6694 are presented in Figure 3.3. The samples immersed in Biodiesel showed no change in weight, indicating neither gain nor loss. In contrast, the samples exposed to the NaOH/methanol solution experienced a weight loss of approximately 4%, likely due to methanol solubilizing the residual resin. By the end of the experiment, the methanol solution turned light green, suggesting the presence of dissolved resin. To further confirm the hypothesis of residual resin washing, the NaOH solution test was repeated with the same sample, and no changes were observed in either the mass of the sample or the color of the solution. Additionally, no changes in hardness were observed for the samples exposed to either Biodiesel or the NaOH/methanol solution, when compared to the unexposed control samples.

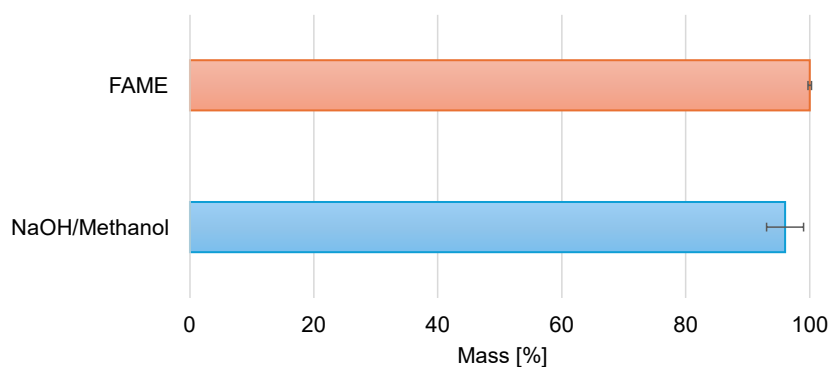


Figure 3.3. Results for gravimetry test of resin DION6694

Based on the review results, stainless steel 316 tubing was selected for the shell. In addition to its excellent chemical resistance, stainless steel offers superior heat conductivity, which enhances the efficient heating of the contactor during the transesterification of soybean oil. Furthermore, this tubing was readily available in the laboratory's stock. Similarly, polypropylene (PP) was chosen as the membrane material due to its availability and chemical resistance. The PP hollow fiber membranes were purchased from Zena Membranes (Brno, Czech Republic) with the specifications described in Table 3.4 and in Figure 3.4. The reactor length was limited to 0.50 m because of the length of the commercial hollow fiber membranes (0.65 m). Finally, bisphenol fumarate polyester resin (Reichhold™ DION6694) was confirmed as the potting resin, providing reliable performance for the application.

Table 3.4. Specifications for PP HFM – Membrane P80 Zena Membranes

Specification	
Membrane type	Hollow fiber – P80
Membrane material	Polypropylene (PP)
Pore size	Average 0.1 μm
Typical flux	170 $\text{L m}^{-2} \text{h}^{-1}$ @ 1 bar - 15°C
OD / ID	530 / 440 μm
Surface treatment	None-hydrophobic
Fiber burst pressure	>5.5 bar
Fiber collapse pressure	>3.5 bar
Strength	2 N / fiber

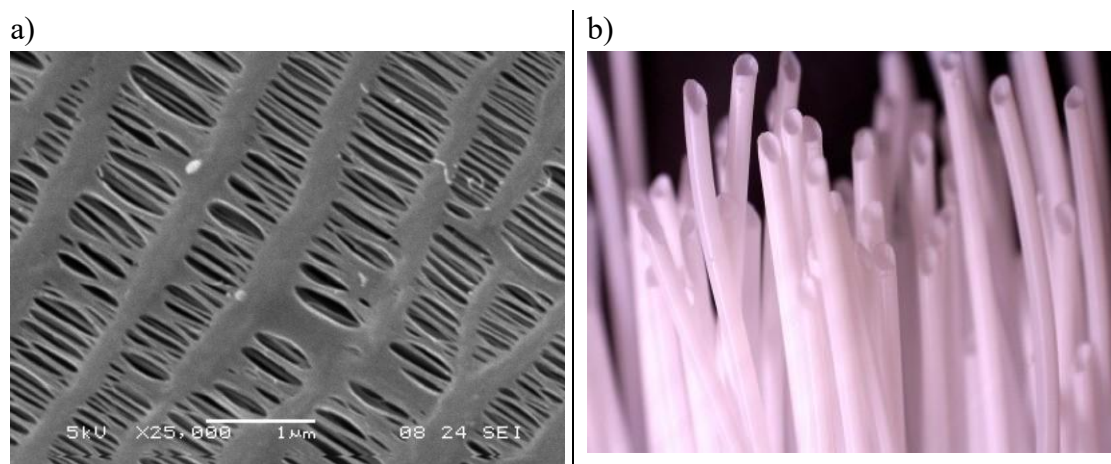
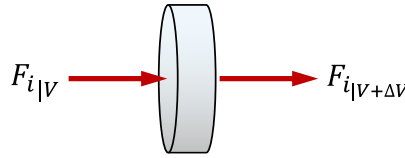


Figure 3.4. Images of the PP HFM – Membrane P80 Zena Membranes. a) SEM of the Surface. b) HFM appearance photo

3.4. Initial Modeling: PFR

A Plug Flow Reactor (PFR) model was developed and solved to guide the selection of the flow configuration, considering both cocurrent and countercurrent setups to improve the extractive reaction process. Additionally, the model helps define the expected system behavior under ideal mixing conditions, assuming negligible mass transfer effects. In this model, the fluid is treated as moving in discrete plugs, with no mixing within each plug, ensuring a uniform reaction profile along the length of the tubular reactor.

Differential Molar Balance



$$F_{i|V} - F_{i|V+\Delta V} + r_i \Delta V = \frac{dN_i}{dt} \quad \text{Equation 3.1}$$

Steady-state: $F_{i|V} - F_{i|V+\Delta V} + r_i \Delta V = 0$

Using derivative definition: $\lim_{\Delta V \rightarrow 0} \frac{F_{i|V+\Delta V} - F_{i|V}}{\Delta V} = r_i$

Differential equation for each species: $\frac{dF_i}{dV} = r_i \quad \text{Equation 3.2}$

As a function of length (z): $\frac{dF_i}{dz} = A_{CS} r_i \quad \text{Equation 3.3}$

The reaction rates for each species (r_i) are presented in Table 3.5. Using Equation 3.3, a system of six ordinary differential equations (ODEs), one for each species, was formulated. Euler's Method was employed to solve this system, using Microsoft ExcelTM, applying the conditions outlined in Table 3.6. The conversion and yield were subsequently calculated using Equation 5.14 and Equation 5.15.

Table 3.5. Reaction Rate for each chemical species

$r_{TG} = -k_1 C_{DG} C_{ME} + k_{-1} C_{TG} C_M$
$r_{DG} = k_1 C_{DG} C_{ME} - k_{-1} C_{TG} C_M - k_2 C_{MG} C_{ME} + k_{-2} C_{DG} C_M$
$r_{MG} = k_2 C_{MG} C_{ME} - k_{-2} C_{DG} C_M - k_3 C_G C_{ME} + k_{-3} C_{MG} C_M$
$r_{ME} = k_1 C_{DG} C_{ME} - k_{-1} C_{TG} C_M + k_2 C_{MG} C_{ME} - k_{-2} C_{DG} C_M + k_3 C_G C_{ME} - k_{-3} C_{MG} C_M$
$r_G = k_3 C_G C_{ME} - k_{-3} C_{MG} C_M$
$r_M = -r_{ME}$

The values for kinetic constants were obtained from NOUREDINI et al. [82]

Table 3.6. Conditions for the solution of the ODEs

Flow setup	Variable	Units	$z = 0$	$z = l_R$
Cocurrent	OFR	L h ⁻¹	0.8	-
	MR	-	6	-
Countercurrent	OFR	L h ⁻¹	0.8	-
	MR	-	-	6

Figure 3.5 presents the conversion and yield profiles for the PFR model. The results indicate that the countercurrent flow configuration achieves the best performance in terms of both conversion and yield. To shift a chemical equilibrium, the concentration of a reactant must be increased or the concentration of a product minimized by removing it—both of which are achieved in the countercurrent setup. While the cocurrent configuration is limited by chemical equilibrium, the countercurrent setup creates alcohol and glycerol concentration gradient profiles that shift the equilibrium of the transesterification reaction, leading to improved conversion and yield. These profiles align with findings from the literature and previous works by the author [82,91,148,11].

Similarly, a comparison of Figure 3.5a and Figure 3.5b shows that lower values of OFR lead to higher conversion and yield, due to the longer residence time of the reactive mixture in the reactor.

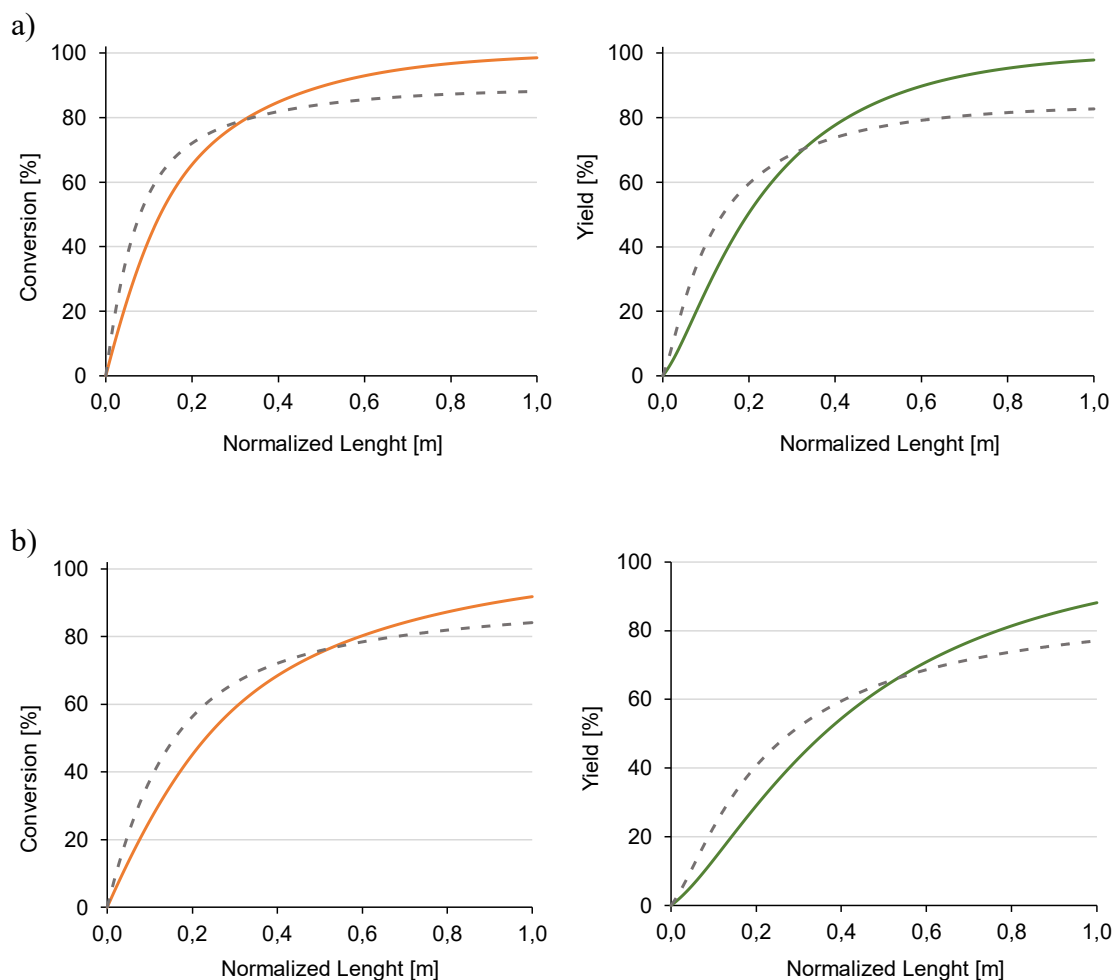


Figure 3.5. Conversion and Yield profiles for the PFR model. MR 6:1; Countercurrent (continuous line) and cocurrent (dotted line). a) OFR = 0,4 L h⁻¹; b) OFR = 0,8 L h⁻¹

3.5. Hollow Fiber Membrane Module Fabrication

A set of three hollow fiber membrane contactors were constructed and leak-tested. The modules featured stainless steel 316 tubing with an 8 mm internal diameter for the housing and polypropylene hollow fiber membranes supplied by Zena Membranes (Brno, Czech Republic). For potting, bisphenol fumarate polyester resin DION6694, provided by Reichhold do Brazil (Mogi das Cruzes – SP, Brazil), was used, with a 6% cobalt octoate solution as the catalyst and MEK as the initiator.

The parameters of the modules (contactors) are summarized in Table 3.7 and the datasheet for the HFM housing is provided in Figure 3.6. Each contactor was immersed in methanol to remove any residual resin and then tested for leaks by circulating distilled water through the membrane bundle side for two hours while monitoring for leaks into the housing side. Any modules exhibiting signs of leakage were discarded and re-fabricated.

Table 3.7. Detailed parameters for membrane contactors.

Component	Parameter	Units	Value
Housing	Outer Diameter	m	0.012
	Inner Diameter	m	0.008
	Length	m	0.70
¹ HFM	Outer Diameter	μm	530
	Inner Diameter	μm	440
	Pore size	μm	0,1
	Active Length	m	0.470
	Number of HFM	Unit	23; 46; 69
	Packing fraction	%	10; 20; 30
Potting	Catalyst: 6% cobalt octoate solution	² phr	0,2
	Initiator: MEK	² phr	2,0

¹ From manufacturer datasheet

² Parts per Hundred Resin

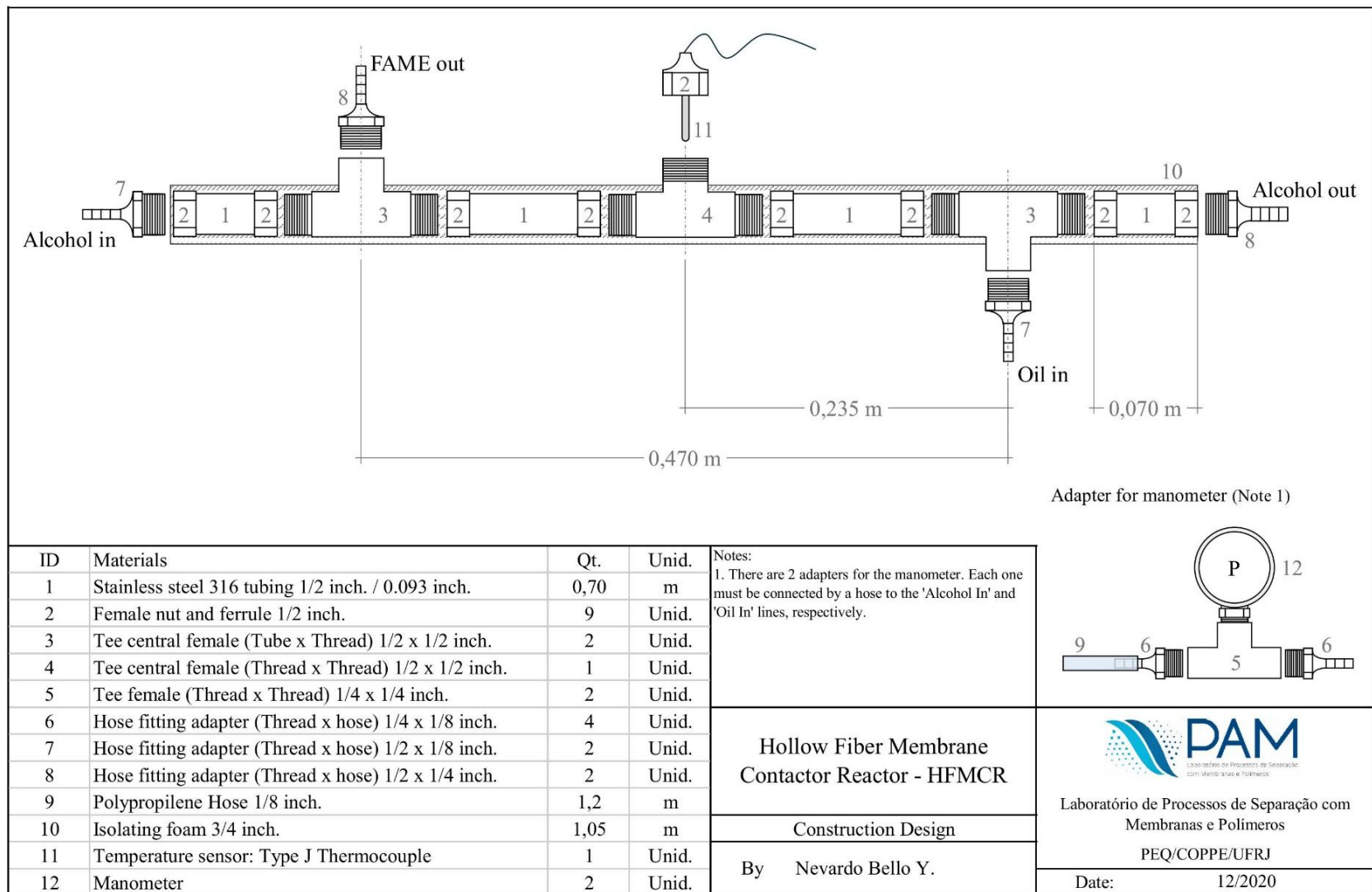
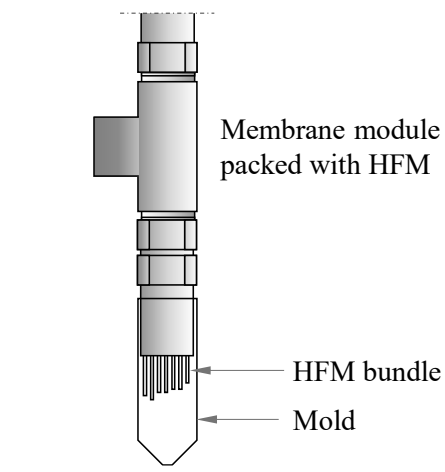
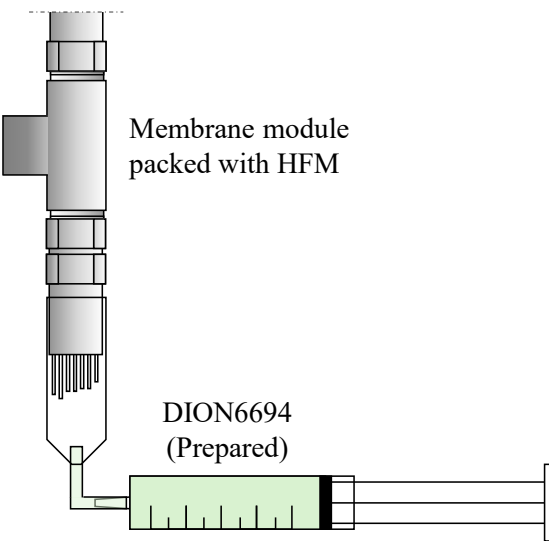


Figure 3.6. Hollow fiber membrane module housing - Construction Datasheet

Potting Process

The objective of the potting process is to create a barrier that prevents mixing between the phases while simultaneously distributing the feed alcohol to the hollow fiber membrane bundle, in a configuration similar to the shell-and-tube arrangement in a heat exchanger. The steps for fabricating the HFM module are outlined in Table 3.8.

Table 3.8. Potting process description

<div>1. Pack the HFM bundle inside the housing, ensuring the membrane ends are sealed to prevent resin penetration.</div> <div>2. Secure the mold to the housing ends to prevent resin leakage.</div>	
<div>Prepare the resin mixture according to the proportions described in Table 3.7.</div> <div>3. Fill a syringe with the resin and hold it vertically to release any air bubbles.</div>	

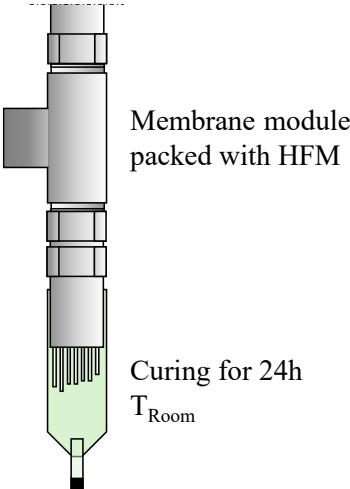
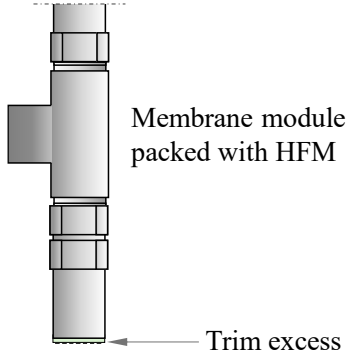
<ol style="list-style-type: none"> 4. Slowly inject the resin to avoid forming air pockets within the potting. 5. Allow the resin to cure for 24 hours at room temperature. 	
<ol style="list-style-type: none"> 6. Trim any excess resin from the module. 7. Inspect the HFM using a microscope to ensure that the membranes are not clogged. 	

Figure 3.7 illustrates a successful potting process of the HFM module. It can be observed that all the hollow fiber membranes are open and free of clogging, while the resin does not show any failures through the potting seal, which could potentially cause leaks during the experimental stage.

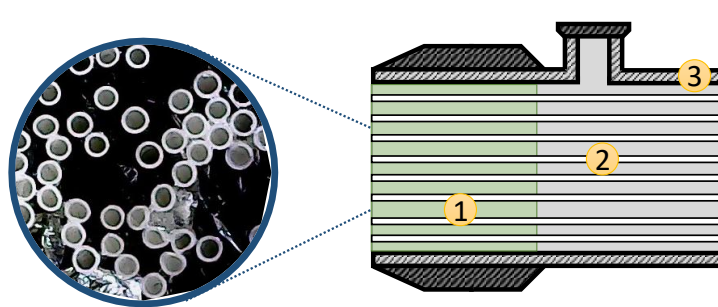


Figure 3.7. HFM module Potting. (a) Cross-section photograph (b) Schematic diagram: 1. DION6694 resin; 2. PP hollow fiber membranes bundle; 3. Stainless steel housing.

3.6. Hollow Fiber Membrane Contactor Reactor Laboratory Scale System

Additional equipment was selected to maintain the variables within the defined parameters. A Remco 3323-2E1-82B diaphragm pump was used for oil feeding, equipped with a bypass and a rotameter to regulate the oil flow rate. Methanol was fed using a Provitec DM 5900 dosing pump with adjustable speed to achieve the desired flow rate. Both the rotameter and dosing pump were pre-calibrated. Pressure gauges (0.0 to 0.5 bar) were installed to monitor the pressure at the inlets of the soybean oil and NaOH/methanol solution. A silicone rubber heating tape (1.80 m x 1/2 inch - 240 Vac), paired with a COEL K48E temperature controller (HCRR - 240Vca), was used to maintain the temperature at the setpoint.

System Setup

Figure 3.8 illustrates the laboratory-scale setup of the hollow fiber membrane contactor reactor system. Soybean oil is fed through the shell-side of the membrane contactor, while the NaOH/methanol solution flows countercurrently through the lumen side. A silicone heating tape is used to heat the contactor body, maintaining the oil phase temperature at $55 \pm 0.5^\circ\text{C}$ using a PID electronic control system. Figure 3.9 shows a picture of the real system installed at the PAM Laboratory.

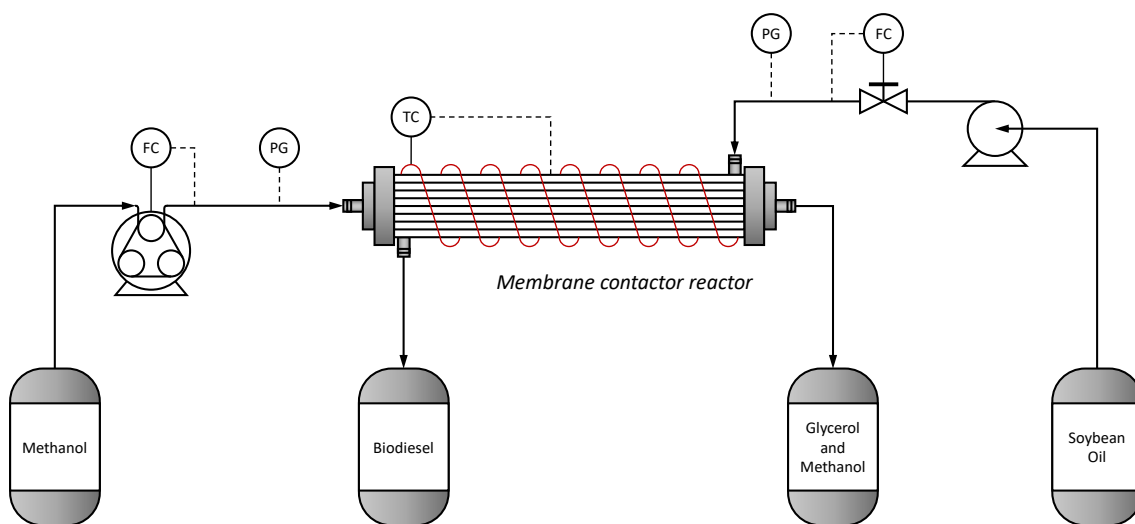


Figure 3.8. Laboratory-scale setup of the hollow fiber membrane contactor reactor system

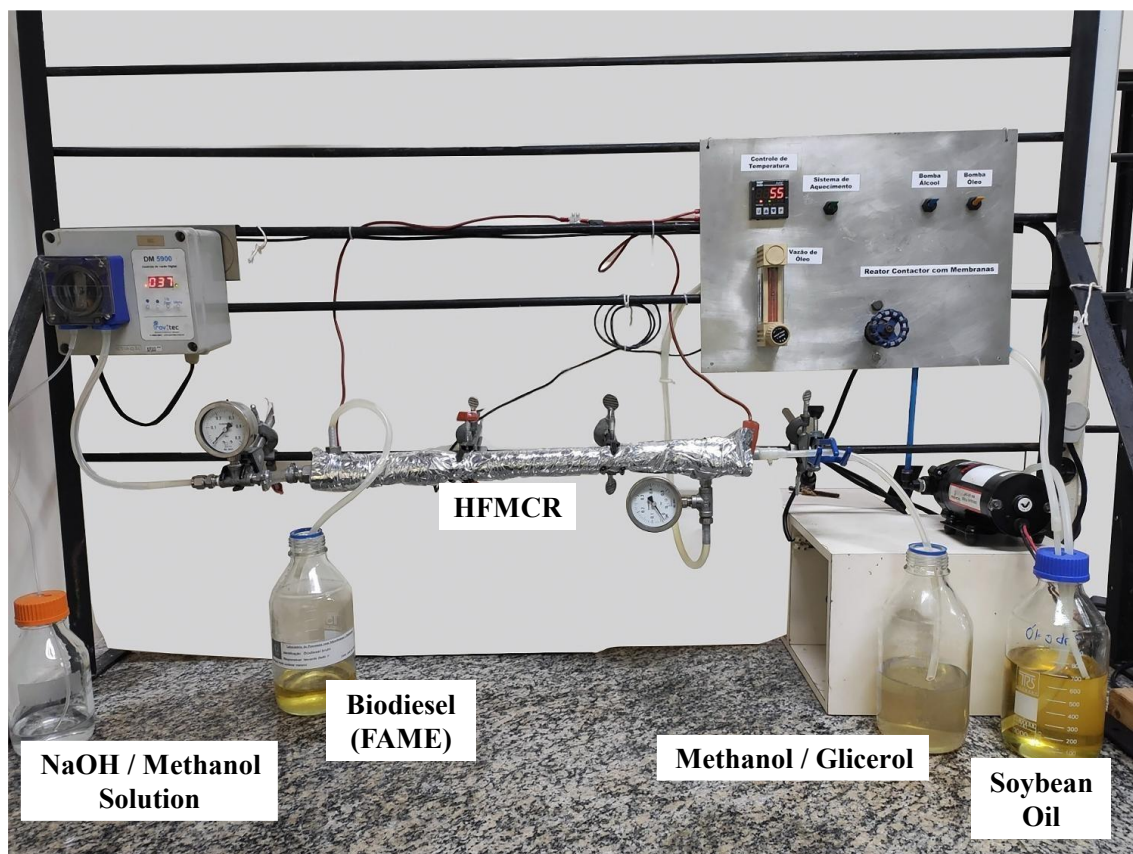


Figure 3.9. Hollow fiber membrane contactor reactor laboratory scale system – PAM Laboratory PEQ/COPPE/UFRJ

3.7. Concluding Remarks

In this chapter, the two main components of the reaction system—the hollow fiber membrane module (HFM) and the peripheral equipment—were designed, fabricated (or purchased), and assembled. The HFM components were selected based on their chemical resistance and availability, with stainless steel tubing chosen for the housing, a polypropylene (PP) hollow fiber membrane, and bisphenol fumarate polyester resin for the potting. A detailed methodology for constructing the modules was developed and documented, including a data sheet for future reference. Three modules were built and tested for leaks before being used in this research. The peripheral equipment, such as pumps, heating devices, and control systems, was also specified and described.

Chapter 4 - Experimental Preliminary Evaluation

This chapter presents the preliminary tests conducted to evaluate the potential of the hollow fiber membrane contactor reactor (HFMCr) for reactive extraction in the production of FAME (biodiesel) through the transesterification of soybean oil. The experiments were carried out using a laboratory-scale system, featuring an HFMCr packed with polypropylene (PP) hollow fiber membranes at a packing fraction of 20%. The study investigated the impact of key parameters, such as oil flow rate (OFR) and methanol-to-oil molar ratio (MR), on the molar rates of reacted triglycerides (TGR) and the produced FAME (FAME_P). Additionally, the glycerol and methanol content in the FAME-rich phase was estimated for each experimental condition.

4.1. Experimental

4.1.1. Materials

Food-grade soybean oil was acquired from Cargill Agrícola S.A. (Uberlândia, MG, Brazil), with specifications provided in Table 4.1. Analytical-grade methanol was obtained from Isofar Ltda. (Duque de Caxias, RJ, Brazil), and sodium hydroxide from Neon Comercial Ltda. (Suzano, SP, Brazil).

Table 4.1. Soybean oil specifications

Property	Unit	Value	Test Method
Acid value	mg KOH g ⁻¹	0.140	ASTM D664
Water content	%wt.	<0.05	ASTM E203

The chemicals used for the gas chromatography analysis included pyridine and n-hexane (ACS grade), as well as the derivatization agent N,O-bis(trimethylsilyl) trifluoroacetamide (BSTFA), and reference standards including methyl oleate, triolein, and glyceryl tridecanoate (internal standard - IS), all of which were purchased from Sigma Aldrich Chemical Company (St. Louis, MO, USA).

A hollow fiber membrane contactor with a packing fraction of 20%, fabricated as described in Section 3.5, was used for the experiments. Additional module parameters are provided in Table 3.7.

4.1.2. Experimental design

The biodiesel was produced by soybean oil transesterification with methanol, using sodium hydroxide as a homogenous basic catalyst. The catalyst was fixed for all experiments at 0.75% wt., relative to the soybean oil weight [132,107]. The temperature was fixed at 55°C, lower than the methanol boiling point to secure a safe operation.

A set of experiments was planned to study variables with previously known relevant influence on vegetable oils transesterification at PFR-type reactors: oil flow rate (OFR) and methanol to oil molar ratio (MR) [107,22,120]. The relevance of other parameters, such as acid value and moisture, was minimized by using refined vegetable oil. Table 4.2 resumes the levels of study for the main variables, including the response variables.

Table 4.2. Selected variables for the evaluation of soybean oil transesterification in a HFMCR.

Variable	Units	Upper	Lower
Oil flow rate (OFR)	L h ⁻¹	0.8	0.4
Methanol to oil molar ratio (MR)	-	9	4
Packing Fraction	%	20	-
Temperature	°C	55	-
Catalyst (NaOH)	%wt.	0.75	-
Reacted Triglycerides (TG _R)	mol h ⁻¹	Response	
Produced FAME (FAME _P)	mol h ⁻¹	Response	

For the assessment of the HFMCR for biodiesel production, the experimental design employed was based on response surface methodology using the Box–Behnken design. A triplicate of the central point was included to verify reproducibility (Table 4.3). To

explore the feasibility of biodiesel production using a HFMCR, only experiments E3, E6, E7, E10, E11, E14, and E15 were conducted in this section. These experiments corresponded to the first module constructed with a packing fraction of 20%.

Table 4.3. Set of experiments performed

Run	E1	E2	E3 ^{CP}	E4	E5	E6 ^{CP}	E7	E8
PF [%]	10	30	20	10	30	20	20	30
MR	4.0	4.0	6.5	9.0	6.5	6.5	4.0	6.5
OFR [L h ⁻¹]	0.6	0.6	0.6	0.6	0.6	0.6	0.4	0.8

Run	E9	E10	E11	E12	E13	E14	E15 ^{CP}
PF [%]	10	20	20	30	10	20	20
MR	6.5	9.0	4.0	9.0	6.5	9.0	6.5
OFR [L h ⁻¹]	0.8	0.8	0.8	0.6	4.0	0.4	0.6

CP: Central Point

4.1.3. Procedure

The methanol/catalyst solution was prepared and filtered just before the transesterification reaction to avoid concentration variations because of the volatility of methanol and to avoid the clogging of the membrane by eventual insoluble suspended particles. Then, the solution was fed through the lumen side of the membrane bundle. Once the alcoholic solution stabilized, the oil feeding started through the contactor shell-side, guaranteeing the exit of air in the whole system. At the same time, the reactor heating started until reaching $55 \pm 0.5^\circ\text{C}$. As soon as the system temperature reached the setpoint, the initial time ($t=0$) was set.

4.2. Characterization and sample analysis

The gas chromatography analysis methodology was developed based on ASTM D6584-17 [149]. In all experiments, samples from the FAME-rich phase were collected every 20 minutes for one hour in vials preloaded with $4.0 \text{ mg} \pm 0.5$ of glyceryl tridecanoate (IS). Each 15 mg sample was derivatized immediately after extraction from the reactor by adding BSTFA as the derivatization agent and pyridine as the catalyst, at room temperature, and the vial volume was brought to 2.0 mL with n-hexane. The derivatization process lasted 60 minutes. All samples were stored at 4°C until analysis.

The derivatized samples were analyzed for FAMES, TGs, and glycerol using an Agilent 7890A Gas Chromatograph (Agilent Technologies Co. Ltd., Shanghai, China), equipped with a flame ionization detector (FID) and a fused silica capillary column DB-5HT (15 m \times 0.320 mm \times 0.10 μ m) (Agilent J&W GC Columns, Shanghai, China). Samples of 1.0 μ L were injected via an autosampler. After 1 minute of stabilization at 80°C, the oven temperature was programmed to increase from 80°C to 100°C at a rate of 10°C/min, followed by an increase from 100°C to 230°C at 20°C/min, and finally from 230°C to 380°C at 25°C/min, where it was held for 10 minutes. The injector and detector temperatures were set at 370°C and 380°C, respectively. Each run lasted 25.5 minutes. Nitrogen was used as the carrier gas, with a flow rate of 8 mL/min and a 2:1 split ratio. Data acquisition and processing were carried out using Certy software (Agilent Technologies Co.). The concentration of methanol was determined by gravimetric volatilization.

The reacted triglycerides (TG_R) [mol h^{-1}] (Equation 4.1) and produced FAME ($FAME_P$) [mol h^{-1}] were estimated by the GC analyses.

$$TG_R [\text{mol h}^{-1}] = TG_{in} - TG_{out} \quad \text{Equation 4.1}$$

where TG_{in} is the molar flow rate of triglycerides in the oil phase at the reactor inlet (calculated from the OFR), and TG_{out} is the molar flow of triglycerides in the oil phase at the reactor outlet. TG_{out} and $FAME_P$ were calculated from gas chromatography data.

4.3. Results and Discussion

The reactive extraction process using an HFMCr allows both reaction and separation steps to be carried out with the same equipment. The glycerin is extracted with methanol just as it is produced and, due to the countercurrent operation, the chemical equilibrium shifts toward the FAME formation. The best results were achieved with a MR of 4:1 and an OFR of 0.4 L h^{-1} , resulting in a TG_R of 0,14 mol h^{-1} and $FAME_P$ of 0,24 mol h^{-1} . This corresponds to a conversion of 34% and a yield of 20%, respectively. The concentration of glycerin in the final product was only 0.06% wt. Figure 4.1 shows the obtained products of each phase and Figure 4.2, the chromatogram of the FAME-rich phase.

a)



b)



Figure 4.1. Obtained products. a) FAME-rich phase; b) Alcohol phase: Glycerin (white solid) + Methanol

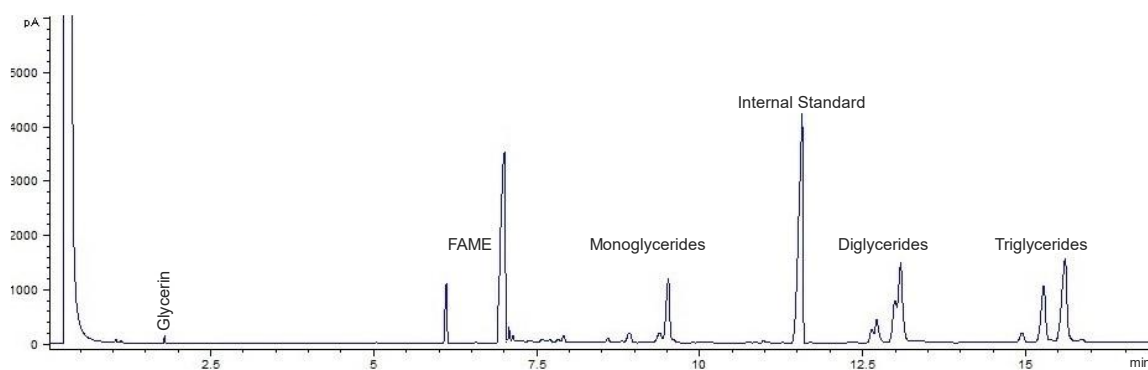


Figure 4.2. FAME-rich phase sample chromatogram.

The performance of PFR-type reactors, such as the HFMCR, is strongly influenced by the flow rate as it directly affects the reactive mass residence time (τ). Low flow rates imply longer residence times, increasing feedstock conversion and product formation rates. In the specific case of vegetable oil transesterification in conventional reactors, the FAME-rich phase and the alcohol-rich phase flow through the same volume in the same direction, so the residence time is the same. In contrast, the operation of an HFMCR allows the independent flow of each phase, both in direction and magnitude, and, therefore, the control of two residence times, τ_F , and τ_A .

4.3.1. Influence of the Oil Flow Rate (OFR)

The OFR is the variable that controls the FAME-rich phase residence time (τ_F), flowing through the shell-side. Figure 4.3 and Figure 4.4 show the effect of the OFR on the molar flux of TG_R and $FAME_P$, respectively. At the central point, the experiments were performed in triplicate to determine the experimental uncertainty. The dispersion was less than 6% for TG, and 2% for $FAME_P$, evidencing satisfactory reproducibility of the experiments. On the other hand, the dispersion of the results at upper and lower levels suggests a relevant effect of the other variable under scrutiny (MR). The analysis of the average values considering the same OFR shows that the TG_R trend is little affected by this variable, with a positive variation of less than 5% in the range of observations. In contrast, the average behavior of $FAME_P$ suggests a slight decrease trend, with a variation of around 10%. This trend is the same as reported for vegetable oil transesterification in PFR-type reactors [107,22,120].

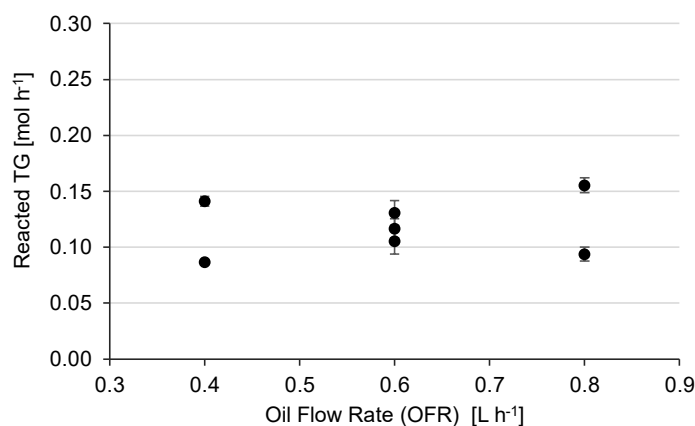


Figure 4.3. Effect of the oil flow rate (OFR) on reacted triglyceride mol rate

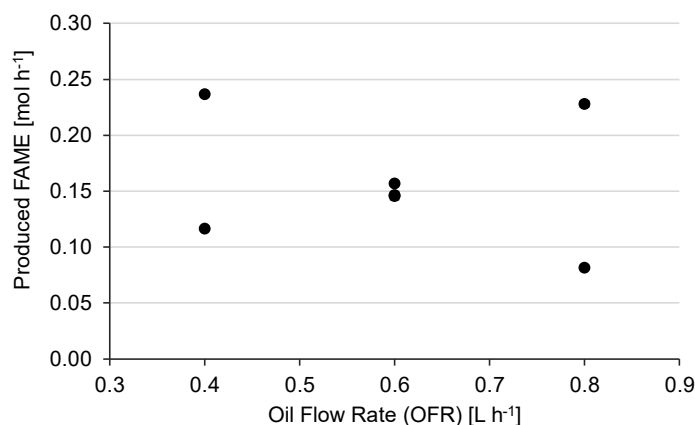


Figure 4.4. Effect of the oil flow rate (OFR) on produced FAME mol rate

4.3.2. Influence of the methanol to oil molar ratio (MR)

One way to shift the chemical equilibrium is to increase the concentration of one of the reactants. For the transesterification of vegetable oils, several research works have been conducted to optimize MR, concluding that the ideal value is about 6:1, slightly less than twice the stoichiometric molar ratio. Higher values do not improve FAME production and lead to a more difficult downstream glycerol stripping operation [79,51,88].

The MR is the variable that controls the alcohol-rich phase residence time (τ_A), flowing through the membrane lumen side. Figure 4.5 shows the influence of the methanol-to-oil molar ratio on the molar flux of TG_R , while Figure 4.6 illustrates its effect on the molar flux of $FAME_P$. Unlike the OFR, the dispersion between the results is negligible, confirming that MR has a stronger influence than OFR, in the range of this investigation, for both the TG_R and the $FAME_P$. Moreover, both variables show an inverse relationship effect on the reaction progress, with a variation of 25% and 55%, respectively. Thus, low values of MR increase the TG_R and the $FAME_P$.

One should be aware that the results cannot be compared with previously reported studies due to the quite different flow dynamic conditions. Inside the HFMCr, the volume of the alcohol-rich phase is set by the packing fraction. Therefore, the MR variable evaluates the effect of the alcohol flow rate and, consequently, its residence time (τ_A). The results reflect the known behavior of a PFR-type reactor, evidencing that the smaller MR, the longer the residence time, and the higher the reaction and product generation rates. However, to better understand the results, it is necessary to observe the distribution of the glycerin into the two phases, as shown in section 4.3.3.

It is important to clarify here that the reaction system was designed in such a way as to avoid reaching 100% of conversion and yield values since this would make it impossible to analyze the influence of the key variables.

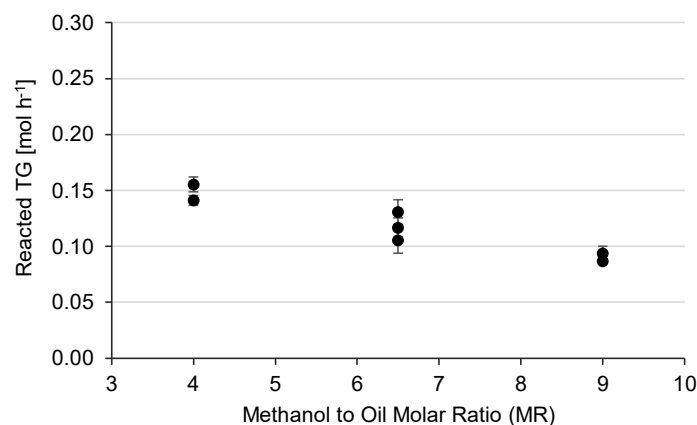


Figure 4.5. Effect of the methanol to oil molar rate (MR) on reacted triglyceride mol rate

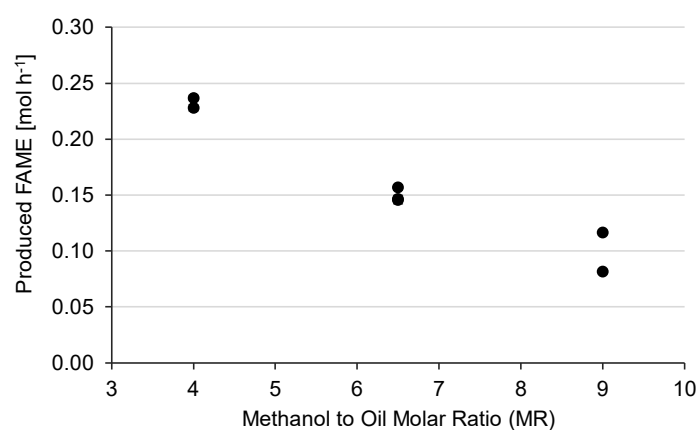


Figure 4.6. Effect of the methanol to oil molar rate (MR) on produced FAME mol rate

4.3.3. Methanol and Glycerol Content in the FAME-rich phase

Figure 4.7 shows the mass distribution of glycerol, while Figure 4.8 presents the mass distribution of methanol in both phases at the output stream. It can be noted that both glycerol and methanol remain in the alcohol-rich phase, with a mass percentage distribution greater than 99.0% wt. and 99.4% wt., respectively. Because of the non-dispersive contact between the phases, the concentration of glycerol and methanol in the FAME-rich phase is defined by the thermodynamic equilibrium at the operating conditions. Several liquid-liquid equilibrium studies for tertiary systems containing soybean oil, methanol, and glycerol report the presence of two immiscible phases. The polar phase includes a mixture of methanol and glycerol, while the non-polar phase is composed of soybean oil. Similarly, the system FAME/methanol/glycerol has partial miscibility, generating two phases: a non-polar phase, rich in FAME, and a polar phase

rich in alcohol. High concentrations of methanol and low concentrations of FAME and glycerol can eventually lead to a one-phase system [150,151].

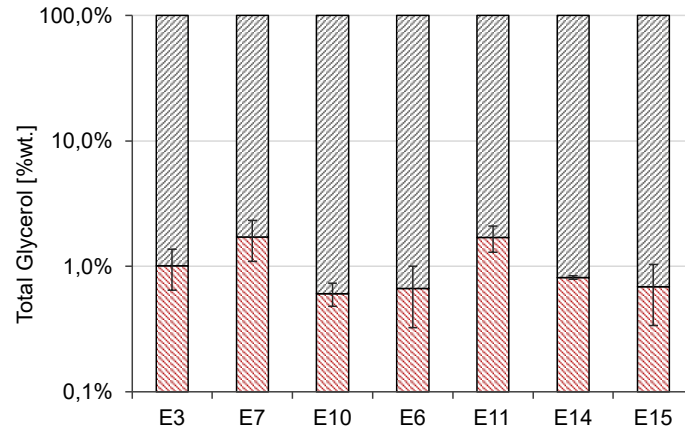


Figure 4.7. Total produced glycerol mass partitioning in both phases, alcohol-rich (black) and FAME-rich (color)

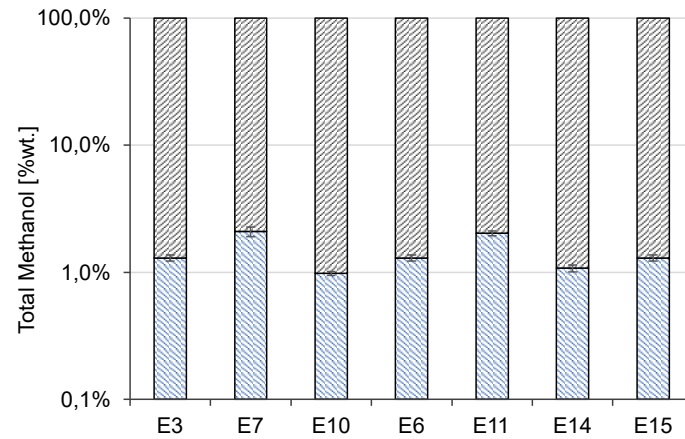


Figure 4.8. Total fed methanol mass partitioning in both phases, alcohol-rich (black) and FAME-rich (color)

In conventional production, the biodiesel purification process begins with the separation of glycerin from the FAME-rich phase. Separation is mandatory not only to guarantee product quality but also to minimize the load of contaminants to be sent to downstream purification stages. Industrial processes use gravitational decanters or centrifuges to achieve the separation [105,92]. The decantation process requires a long residence time to reach lower glycerin concentration, increasing the overall production time and making necessary larger volume separation vessels. On the other hand, the centrifugation process reduces the separation time but increases energy consumption [152]. Achieving a more efficient separation would not only decrease process time and energy consumption but

also minimize the downstream purification process load, contributing significantly to reducing production costs. The results of the glycerin and methanol distribution show that the use of an HFMCR is successful in achieving a simultaneous reaction/separation, as an intensified process. The separation unit of conventional equipment can therefore be eliminated with the consequent increase in the productivity of the process due to the reduction of both processing time and presence of contaminants in the FAME-rich phase.

4.3.4. Operation of a HFMCR for Biodiesel Production in a Countercurrent Setup

The operation of the HFMCR can be further explained based on the observed results. The oil flows through the shell-side and fills the pores because of the hydrophobicity of the PP membranes. At the same time, the alcohol flows in a countercurrent mode through the lumen side of the hollow fiber membranes. The contact between both phases and, consequently, the transesterification reaction, occurs on the surface of filled pores (Figure 4.9). Because of the low solubility of the glycerol/methanol mixture in the FAME-rich phase, the methanol present in the alcohol-rich phase acts as an extractant solvent for glycerol, achieving a reactive extraction.

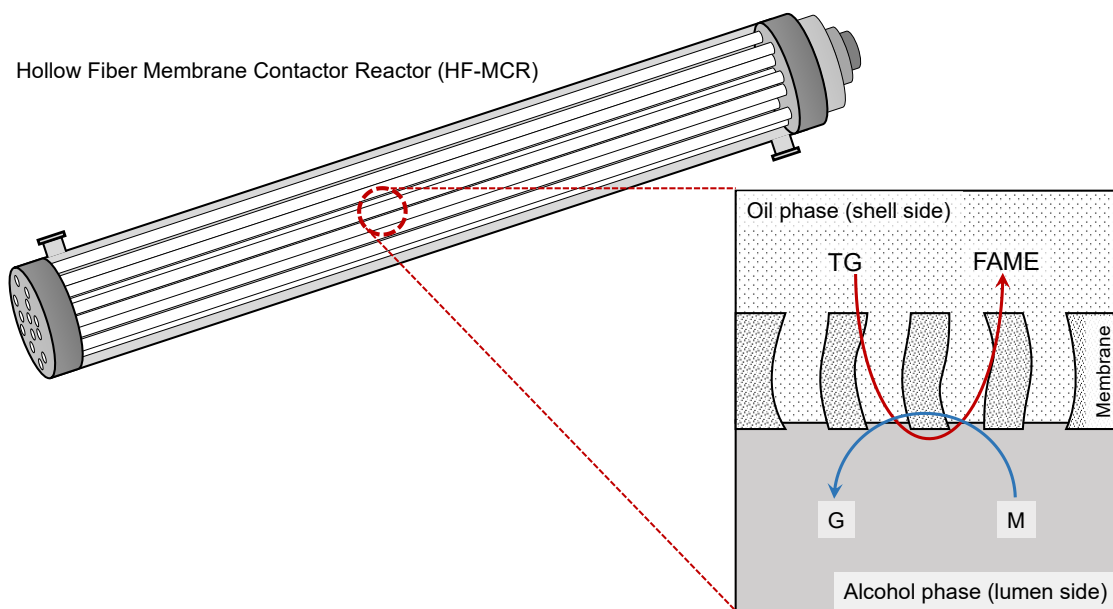


Figure 4.9. Schematic diagram of phase contacts and reaction path at the microporous membrane wall for the FAME production in an HFMCR operating in countercurrent flow. Triglyceride (TG); Methanol (M); Glycerol (G); Fatty Acid Methyl Ester (FAME).

Based on the observed results, it is possible therefore to illustrate a qualitative behavior of the HFMCR operation (Figure 4.10). One can observe that both FAME and glycerol concentration increase along the length of the reactor. However, in opposite directions. Thus, at length $L/L_{\max} = 0$, glycerol concentration is the highest, and FAME concentration is zero. At the opposite end, at length $L/L_{\max} = 1$, glycerol concentration is zero, and FAME concentration is the highest. This condition establishes a concentration gradient along the reactor length for both glycerol and FAME, shifting the chemical equilibrium of the transesterification reaction (Figure 2.9) and increasing TG_R and $FAME_P$.

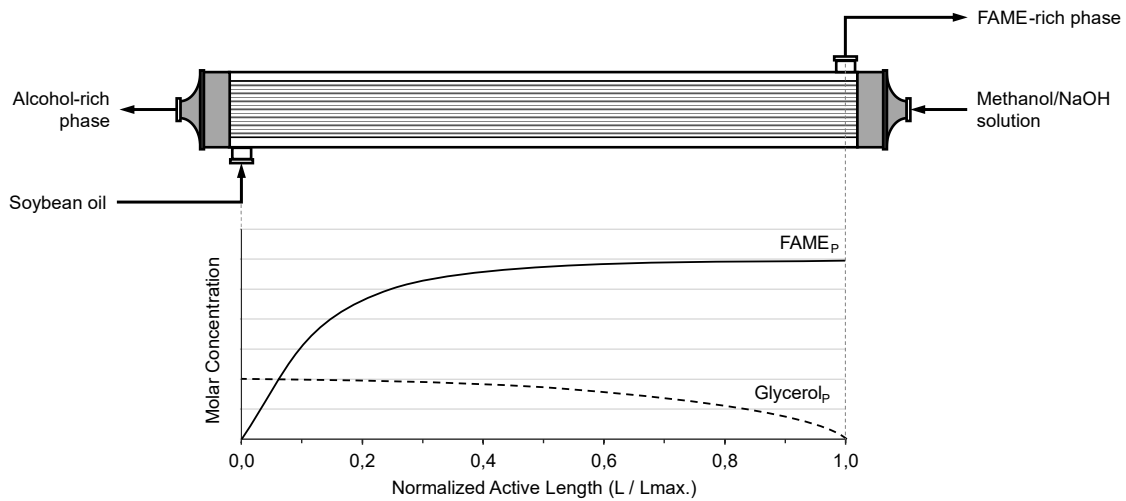


Figure 4.10. Qualitative schematic representation of the concentration profiles in the HFMCR operation (countercurrent mode setup), based on the experimental results obtained.

The results showed that the lower the MR, the higher the residence time of the alcoholic phase inside the HFMCR. Higher residence time increases the concentration gradient of the glycerin along the length, shifting the chemical equilibrium to increase the TG_R and the $FAME_P$. In the same way, a lower MR means a reduction in methanol consumption, improving process productivity. Taking into account these effects, it is necessary to establish however a minimum limit: the MR must be greater than the stoichiometric ratio (e.g. $MR > 3$) to avoid any change in the reaction kinetics.

4.4. Final Remarks

In this chapter, fatty acid methyl esters (FAME), or biodiesel, were produced through the transesterification of soybean oil using HFMCR technology in a reactive extraction

process. The membrane contactor offers significant advantages over traditional methods by improving phase contact in a non-dispersive way while reducing energy consumption associated with the stirred systems.

The countercurrent setup proved effective in extracting glycerol from the FAME-rich phase, using methanol as the extraction solvent. This intensified approach not only facilitates glycerol removal but also improves the overall efficiency and productivity of the biodiesel production process while addressing the potential to overcome the limitations imposed by the chemical equilibrium of the transesterification reaction.

In the same way, the use of the HFMCR minimized the challenges associated with glycerol separation and reduced contaminants in downstream purification, resulting in increased process productivity. Among the variables investigated, the methanol-to-oil molar ratio (MR) had a significant effect on the reacted triglycerides (TG_R) and produced FAME ($FAME_P$), which could lead to lower methanol consumption and reduced operational costs. The best results were achieved with a methanol-to-oil molar ratio of 4:1 and an oil flow rate of 0.4 L h^{-1} , yielding a TG_R of 0.14 mol h^{-1} and a $FAME_P$ of 0.24 mol h^{-1} , which corresponds to a 34% conversion and a 20% yield. The final biodiesel product had a low glycerin concentration of just 0.06% by weight.

Chapter 5 - Modeling and Validation of HFMCR Performance in Biodiesel Production

Process modeling is essential in the chemical industry as it provides a thorough understanding of physicochemical dynamics, enabling the optimization of process performance and operating conditions while minimizing the need for extensive experimental testing, thus saving both time and resources. Effective modeling is also crucial in designing safer and more sustainable processes, improving process control, enhancing product quality, and supporting the economic and environmental sustainability of chemical manufacturing.

This chapter focuses on the development of a mathematical model designed to predict the performance of a HFMCR in the base-catalyzed transesterification of soybean oil for the production of FAME. The model represents the reactor as a batch-in-series system, incorporating mass transfer limitations and flux through the membrane, using a resistance-in-series approach alongside empirical correlations to calculate the Sherwood number. The accuracy of the model was validated through experimental data obtained from a laboratory reaction system. To improve the accuracy of the model, a sensitivity analysis was conducted to evaluate the impact of each parameter of the empirical correlation (Equation 5.10) on conversion and yield. Based on the results of the sensitivity analysis, the parameters of this empirical correlation were estimated. Finally, the improved model was used to investigate the effects of key variables—oil flow rate (OFR), methanol-to-oil molar ratio (MR), and packing fraction (PF)—on response variables.

5.1. Model Development

A two-dimensional model was developed for FAME production in a HFMCR. Figure 5.1 illustrates the hydraulic setup of the membrane contactor used for the model and the laboratory test for model validation. The oil phase (α) is fed through the shell-side, filling

the membrane pores by chemical affinity with the membrane material. Simultaneously, the alcohol phase (β) flows in a counter-current through the lumen of the hollow fiber membranes.

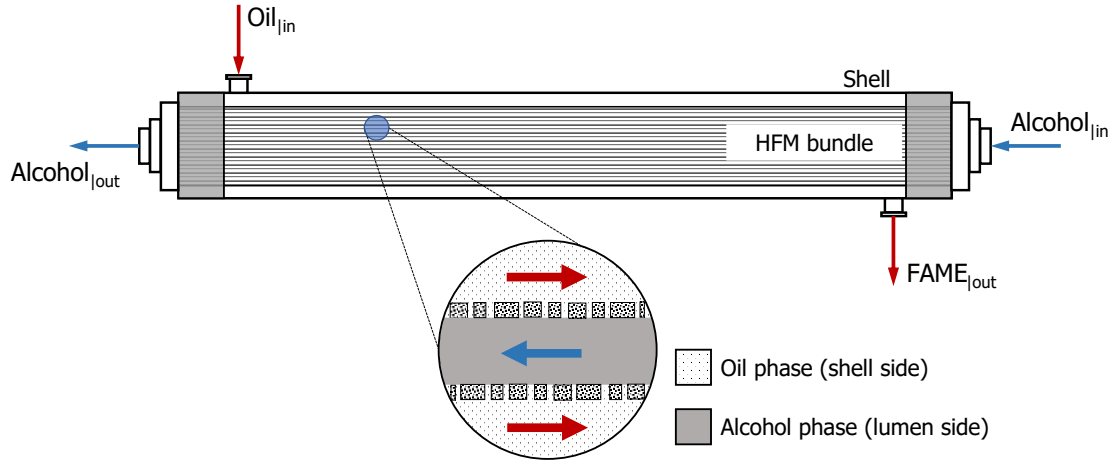


Figure 5.1. Hollow fiber membrane contactor reactor counter-current setup

5.1.1. Batch-in-series Modeling

A key characteristic of membrane contactors is that the volumes of the shell and lumen phases are determined by the construction design and remain constant, irrespective of the flow rates. Consequently, the flow rates influence only the residence time of each phase within the reactor. Due to this, the batch-in-series model is a more appropriate representation of alkali-catalyzed transesterification of soybean oil in a HFMCR. In the modeling process, each membrane pore acts as a batch reactor, with the reaction taking place instantaneously at the reactive layer (interphase). Figure 5.2 presents a schematic illustration of the modeling used for FAME production in the HFMCR.

The modeling development includes several assumptions:

- The system is in steady state.
- The temperature was kept constant (isothermal).
- Chemical reaction occurs and equilibrium is established inside the reaction layer.
- Radial concentration inside the HFMCR was negligible.
- Distribution coefficients between the phases are constant. All glycerides (TG, DG, MG, and FAME) remain in the oil phase (α), while all glycerin produced remains in the alcohol phase (β) [150,151].

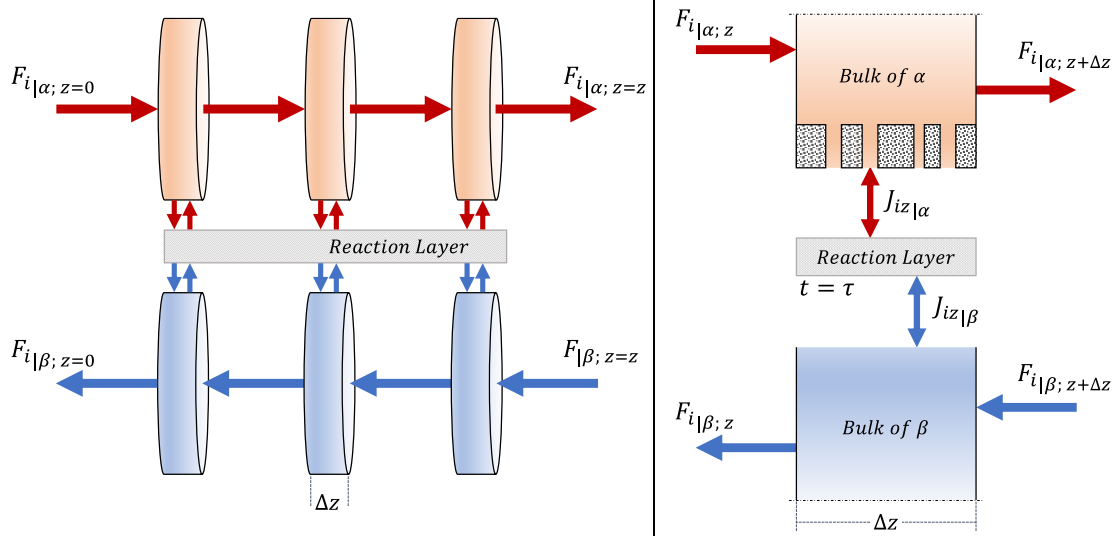


Figure 5.2. Batch-in series modelling for HFMCR in counter-current FAME production

Mass Balance in the HFMCR

$$F_{i|p; z} - F_{i|p; z+\Delta z} + A_{ms} \cdot J_{iz|p} \cdot \Delta z = 0 \quad \text{Equation 5.1}$$

$$\frac{dF_{i|p}}{dz} = (\pi \cdot d_{out} \cdot n_m) \cdot J_{iz|p} \quad \text{Equation 5.2}$$

Where $F_{i|p}$ represents the molar flow of component i on the phase p , A_{ms} denotes the outer surface area of the hollow fiber, $J_{iz|p}$ is the molar flux of component i on the phase p , d_{out} represents the outer diameter of the membrane fiber, and n_m is the number of hollow fiber membranes. Equation 5.2 represents the expression used to calculate the molar flow profile along the length for each species, as a function of surface membrane area (A_{ms}) and molar flux (J_{iz}). The molar flux of each species through the membrane (J_{iz}) is given by Equation 5.3, which expresses it as a function of a proportionality constant (K_i) and the concentration gradient driving the transfer (ΔC). This proportionality constant, known as the mass transfer coefficient, quantifies the rate at which mass transfer occurs between phases.

$$J_{iz|p} = K_{i|p} \Delta C = K_{i|p} (C_{i|p} - C_i^*) \quad \text{Equation 5.3}$$

Where $C_{i|p}$ is the concentration of component i at the bulk of phase p , and C_i^* is the concentration of component i at the reaction layer.

Concentration at the Reaction Layer (C_i^*)

Since each pore of the hollow fiber membrane acts as a reactor, the concentration at the reaction layer (RL) was determined using a batch model, as illustrated in Figure 5.3.

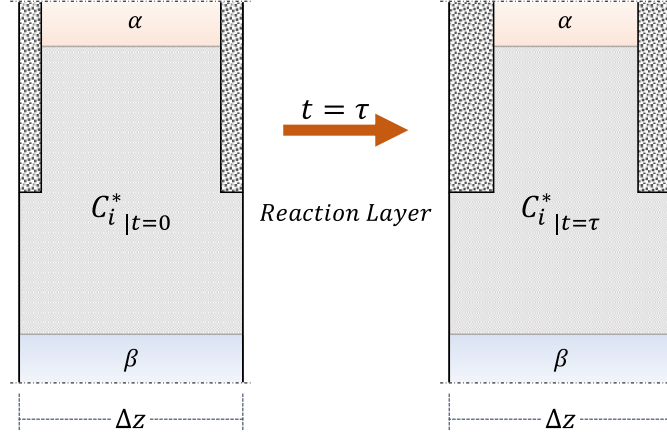


Figure 5.3. Batch reactor model

From the mass balance for a batch reactor:

$$\left(\frac{dN_i}{dt} \right)_{|RL} = r_i V_{\Delta z} \quad \text{Equation 5.4}$$

$$N_{i|t=\tau} = N_{i|t=0} + r_i V_{\Delta z} dt \quad \text{Equation 5.5}$$

$$C_{i|t=\tau}^* = C_{i|t=0}^* + r_i \tau_{Av} \quad \text{Equation 5.6}$$

Where N_i denotes the moles of component i , $V_{\Delta z}$ represents the differential constant volume for each batch reactor, and r_i is the reaction rate of component i . The average residence time (τ_{Av}) for each phase was constant and calculated as outlined in Equation 5.7 and Equation 5.8 [153]:

$$dt = \tau = \frac{\tau_\alpha + \tau_\beta}{2} \quad \text{Equation 5.7}$$

$$\tau_{|p} = \frac{V_{|p}}{v_{0|p}} = \frac{A_{CS|p} dz}{v_{0|p}} \quad \text{Equation 5.8}$$

The τ_α and τ_β represent the residence times for phase α (FAME-rich) and phase β (alcohol-rich), respectively, $V_{|p}$ is the differential volume, and $v_{0|p}$ denotes the volume flow rate of each phase p . Similarly, $A_{CS|p}$ represents the cross-sectional area of phase p , and dz is the differential length (see Equation 5.2).

Kinetics of the Transesterification Reaction

The kinetics of transesterification involves three consecutive and reversible reactions that produce glycerol and biodiesel (fatty acid methyl esters - FAME) as the final products, with diglycerides and monoglycerides acting as intermediates, as illustrated in Figure 2.9. The reaction rates (r_i) for each species formed or consumed during soybean transesterification are presented in Table 5.1. The kinetic constants used in the analysis were obtained experimentally by Nouredini et al. [82].

Table 5.1. Reaction Rate for each chemical species

$r_{TG} = -k_1 C_{DG} C_{ME} + k_{-1} C_{TG} C_M$
$r_{DG} = k_1 C_{DG} C_{ME} - k_{-1} C_{TG} C_M - k_2 C_{MG} C_{ME} + k_{-2} C_{DG} C_M$
$r_{MG} = k_2 C_{MG} C_{ME} - k_{-2} C_{DG} C_M - k_3 C_G C_{ME} + k_{-3} C_{MG} C_M$
$r_{ME} = k_1 C_{DG} C_{ME} - k_{-1} C_{TG} C_M + k_2 C_{MG} C_{ME} - k_{-2} C_{DG} C_M + k_3 C_G C_{ME} - k_{-3} C_{MG} C_M$
$r_G = -k_3 C_G C_{ME} + k_{-3} C_{MG} C_M$
$r_M = r_{ME}$

5.1.2. Shell-side (phase α) Mass Transfer Coefficient

Since phase α fills the membrane pores, the shell-side mass transfer coefficient ($K_{i|shell}$) could be calculated using a resistances-in-series approach that must account for two resistances: the FAME-rich mass transfer resistance, corresponding to the boundary layer of phase α ($k_{i|\alpha}$) and the resistance of the membrane itself ($k_{i|m}$) as depicted in Equation 5.9.

$$\frac{1}{K_{i|shell}} = \frac{1}{k_{i|\alpha}} + \frac{1}{k_{i|m}} \quad \text{Equation 5.9}$$

FAME-rich phase mass transfer coefficient ($k_{i|\alpha}$)

Due to the complex geometry, fiber arrangement, and fluid flow pattern, the shell-side mass transfer coefficient, represented by the Sherwood number, can be estimated using a general correlation (Equation 5.10) [36,38]. The diffusion coefficients were estimated using methods described by Miyabe et al. and Prausnitz et al. [154,155].

$$Sh = \frac{k_{i|\alpha} d_h}{D_{iM}} = A (1 - \phi)^\omega \left(\frac{d_h}{l}\right)^\gamma Re^\delta Sc^\theta \quad \text{Equation 5.10}$$

Where Sh , Re , and Sc , are the dimensionless numbers of Sherwood, Reynolds, and Schmidt, respectively; d_h represents de hydraulic diameter, and D_{iM} is the diffusion coefficient of component i in the mixture. Additionally, ϕ denotes the packing fraction and l the active length of the HFMCR. The parameters of the empirical correlation, A , ω , γ , δ , and θ , were obtained from Prasad and Sirkar [35].

Membrane mass transfer coefficient ($k_{i|m}$)

The membrane mass transfer coefficient was estimated using the methods described by Prasad and Sirkar, assuming unhindered diffusion through organic fluid-filled pores (Equation 5.11) [24,35,34].

$$k_{i|m} = \frac{2 \cdot \varepsilon \cdot D_{iM}}{\bar{\tau} (d_{out} - d_{im})} \quad \text{Equation 5.11}$$

5.1.3. Lumen-side (phase β) Global Mass Transfer Coefficient

Given that the alcohol phase does not fill the membrane pores, only the mass transfer resistance associated with the boundary layer of the alcohol phase (β) is considered (Equation 5.12).

$$K_{i|Lumen} = k_{i|\beta} \quad \text{Equation 5.12}$$

The L  v  que correlation (Equation 5.13) was used to determine the tube side mass transfer coefficient ($K_{i|Lumen}$) for the lumen side of the HFMCR. This correlation is applicable under laminar flow conditions for systems with a $Gz > 6$ [36].

$$Sh = \frac{k_{i|\beta} d_{im}}{D_{iM}} = 1.62 \cdot \left(\frac{dh}{l}\right)^{0.33} \cdot Re^{0.33} \cdot Sc^{0.33} \quad \text{Equation 5.13}$$

Where d_{im} represents de inner fiber diameter, and $k_{i|\beta}$ is the mass transfer resistance associated with the boundary layer of the alcohol phase.

5.1.4. Model Solution

From Equation 5.2, a system of six ordinary differential equations (ODEs), one for each species, was formulated. Euler's Method was employed to solve this system, which was implemented in Microsoft Excel™. The solution of the model involves calculating the variables described by Equations 5.2 to 5.13 as functions of reactor length. Therefore, these variables are recalculated at each integration step as part of the algorithm used to solve the model (Figure 5.4).

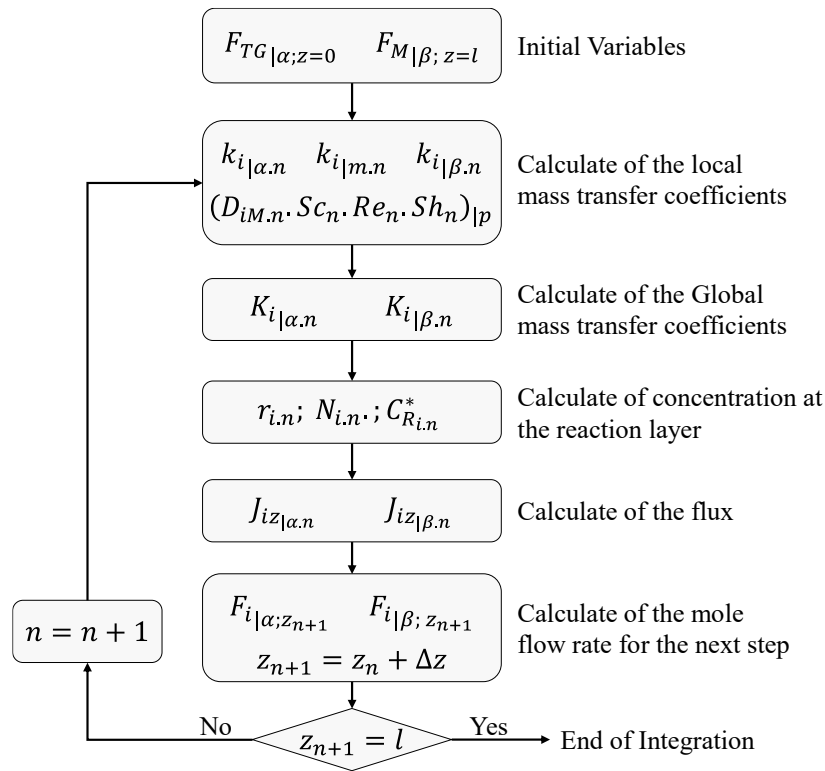


Figure 5.4. Algorithm for model solution

5.1.5. Estimation of Parameters for the Shell-Side Sherwood General Correlation

Sensitivity analysis

A sensitivity analysis of the parameters A , ω , γ , δ , and θ , for the shell-side Sherwood general correlation (Equation 5.10), was initially conducted to identify which parameters significantly impact the response variables: conversion (C_{TG}) and yield (Y_{FAME}). In parameter estimation, sensitivity refers to the degree of influence a single parameter exerts on the response variables. A highly sensitive parameter causes large variations in

the response variable with small changes [156]. For this work, the parameter values reported by Prasad and Sirkar [35] (see Table 2.3) were used as the initial values for the sensitivity analysis. Each parameter was incrementally increased by 10%, up to 150%, and decreased by 10%, down to 30% of the initial value. The correlation between the results was then calculated and analyzed.

Parameter Estimation

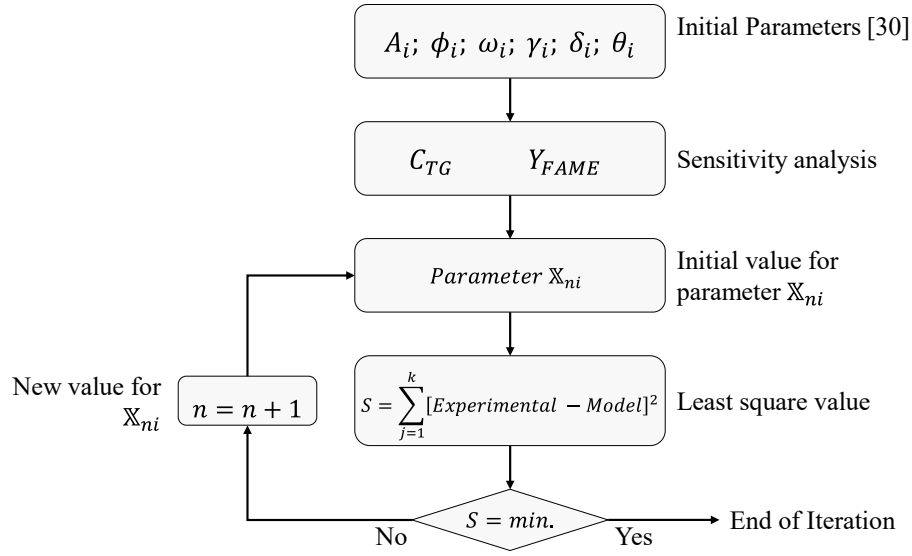


Figure 5.5. Algorithm for the estimation of parameters for shell-side Sherwood general correlation

The least squares method is used for parameter estimation, using as a function objective to minimize the difference between the model's predicted values and the experimental response variables. The experimental data presented in Section 5.3 were used for this process. Estimation begins with the most sensitive parameters, gradually moving to the less sensitive ones based on the sensitivity analysis results. The algorithm for estimating parameters related to the general correlation for the shell-side Sherwood number (Equation 5.10) is shown in Figure 5.5. This iterative process enables accurate parameter estimation, enhancing the predictive accuracy of the correlation.

5.2. Model Validation

5.2.1. Experimental Design

FAME was produced via the transesterification of soybean oil with methanol, using sodium hydroxide as a homogeneous basic catalyst. A series of experiments were designed to study variables previously identified as having a significant influence on the transesterification of vegetable oils in plug flow reactors, specifically the oil flow rate (OFR) and the methanol-to-oil molar ratio (MR) [107,22,120]. These variables were previously studied and reported by the author, and the experimental design aimed to extend the results obtained in earlier work [6]. Additionally, the effect of packing fraction was incorporated into the research. The objective was to develop an empirical model to estimate the mass transfer coefficient on the shell-side (Equation 5.10). The influence of other parameters was minimized by using refined vegetable oil. Table 5.2 summarizes the levels of study for the primary variables, including the response variables.

Table 5.2. Selected variables for the evaluation of soybean oil transesterification in a HFMCR

Variable	Units	Upper	Middle	Lower
Oil flow rate (OFR)	L h ⁻¹	0.8	0.6	0.4
Methanol to oil molar ratio (MR)	-	9	6.5	4
Packing fraction	%	30	20	10
Temperature	°C	55	-	-
Catalyst (NaOH)	%wt.	0.75	-	-
TG Conversion (C _{TG})	%	Response		
FAME Yield (Y _{FAME})	%	Response		

Where:

$$C_{TG} = \frac{TG_{in} - TG_{out}}{TG_{in}} \cdot 100 \quad \text{Equation 5.14}$$

$$Y_{FAME} = \frac{FAME_{out}}{3TG_{in}} \quad \text{Equation 5.15}$$

TG_{in} represents the molar flow rate of triglycerides in phase α at the reactor inlet, while TG_{out} represents the molar flow rate of triglycerides in phase α at the reactor outlet. Similarly, $FAME_{out}$ indicates the molar flow rate of fatty acid methyl esters in phase α at the reactor outlet. The values of TG_{out} and $FAME_{out}$ for each experiment were determined using gas chromatography (GC) analysis.

The experimental design employed in this study was based on the response surface methodology, specifically utilizing the Box–Behnken design (Table 5.3). The experiments conducted in this section complete the experimental framework of the research, which, in the preceding chapter, evaluated the feasibility of biodiesel production using a module with a PF of 20%.

Table 5.3. Set of experiments performed

Run	E1	E2	E3 ^{CP}	E4	E5	E6 ^{CP}	E7	E8
PF [%]	10	30	20	10	30	20	20	30
MR	4.0	4.0	6.5	9.0	6.5	6.5	4.0	6.5
OFR [L h ⁻¹]	0.6	0.6	0.6	0.6	0.6	0.6	0.4	0.8

Run	E9	E10	E11	E12	E13	E14	E15 ^{CP}
PF [%]	10	20	20	30	10	20	20
MR	6.5	9.0	4.0	9.0	6.5	9.0	6.5
OFR [L h ⁻¹]	0.8	0.8	0.8	0.6	4.0	0.4	0.6

CP: Central Point

5.2.2. Materials

Soybean oil (food grade) was obtained from Cargill Agrícola S.A. (Uberlândia – MG, Brazil); with specifications shown in Table 5.4. Analytical grade methanol was purchased from Isofar Ltda. (Duque de Caxias – RJ, Brazil) and Sodium hydroxide from Neon Comercial Ltda. (Suzano – SP, Brazil).

Table 5.4. Soybean oil specifications

Property	Unit	Value	Test Method
Acid value	mg KOH g ⁻¹	0.140	ASTM D664
Water content	%wt.	<0.05	ASTM E203

The chemicals used for the gas chromatography analysis included pyridine and n-hexane (ACS grade), as well as the derivatization agent N,O-bis(trimethylsilyl) trifluoroacetamide (BSTFA), and reference standards including methyl oleate, triolein, and glyceryl tridecanoate (internal standard - IS), all of which were purchased from Sigma Aldrich Chemical Company (St. Louis, MO, USA).

Three hollow fiber membrane modules, fabricated as outlined in Section 3.5, were used for model validation. The module parameters are listed in Table 3.7.

5.2.3. Characterization and Sample Analysis

The gas chromatography analysis methodology was developed based on ASTM D6584-17 [149]. In all experiments, samples from the FAME-rich phase were collected every 20 minutes for one hour in vials preloaded with $4.0 \text{ mg} \pm 0.5$ of glyceryl tridecanoate (IS). Each 15 mg sample was derivatized immediately after extraction from the reactor by adding BSTFA as the derivatization agent and pyridine as the catalyst, at room temperature, and the vial volume was brought to 2.0 mL with n-hexane. The derivatization process lasted 60 minutes. All samples were stored at 4°C until analysis.

The derivatized samples were analyzed for FAMES, TGs, and glycerol using an Agilent 7890A Gas Chromatograph (Agilent Technologies Co. Ltd., Shanghai, China), equipped with a flame ionization detector (FID) and a fused silica capillary column DB-5HT ($15 \text{ m} \times 0.320 \text{ mm} \times 0.10 \text{ }\mu\text{m}$) (Agilent J&W GC Columns, Shanghai, China). Samples of 1.0 μL were injected via an autosampler. After 1 minute of stabilization at 80°C, the oven temperature was programmed to increase from 80°C to 100°C at a rate of 10°C/min, followed by an increase from 100°C to 230°C at 20°C/min, and finally from 230°C to 380°C at 25°C/min, where it was held for 10 minutes. The injector and detector temperatures were set at 370°C and 380°C, respectively. Each run lasted 25.5 minutes. Nitrogen was used as the carrier gas, with a flow rate of 8 mL/min and a 2:1 split ratio. Data acquisition and processing were carried out using Cerity software (Agilent Technologies Co.). The concentration of methanol was determined by gravimetric volatilization.

5.3. Results and Discussion

5.3.1. Model Validation

The values predicted by the model for the response variables, C_{TG} and Y_{FAME} , were compared to the experimental results, as shown in Figure 5.6 and Figure 5.7, respectively. Overall, the fit between the experimental data and the predicted values was less than

satisfactory under the tested conditions. The correlation coefficients were 68% for C_{TG} and 72% for Y_{FAME} .

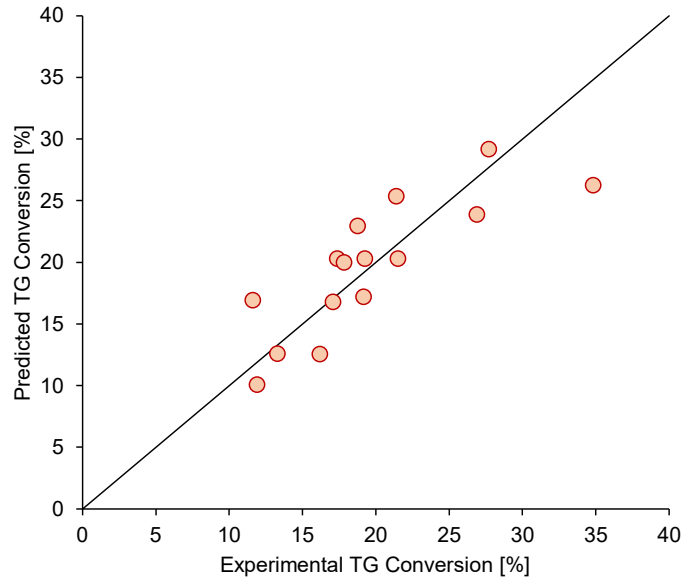


Figure 5.6. Predicted vs. Experimental results for conversion (C_{TG})

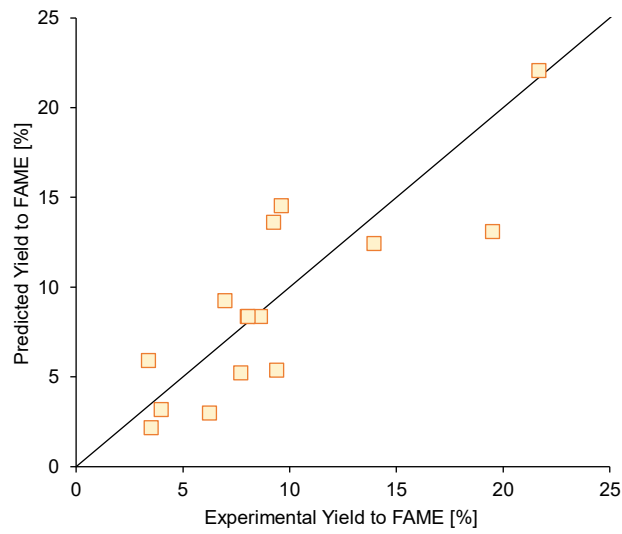


Figure 5.7. Predicted vs. Experimental results for yield (Y_{FAME})

To improve the accuracy of the model, the parameters of the empirical correlation used to calculate the shell-side mass transfer coefficient (Equation 5.10) were estimated. Prior to this estimation, a sensitivity analysis was conducted to assess the impact of each parameter on conversion and yield, enhancing the precision of the parameter calculations.

5.3.2. Estimation of Parameters for the Shell-side Sherwood General Correlation

Sensitivity Analysis

Figure 5.8 summarizes the sensitivity analysis for each parameter of Sherwood (Sh) shell-side empirical correlation (Equation 5.10): A , ω , γ , δ , and θ . Pearson and Spearman correlations were employed to determine the impact of each parameter on the response variables: conversion (C_{TG}) and yield (Y_{FAME}).

The Pearson correlation measures the linear relationship between two continuous variables, assuming a normal distribution. Its values range from -1 (indicating a perfect negative linear relationship) to 1 (indicating a perfect positive linear relationship), with 0 representing no linear relationship. In contrast, the Spearman correlation is a non-parametric measure that assesses monotonic relationships, where one variable consistently increases or decreases with the other, though not necessarily at a constant rate. Like Pearson, Spearman ranges from -1 to 1, with values near these extremes indicating strong monotonic relationships, and 0 representing no monotonic relationship. However, Spearman does not assume normality and can capture both linear and non-linear monotonic relationships [156,157].

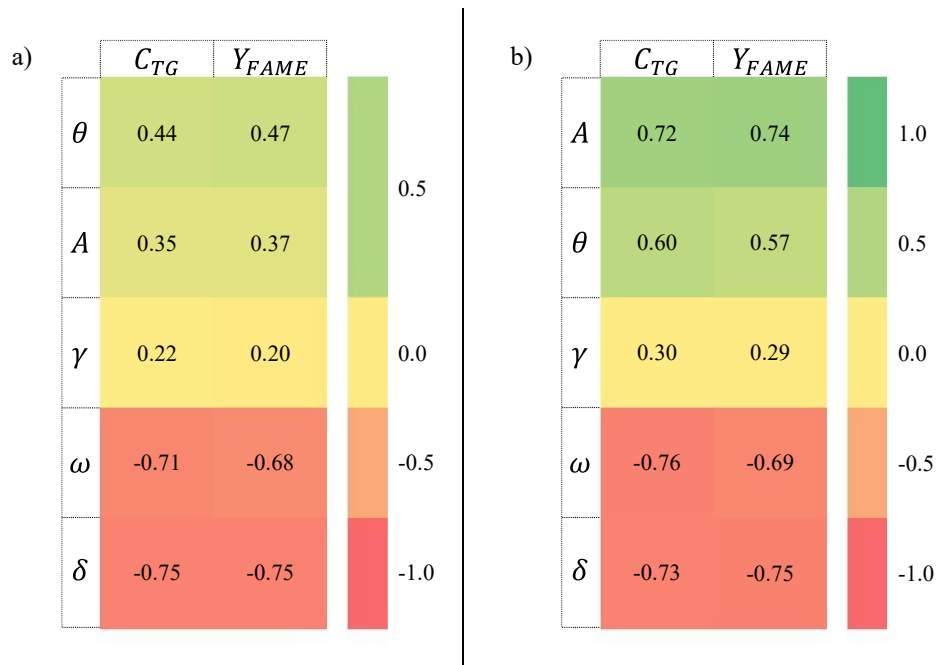


Figure 5.8. Sensitivity analysis for parameters of the shell-side Sherwood general correlation.
a) Pearson correlation; b) Spearman correlation

To determine whether a parameter exhibits a linear, monotonic, or no relationship, the Pearson and Spearman correlation values should be compared. If the Pearson correlation is closer to 1 or -1, the relationship is considered linear; if the Spearman correlation is closer to these limits, it suggests a monotonic relationship. When both correlations are near the same limit with a small difference between them, it indicates a strong linear relationship. Conversely, values near zero suggest that the parameter has neither a linear nor a monotonic relationship.

The analysis concluded that parameter δ exhibits a negative linear correlation, with values of -0.75 for both conversion and yield, while parameter ω shows a negative monotonic correlation, with values of -0.76 for conversion and -0.68 for yield. Similarly, parameters A and θ display a positive monotonic relationship, with values of 0.72 and 0.60 for conversion, and 0.74 and 0.57 for yield. In contrast, parameter γ shows neither a linear nor a monotonic correlation. Based on these findings, the estimation process begins with the most sensitive parameters and gradually progresses to the less sensitive ones in the following order: δ , A , ω , θ , and finally γ .

Parameters Estimation

Table 5.5 summarizes the parameters estimated for TG and FAME, applied to the empirical correlation for Sh (Equation 5.10). Due to the difficulty in finding data to calculate some properties for MG and DG, the parameters estimated for TG were also applied to these chemical species.

Table 5.5. Parameters estimated for TG and FAME applied to empirical Sh correlation

i	A	ω	γ	δ	θ	Re	ϕ
TG	6.58	4.74	1.34	0.60	0.44	0.2 – 2.0	0.10 – 0.30
FAME	6.22	1.75	1.57	0.60	0.32		

The results of the parameter estimation were compared with some empirical correlations for shell-side mass transfer, as presented in Table 5.6. These empirical correlations were originally developed for liquid-liquid systems in parallel flow and handmade randomly-packed modules, with reported ranges of Re and ϕ consistent with those used in this work.

Table 5.6. Empirical correlations for shell-side mass transfer for liquid-liquid systems, handmade, parallel flow, and randomly-packed modules

Authors	Gawronski and Wrzeńska	Basu et al.	Prasad and Sirkar
Parameters			
A	0.09	17.4	5.85
ω	1.0	1.0	1.0
γ	0	1.0	1.0
δ	$0.8-0.16\phi$	0.60	0.60
θ	0.33	0.33	0.33
Re	0 – 10	1 – 100	0 – 500
ϕ	0.21 – 0.80	0.25 – 0.48	0.04 – 0.40
Feed	Ethanol in aqueous solution	Phenol in methyl isobutyl ketone	Aqueous solutions of phenol, succinic acid, and acetic acid
Extractant	n-octanol	Sodium hydroxide solutions	Methyl isobutyl ketone, n-butanol, and xylene
Ref.	[25]	[42]	[35]

However, these correlations were based on extraction processes where key transport properties, such as viscosity and density, do not undergo significant changes during extraction. In contrast, the current work focuses on an extractive reaction, which results in variations in these transport properties, in both phases, as the reaction progresses along the length of the reactor. Additionally, the liquids used in this study differ from those used in the reported correlations, as a mixture of soybean oil and FAME was used, with the FAME concentration increasing as the reaction proceeds. In the absence of reported estimations for extractive reactions in a HFMCR, the values reported in Table 5.6 were used as a general guide to estimate the order of magnitude for each parameter.

The estimated values for the independent parameter A fall within the range reported in the literature and closely align with those provided by Prasad and Sirkar. Parameter ω , related to the free fraction $(1 - \phi)$, and parameter γ , linked to the HFMCR geometry (d_h/l) , are influenced by the packing fraction, housing diameter, and active length. However, the estimated values for ω and γ deviate from the linear relationships previously reported, as these parameters were not evaluated in the studies referenced in Table 5.6.

The parameter δ is linked to the Reynolds (Re) number and remains constant due to the hydraulic characteristics of the system used in this study, which operated within a limited Re (see Table 5.5). This makes it difficult to observe any significant effect of the δ parameter on the estimation of Sh. Additionally, the parameter θ , associated with the Schmidt (Sc) number, remained unchanged for FAME, while a slight increase was observed for TG. This increase is likely attributed to the higher viscosity of soybean oil (TG).

Improved Model Adjustment

The comparison between the values predicted by the model using the parameters reported by Prasad and Sirkar and those estimated in the present research study, for each response variable— C_{TG} and Y_{FAME} — are presented in Figure 5.11Figure 5.9 and Figure 5.10, respectively. An improvement in the fit between the experimental data and the predicted values is observed, with satisfactory correlation coefficients of 81% for C_{TG} and 88% for Y_{FAME} .

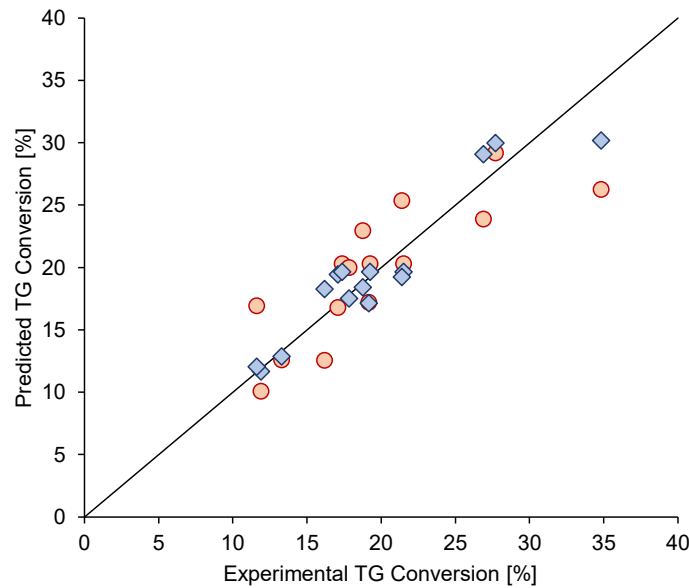


Figure 5.9. Adjusted Correlation: Predicted vs. Experimental results for conversion (C_{TG})
Orange circles Prasad and Sirkar parameters; Blue diamonds estimated parameters

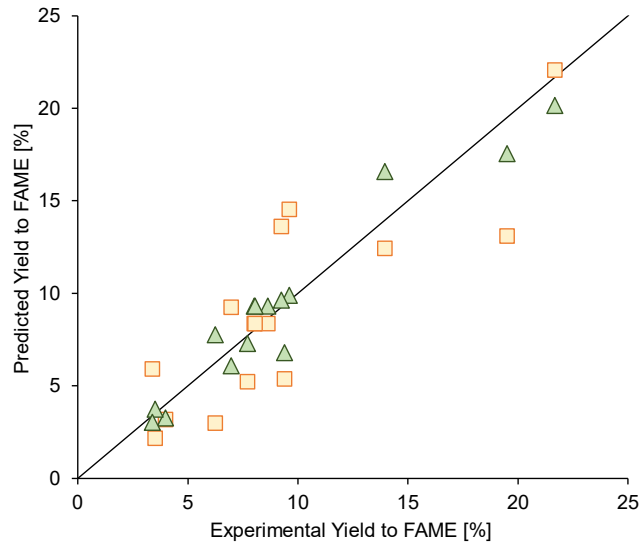


Figure 5.10. Adjusted Correlation: Predicted vs. Experimental results for yield (Y_{FAME})
Yellow squares Prasad and Sirkar parameters; Green triangles estimated parameters

5.3.3. Response Surfaces

Based on the experimental results and adjusted modeling, response surfaces were constructed to illustrate the effects of PF, OFR, and MR on triglyceride conversion (C_{TG}) (Figures 5.11, to 5.13) and yield to FAME (Y_{FAME}) (Figures 5.14 to 5.16).

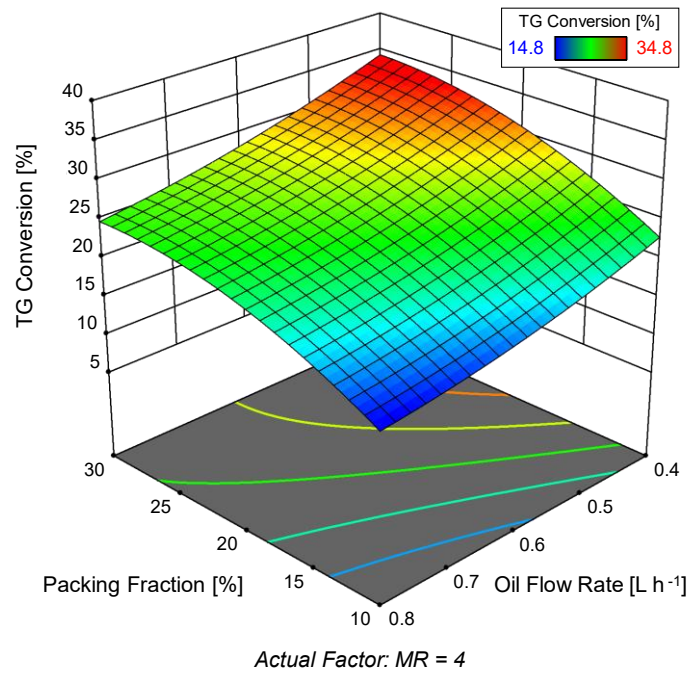


Figure 5.11. Effect of OFR and PF on the TG conversion (C_{TG}). $MR = 4:1$.

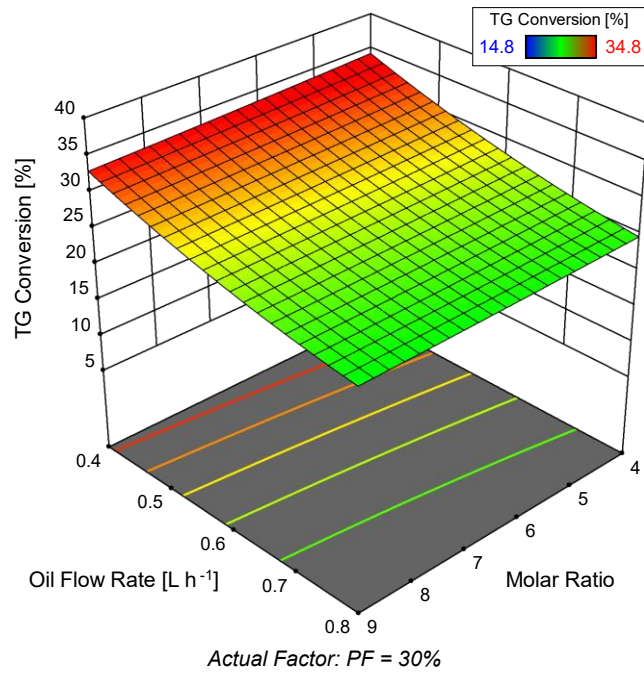


Figure 5.12. Effect of OFR and MR on the TG conversion (C_{TG}). PF = 30%.

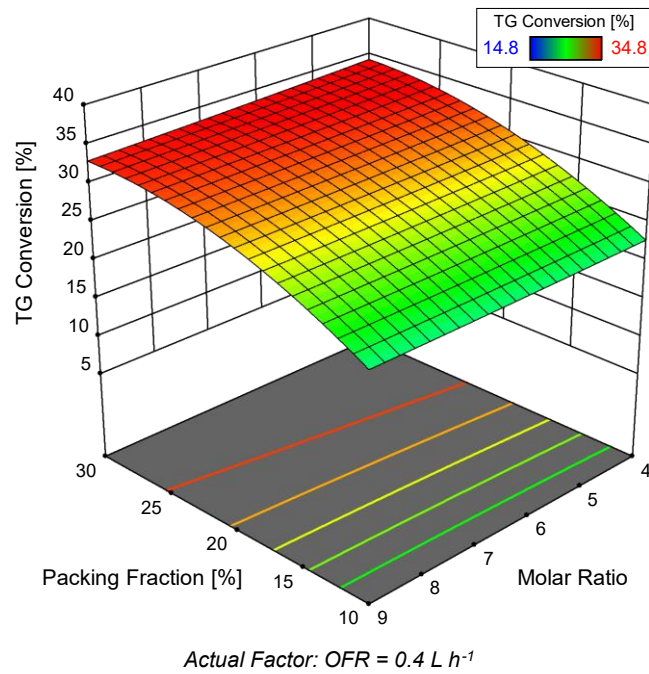


Figure 5.13. Effect of PF and MR on the TG conversion (C_{TG}). OFR = 0.4 L h⁻¹.

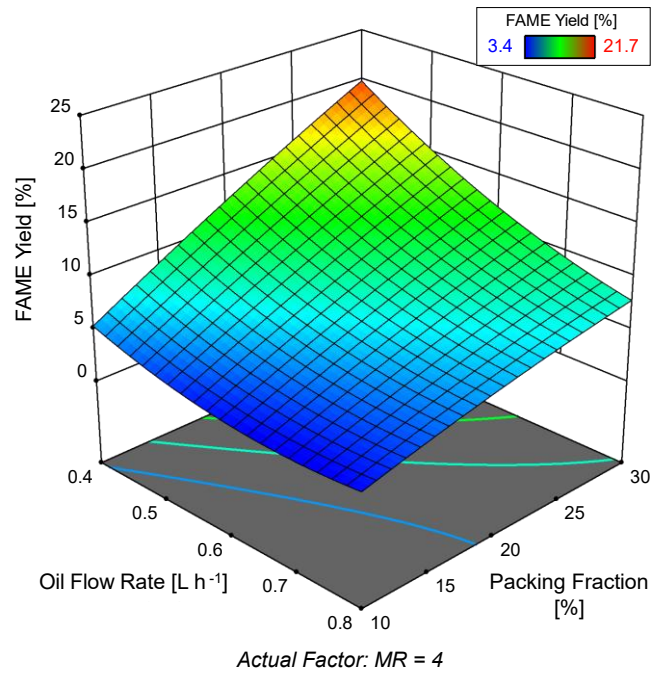


Figure 5.14. Effect of OFR and PF on the yield to FAME (Y_{FAME}). MR = 9:1

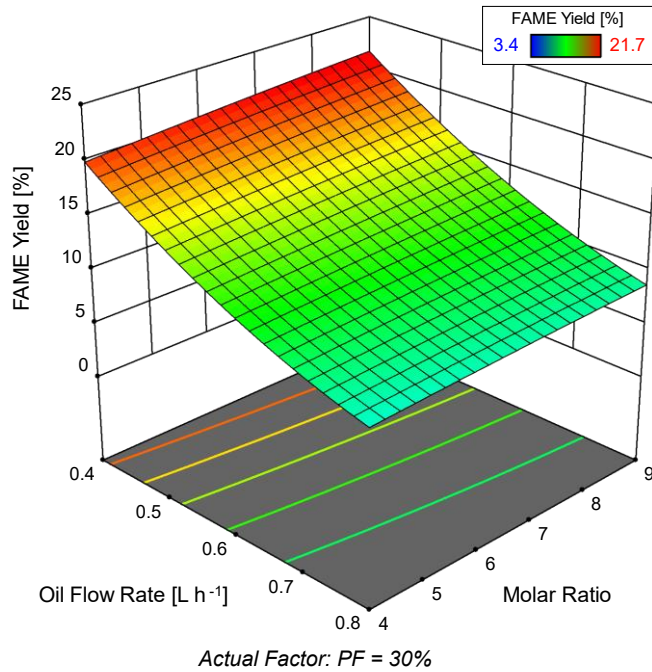


Figure 5.15. Effect of OFR and MR on the yield to FAME (Y_{FAME}). PF = 30%

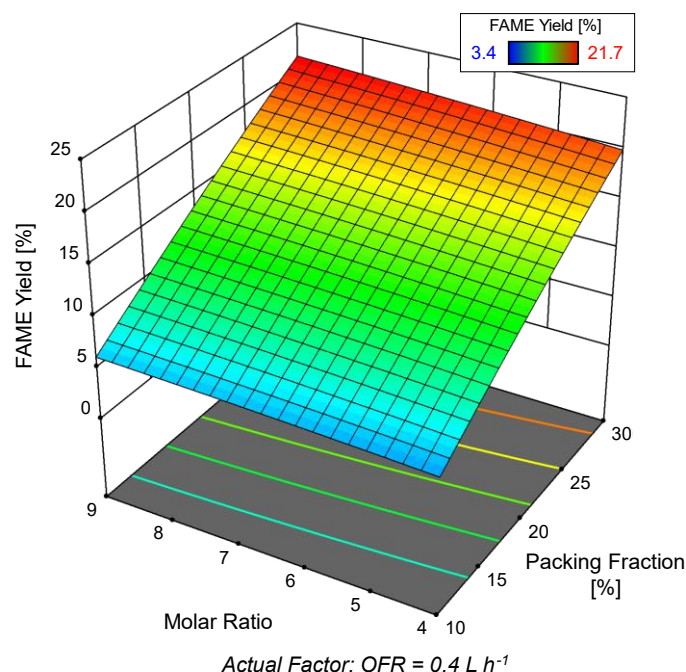


Figure 5.16. Effect of MR and PF on the yield to FAME (Y_{FAME}). $OFR = 0.4 \text{ L h}^{-1}$.

Effect of Oil Flow Rate (OFR)

Conversion and yield are significantly influenced by the OFR, as shown in Figures 5.11 and 5.12, and Figures 5.14 and 5.15, respectively. As the OFR increases, the residence time of the FAME-rich phase within the reactor decreases, resulting in lower conversion and yield. These results are consistent with previous studies on the transesterification of vegetable oil in tubular reactors [22,107,120].

Effect of methanol-to-oil Molar Ratio (MR)

Due to the independent flow of the alcohol phase, the molar ratio (MR) affects the residence time of the alcohol-rich phase. In a counter-current flow setup, lower MR values are expected to extend the residence time, enhancing the glycerol concentration gradient along the active length and shifting the chemical equilibrium to improve both conversion and yield. However, the effect on conversion is minimal, with only a 2% increase observed when the MR decreases from 9 to 4 (Figures 5.12 and 5.13). Conversely, the yield shows a slight opposite trend, increasing from 19.8% to 21.5% as the MR rises from 4 to 9 (Figures 5.15 and 5.16).

These results suggest a potential reduction in the excess methanol required for the base-catalyzed transesterification of triglycerides. Most authors recommend a molar ratio (MR) of approximately 6:1 for stirred processes [51,88], which corresponds to an excess of two times the stoichiometric amount.

Effect of Packing Fraction (PF)

The PF influences two key variables for the HFMCR: the surface area available for mass transfer and the residence time of the FAME-rich and alcohol phases. Higher values of PF enhance both conversion and yield by increasing the membrane surface area (A_{ms}) and improving mass transfer (Equation 5.2). However, an increase in packing fraction also increases the volume of the alcohol phase inside the reactor, consequently increasing the residence time of the alcohol-rich phase. In contrast, for the FAME-rich phase, increased packing fraction reduces the free volume available, thereby decreasing its residence time. To fully understand the behavior of the HFMCR, it is important to consider the combined effect of PF with the OFR and the MR.

Figures 5.11 and 5.13 illustrate the effect of PF on conversion. Higher values of PF lead to a non-linear increase in conversion. A local maximum of approximately 35% is reached when the packing fraction approaches 30%, with an oil flow rate of 0.4 L h^{-1} and a molar ratio of 4. For yield, Figures 5.14 and 5.16 depict the effect of packing fraction, showing a linear increase as the packing fraction rises. The maximum yield is 22% when the oil flow rate is 0.4 L h^{-1} and the molar ratio is 9.

At the initial reactor length, TG reacts rapidly, converting into DG, MG, and FAME (Figure 2.9). However, FAME formation occurs more slowly than TG conversion, as one mole of FAME is produced per reaction step. As a result, TG is consumed at a faster rate than FAME is formed, which explains the linear behavior for yield. The effect of PF on conversion aligns with expectations, as higher PF increases contact between the hollow fiber membranes, effectively reducing the surface area available for mass transfer.

5.4. Effect of the hydrophilicity of the membrane: Mass transfer coefficient inside the membrane

As mentioned in Section 2.1.3, one of the main challenges for the widespread use of hollow fiber membrane modules as contactors is the significant impact of membrane resistance on mass transfer [24,34,35]. Therefore, the model developed was used to observe the effect of mass transfer resistance (see Equation 5.9) in both the FAME-rich phase ($1/k_\alpha$) and the membrane ($1/k_m$) on conversion and yield, with the results shown in Figure 5.17.

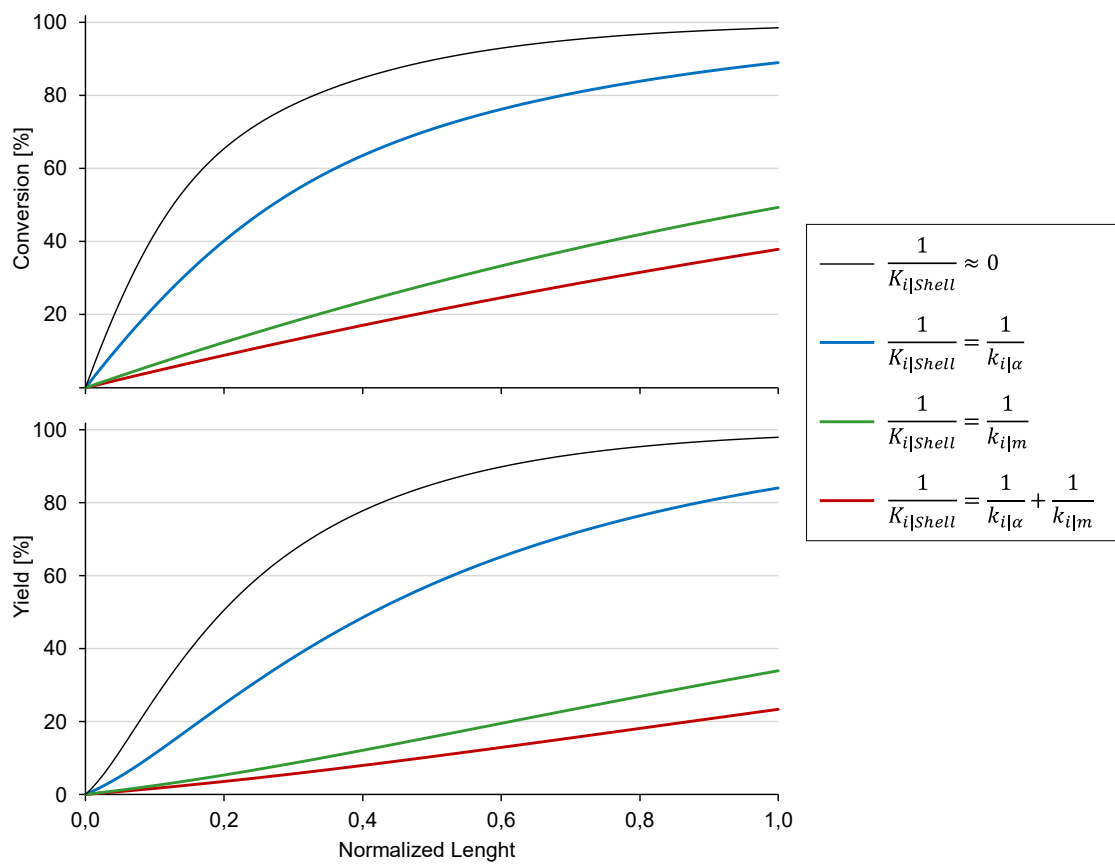


Figure 5.17. Effect of the shell-side mass transfer resistance on the conversion and yield.

The dotted lines depict the conversion and yield obtained by considering only the intrinsic kinetics of the transesterification reaction, ignoring mass transfer effects. The blue lines represent the shell-side resistance influenced exclusively by the FAME-rich phase resistance, without accounting for membrane resistance. Conversely, the green lines show the shell-side resistance with only membrane resistance considered, excluding the FAME-rich phase resistance. Finally, the red lines illustrate the resistance-in-series model used

in this work, which combines the effects of both the FAME-rich phase resistance and membrane resistance on the overall shell-side resistance.

Figure 5.17 illustrates the significant impact of membrane mass transfer resistance on the overall shell-side resistance, in line with findings reported in the literature. Within the membrane pores, mass transfer occurs exclusively by diffusion, influenced by key membrane properties such as porosity, tortuosity, and thickness, as described in Equation 5.11. In the studied system, the FAME-rich phase fills the membrane pores due to its lower polarity and the hydrophobic nature of the PP hollow fiber membrane. As a result, a molecule from the FAME-rich phase must travel from the bulk of the FAME-rich phase, pass through the boundary layer (associated with FAME-rich phase resistance), and move through the membrane pores to reach the interface, where the reaction occurs. After the reaction, the FAME molecules must return to the bulk of the FAME-rich phase. The higher viscosity of the FAME-rich phase increases the mass transfer resistance of the membrane, by reducing diffusion coefficients.

To improve mass transfer in the HFMCR for FAME production, a hydrophilic membrane may be used as an alternative to the PP membrane. The alcohol-rich phase, owing to its higher polarity, would fill the membrane pores. As the alcohol phase exhibits lower viscosity, the resistance to mass transfer would decrease, thereby optimizing the process. This improvement is especially relevant, given that the transesterification of soybean oil takes place at the phase interface.

5.5. Model-based design of membrane contactor

Based on the results of the model, the HFMCR packing fraction and operational parameters were optimized to maximize conversion and yield. The selected conditions included an OFR of 0.4 L h^{-1} , a PF of 30%, and a MR of 6:1. To ensure compliance with the required biodiesel quality standards, a target conversion of 98.5% and yield of 97.0% was set, as shown in Table 2.5. Consequently, the active length was calculated to be 9.72 m. Figure 5.18 illustrates the conversion and yield profiles, while Figure 5.19 presents the molar flow rate profiles for each species.

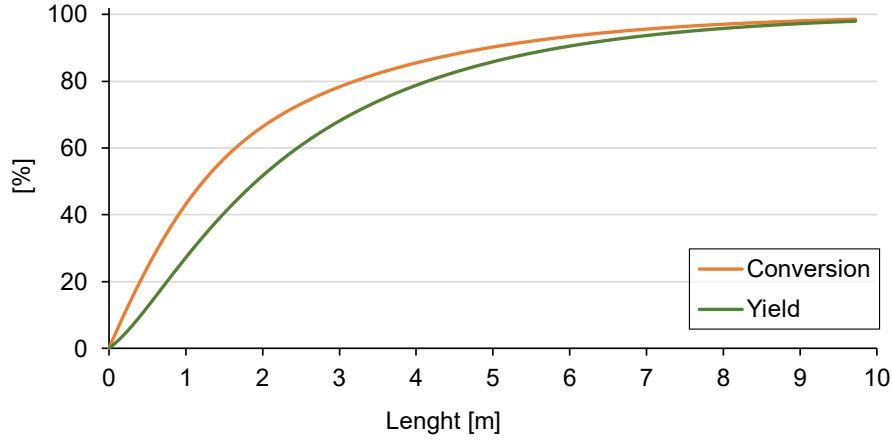


Figure 5.18. Profile of conversion and yield for the HFMR.
OFR 0.4 L h^{-1} ; PF 30%, and MR 6:1

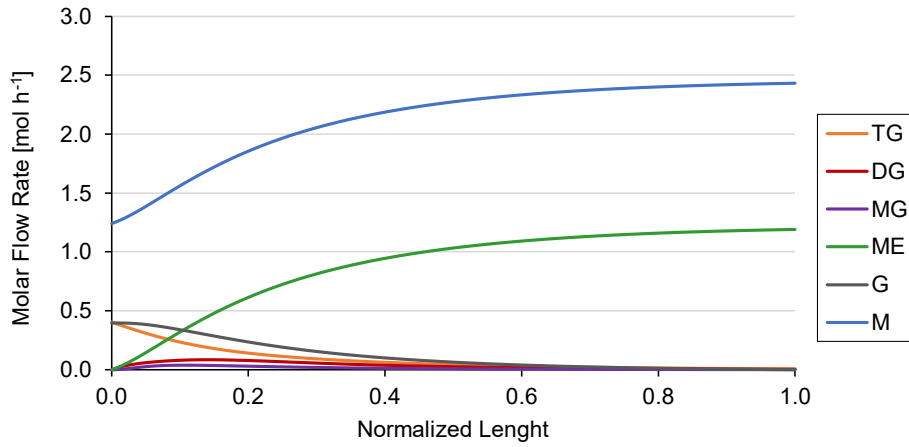


Figure 5.19. Molar flow rate profile for the HFMR.
OFR 0.4 L h^{-1} ; PF 30%, and MR 6:1

5.6. Final Remarks

The mathematical model proposed in this work effectively describes the behavior of the hollow fiber membrane contactor reactor (HFMCr) for biodiesel (FAME) production. The parameters for the general correlation of the shell-side Sherwood number were estimated using experimental data, and a sensitivity analysis was conducted to evaluate their impact on conversion and yield. In an HFMCr operating in a counter-current setup, lower molar rates can be used compared to traditional production processes, achieving a conversion of 35% and a yield of 20% under conditions of 30% packing fraction (PF), a molar ratio (MR) of 4:1, and a soybean oil flow rate (OFR) of 0.4 L h^{-1} .

Biodiesel (FAME) production in an HFMCr offers advantages for downstream separation and purification operations. The non-dispersive interaction between the reactive phases ensures phase independence throughout the process, preventing the formation of emulsions that could otherwise complicate and hinder the efficiency of downstream purification stages.

Conclusions and Recommendations

A comprehensive investigation was undertaken to evaluate the hypothesis that facilitating simultaneous reaction and byproduct removal through liquid-liquid extraction via a membrane contactor can improve the efficiency of base-catalyzed transesterification for continuous biodiesel production from soybean oil. A hollow fiber microporous membrane contactor reactor, specifically designed for this application, established optimal operating conditions for experimental validation, supported by a corresponding mathematical model. This intensified approach significantly enhanced glycerol removal, thereby improving the overall efficiency of the biodiesel production process using soybean oil as feedstock. By overcoming the limitations imposed by the chemical equilibrium of the transesterification reaction, this method presents a promising solution for industrial-scale biodiesel production, optimizing both process performance and product yield.

The experimental results indicate that the HFMCR effectively enhances phase contact, thereby facilitating glycerol extraction and optimizing the alkali-catalyzed transesterification of soybean oil. Methanol functions as both a reactant and an efficient solvent for glycerol extraction. The countercurrent configuration significantly reduced the glycerol concentration to 0.06% wt in the final biodiesel product, with a conversion rate of 34% and a yield of 20%. The HFMCR successfully addressed long-standing challenges related to glycerol separation and contaminants in downstream purification, thereby substantially improving process productivity. By adhering to the principles of reactive extraction, this method not only resolved the issues associated with glycerol separation but also enhanced the overall efficiency of the biodiesel production process, thereby confirming the suitability of the HFMCR for this application.

The reaction system, consisting of the hollow fiber membrane module and peripheral equipment, was successfully designed, fabricated, and assembled to meet the requirements for industrial biodiesel production. This process demonstrated the feasibility of developing custom membrane modules with high chemical resistance, which could potentially be adapted for various industrial applications. The construction methodology and accompanying data sheets were thoroughly documented, establishing a solid foundation for future work. Furthermore, the selection and integration of peripheral

equipment, such as pumps, heating devices, and control systems, were carefully executed to deliver a fully functional laboratory-scale setup for experimental evaluations of biodiesel production.

The selected operational variables for investigation included oil flow rate (OFR), methanol-to-oil molar ratio (MR), and packing fraction (PF). The results highlighted the significant influence of these variables on transesterification conversion and yield within the hollow fiber membrane contactor reactor system. Lower OFR values were found to enhance both conversion and yield, consistent with previous studies. Notably, the MR, within the tested range of 4:1 to 9:1, showed minimal impact on conversion and yield, indicating that the excess methanol required for base-catalyzed transesterification could potentially be reduced. The packing fraction (PF) has emerged as a crucial factor, demonstrating significant interactions with both the organic flow rate (OFR) and mass ratio (MR). Higher PF values were shown to enhance conversion and yield by improving mass transfer; however, they also modify the residence time of each phase. Optimal experimental conditions for an active length of 0.47 m, yielding a conversion of 35% and a yield of 20%, were achieved with an OFR of 0.4 L h^{-1} , an MR of 4:1, and a PF of 30%. These findings offer valuable insights for optimizing the hollow fiber membrane contactor reactor (HFMCr) system.

The mathematical model developed provides a comprehensive description of the performance of HFMCr for biodiesel production from soybean oil. The parameters for the general correlation of the shell-side Sherwood number were estimated using experimental data, and a sensitivity analysis was undertaken to evaluate their impact on conversion and yield. Using the model, it was concluded that shell-side mass transfer is mainly controlled by membrane resistance, which is impacted by the higher viscosity of the FAME-rich phase filling the membrane pores. The model also predicts that an active HFMCr length of 9.72 m can achieve a conversion of 98.5% and a yield of 97.0%, meeting the necessary quality standards for biodiesel as a biofuel. These results were obtained under the conditions of an OFR of 0.4 L h^{-1} , an MR of 6:1, and a PF of 30%, demonstrating the potential of the HFMCr system for efficient biodiesel production.

The application of HFMCr technology presents a highly effective solution for biodiesel production by enhancing the process through reactive extraction, shifting chemical equilibrium, and reducing the demands on downstream purification stages. These benefits

position HFMCRs as a highly attractive alternative for continuous biodiesel production, facilitating the development of more cost-effective and sustainable processes. Furthermore, HFMCr technology holds substantial potential for improving the efficiency of reactive extraction in other esterification and transesterification processes. Given the essential role of esterification in the chemical industry, HFMCr technology represents a significant opportunity for expanding its application to other analogous liquid-phase separation challenges, thereby advancing industrial manufacturing. Additionally, this technology has the potential to considerably reduce the energy consumption typically associated with conventional stirred systems, as it eliminates the need for stirring. This results in a more efficient and sustainable approach to biodiesel production.

Recommendations for Future Research

It is recommended to conduct a comprehensive evaluation of the durability of the membrane and operational life under continuous conditions to assess its resistance to fouling, chemical degradation, and physical wear. Such an assessment would provide crucial data regarding the optimal service life of the hollow fiber membranes, enabling the development of effective maintenance or replacement strategies to ensure consistent performance and cost-efficiency in biodiesel production.

Future research should focus on optimizing the flow dynamics within the HFMCr system to enhance mass transfer. Modifying flow configurations or implementing advanced flow control mechanisms may improve phase contact and reduce mass transfer resistance, thereby increasing conversion rates and yield. Investigating various flow patterns or employing computational fluid dynamics (CFD) simulations would provide valuable insights into optimizing flow conditions, thereby further enhancing the performance and efficiency of the reactor for continuous biodiesel production.

References

- [1] CALVIN, K. et al. **IPCC, 2023: Climate Change 2023: Synthesis Report**. [s.l.] Intergovernmental Panel on Climate Change (IPCC), 25 jul. 2023. Disponível em: <<https://www.ipcc.ch/report/ar6/syr/>>. Acesso em: 15 fev. 2025.
- [2] STANKIEWICZ, A. I.; MOULIJN, J. A. Process Intensification: Transforming Chemical Engineering. **AICHE - Chemical Engineering Progress**, 1 jan. 2000.
- [3] FOUAD, E. A.; BART, H. -J. Separation of Zinc by a Non-dispersion Solvent Extraction Process in a Hollow Fiber Contactor. **Solvent Extraction and Ion Exchange**, v. 25, n. 6, p. 857–877, out. 2007.
- [4] PABBY, A. K.; SASTRE, A. M. State-of-the-art review on hollow fibre contactor technology and membrane-based extraction processes. **Journal of Membrane Science**, v. 430, p. 263–303, mar. 2013.
- [5] AGRAHARI, G. K. et al. Membrane contactor for reactive extraction of succinic acid from aqueous solution by tertiary amine. **Chemical Engineering Research and Design**, v. 92, n. 11, p. 2705–2714, nov. 2014.
- [6] BELLO YAYA, N.; HABERT, A. C.; KRONEMBERGER, F. D. A. Evaluation of a hollow fiber membrane contactor reactor for reactive extraction in biodiesel production. **Chemical Engineering and Processing - Process Intensification**, v. 194, p. 109574, dez. 2023.
- [7] LUIS, P. Membrane contactors. Em: **Fundamental Modelling of Membrane Systems**. [s.l.] Elsevier, 2018. p. 153–208.
- [8] DRIOLI, E.; CURCIO, E.; DI PROFIO, G. State of the Art and Recent Progresses in Membrane Contactors. **Chemical Engineering Research and Design**, v. 83, n. 3, p. 223–233, mar. 2005.
- [9] DE ARAUJO KRONEMBERGER, F. **Produção de Ramnolipídeos por Pseudomonas Aeruginosa PA1 em Biorreator com Oxigenação por Contactor de Membranas**. Tese de Doutorado—Rio de Janeiro, RJ. Brasil: Instituto Alberto Luiz Coimbra de Pós-graduação e Pesquisa de Engenharia – COPPE – Universidade Federal do Rio de Janeiro, out. 2007.
- [10] DE SOUZA MORAES, L. **Extração Líquido-Líquido de Ácido Succínico Usando Contactores com Membranas de Fibra Oca**. Dissertação de Mestrado—Rio de Janeiro, RJ. Brasil: Instituto Alberto Luiz Coimbra de Pós-graduação e Pesquisa de Engenharia – COPPE – Universidade Federal do Rio de Janeiro, fev. 2011.
- [11] NORIEGA VALENCIA, M. A. N. **Produção de biodiesel num reator de filme líquido descendente assistido por membranas**. Tese de Doutorado—Rio de Janeiro, RJ. Brasil: Instituto Alberto Luiz Coimbra de Pós-graduação e Pesquisa de Engenharia – COPPE – Universidade Federal do Rio de Janeiro, nov. 2016.

- [12] BRANDÃO DE SOUZA MENDES, F. **Remoção de CO₂ de Ambientes Confinados Utilizando Contactores com Membranas e Água do Mar Sintética como Absorvente**. Dissertação de Mestrado—Rio de Janeiro, RJ. Brasil: Instituto Alberto Luiz Coimbra de Pós-graduação e Pesquisa de Engenharia – COPPE – Universidade Federal do Rio de Janeiro, out. 2017.
- [13] EVANGELISTA DA SILVA ANTUNES, E. C. **Recuperação de Ácido Succínico Através de Extração Líquido-Líquido Usando Contactor de Membrana**. Dissertação de Mestrado—Rio de Janeiro, RJ. Brasil: Instituto Alberto Luiz Coimbra de Pós-graduação e Pesquisa de Engenharia – COPPE – Universidade Federal do Rio de Janeiro, dez. 2018.
- [14] DE FREITAS CAETANO, V. **Membranas Hidrofóbicas para a Remoção de CO₂ em Espaços Confinados Utilizando Contactores Gás-Líquido**. Dissertação de Mestrado—Rio de Janeiro, RJ. Brasil: Instituto Alberto Luiz Coimbra de Pós-graduação e Pesquisa de Engenharia – COPPE – Universidade Federal do Rio de Janeiro, jul. 2023.
- [15] KISS, A. A.; BILDEA, C. S. A review of biodiesel production by integrated reactive separation technologies. **Journal of Chemical Technology & Biotechnology**, v. 87, n. 7, p. 861–879, jul. 2012.
- [16] OH, P. P. et al. A review on conventional technologies and emerging process intensification (PI) methods for biodiesel production. **Renewable and Sustainable Energy Reviews**, v. 16, n. 7, p. 5131–5145, set. 2012.
- [17] WAN OSMAN, W. N. A. et al. Comparative review of biodiesel production and purification. **Carbon Capture Science & Technology**, v. 13, p. 100264, dez. 2024.
- [18] HAJILARY, N.; REZAKAZEMI, M.; SHIRAZIAN, S. Biofuel types and membrane separation. **Environmental Chemistry Letters**, v. 17, n. 1, p. 1–18, mar. 2019.
- [19] GEBREMARIAM, S. N.; MARCHETTI, J. M. Economics of biodiesel production: Review. **Energy Conversion and Management**, v. 168, p. 74–84, jul. 2018.
- [20] HAJJARI, M. et al. A review on the prospects of sustainable biodiesel production: A global scenario with an emphasis on waste-oil biodiesel utilization. **Renewable and Sustainable Energy Reviews**, v. 72, p. 445–464, maio 2017.
- [21] BASHIR, M. A. et al. Recent development of advanced processing technologies for biodiesel production: A critical review. **Fuel Processing Technology**, v. 227, p. 107120, mar. 2022.
- [22] NORIEGA, M. A.; NARVÁEZ, P. C.; HABERT, A. C. Simulation and validation of biodiesel production in Liquid-Liquid Film Reactors integrated with PES hollow fibers membranes. **Fuel**, v. 227, p. 367–378, set. 2018.
- [23] GOMES, M. C. S.; ARROYO, P. A.; PEREIRA, N. C. Influence of oil quality on biodiesel purification by ultrafiltration. **Journal of Membrane Science**, v. 496, p. 242–249, dez. 2017.

- [24] GABELMAN, A.; HWANG, S.-T. Hollow fiber membrane contactors. **Journal of Membrane Science**, 1999.
- [25] GAWRONSKI, R. Kinetics of solvent extraction in hollow-fiber contactors. **Journal of Membrane Science**, v. 168, n. 1–2, p. 213–222, 15 abr. 2000.
- [26] DRIOLI, E.; GIORNO, L. (EDS.). **Membrane Operations: Innovative Separations and Transformations**. 1. ed. [s.l.] Wiley, 2009.
- [27] BAKER, R. W. **Membrane technology and applications**. Fourth edition ed. Hoboken, NJ: Wiley, 2024.
- [28] YANG, M.; CUSSLER, E. L. Designing hollow-fiber contactors. **AIChE Journal**, v. 32, n. 11, p. 1910–1916, nov. 1986.
- [29] YANG, X. et al. Membrane module design and dynamic shear-induced techniques to enhance liquid separation by hollow fiber modules: a review. **Desalination and Water Treatment**, v. 51, n. 16–18, p. 3604–3627, abr. 2013.
- [30] WAN, C. F. et al. Design and fabrication of hollow fiber membrane modules. **Journal of Membrane Science**, v. 538, p. 96–107, set. 2017.
- [31] MAT, N. C.; LOU, Y.; LIPSCOMB, G. G. Hollow fiber membrane modules. **Current Opinion in Chemical Engineering**, v. 4, p. 18–24, maio 2014.
- [32] LI, D.; WANG, R.; CHUNG, T.-S. Fabrication of lab-scale hollow fiber membrane modules with high packing density. **Separation and Purification Technology**, v. 40, n. 1, p. 15–30, nov. 2004.
- [33] GÜNTHER, J. et al. A numerical approach to study the impact of packing density on fluid flow distribution in hollow fiber module. **Journal of Membrane Science**, v. 348, n. 1–2, p. 277–286, fev. 2010.
- [34] DRIOLI, E.; CRISCUOLI, A.; CURCIO, E. **Membrane contactors: fundamentals, applications and potentialities**. 1st ed ed. Amsterdam ; Boston: Elsevier, 2006.
- [35] PRASAD, R.; SIRKAR, K. K. Dispersion-free solvent extraction with microporous hollow-fiber modules. **AIChE Journal**, v. 34, n. 2, p. 177–188, fev. 1988.
- [36] SHEN, S.; KENTISH, S. E.; STEVENS, G. W. Shell-Side Mass-Transfer Performance in Hollow-Fiber Membrane Contactors. **Solvent Extraction and Ion Exchange**, v. 28, n. 6, p. 817–844, 29 out. 2010.
- [37] YOUNAS, M.; BOCQUET, S. D.; SANCHEZ, J. Extraction of aroma compounds in a HFMC: Dynamic modelling and simulation. **Journal of Membrane Science**, v. 323, n. 2, p. 386–394, out. 2008.
- [38] LIANG, T.; LONG, R. L. Corrections to Correlations for Shell-Side Mass-Transfer Coefficients in the Hollow-Fiber Membrane (HFM) Modules. **Industrial & Engineering Chemistry Research**, v. 44, n. 20, p. 7835–7843, 1 set. 2005.

- [39] SHEN, S. et al. Comparison of shell side mass transfer correlations in randomly packed hollow fiber membrane modules. **Desalination and Water Treatment**, v. 17, n. 1–3, p. 52–56, maio 2010.
- [40] BUONOMENNA, M. G.; DRIOLI, E. Solvent free selective oxidation of benzyl alcohol to benzaldehyde using a membrane contactor unit. **Applied Catalysis B: Environmental**, v. 79, n. 1, p. 35–42, fev. 2008.
- [41] DAHURON, L.; CUSSLER, E. L. Protein extractions with hollow fibers. **AIChE Journal**, v. 34, n. 1, p. 130–136, jan. 1988.
- [42] BASU, R.; PRASAD, R.; SIRKAR, K. K. Nondispersive membrane solvent back extraction of Phenol. **AIChE Journal**, v. 36, n. 3, p. 450–460, mar. 1990.
- [43] KOO, S.; SANGANI, A. S. Mass transfer coefficients for laminar longitudinal flow in hollow-fibre contactors. **Journal of Fluid Mechanics**, v. 484, p. 255–282, 10 jun. 2003.
- [44] ASIMAKOPOULOU, A.; KARABELAS, A. A study of mass transfer in hollow-fiber membrane contactors—The effect of fiber packing fraction. **Journal of Membrane Science**, v. 282, n. 1–2, p. 430–441, 5 out. 2006.
- [45] ASHRAFIZADEH, S. N.; KHORASANI, Z. Ammonia removal from aqueous solutions using hollow-fiber membrane contactors. **Chemical Engineering Journal**, v. 162, n. 1, p. 242–249, 1 ago. 2010.
- [46] AGRAHARI, G. K.; VERMA, N.; BHATTACHARYA, P. K. Application of hollow fiber membrane contactor for the removal of carbon dioxide from water under liquid–liquid extraction mode. **Journal of Membrane Science**, v. 375, n. 1–2, p. 323–333, jun. 2011.
- [47] ZHU, Z. et al. An experimental study on synthesis of glycolic acid via carbonylation of formaldehyde using PTFE membrane contactor. **Journal of Membrane Science**, v. 586, p. 259–266, set. 2019.
- [48] ESAN, A. O. et al. A concise review on alternative route of biodiesel production via interesterification of different feedstocks. **International Journal of Energy Research**, v. 45, n. 9, p. 12614–12637, jul. 2021.
- [49] TOPARE, N. S. et al. A short review on approach for biodiesel production: Feedstock's, properties, process parameters and environmental sustainability. **Materials Today: Proceedings**, v. 57, p. 1605–1612, 2022.
- [50] D02 COMMITTEE. **ASTM D6751: Specification for Biodiesel Fuel Blend Stock (B100) for Middle Distillate Fuels**. ASTM International, , mar. 2023. Disponível em: <<http://www.astm.org/cgi-bin/resolver.cgi?D6751-20A>>. Acesso em: 2 fev. 2025
- [51] MEHER, L.; VIDYASAGAR, D.; NAIK, S. Technical aspects of biodiesel production by transesterification—a review. **Renewable and Sustainable Energy Reviews**, v. 10, n. 3, p. 248–268, jun. 2006.

- [52] VERMA, P.; SHARMA, M. P. Review of process parameters for biodiesel production from different feedstocks. **Renewable and Sustainable Energy Reviews**, v. 62, p. 1063–1071, set. 2016.
- [53] MAHMUDUL, H. M. et al. Production, characterization and performance of biodiesel as an alternative fuel in diesel engines – A review. **Renewable and Sustainable Energy Reviews**, v. 72, p. 497–509, maio 2017.
- [54] SURESH, M.; JAWAHAR, C. P.; RICHARD, A. A review on biodiesel production, combustion, performance, and emission characteristics of non-edible oils in variable compression ratio diesel engine using biodiesel and its blends. **Renewable and Sustainable Energy Reviews**, v. 92, p. 38–49, set. 2018.
- [55] NARVÁEZ RINCÓN, P. C. **Producción de ésteres metílicos de ácidos grasos en un reactor de película líquida descendente**. Tesis de Doctorado—Bogotá D. C.: Universidad Nacional de Colombia, 2006.
- [56] INTERNATIONAL ENERGY AGENCY, IEA. **Transport biofuels**. , dez. 2024. Disponível em: <<https://www.iea.org/reports/renewables-2023/transport-biofuels>>. Acesso em: 20 dez. 2024
- [57] RENEWABLES IN ENERGY DEMAND. **REN21. 2024 - Renewables 2024 Global Status Report Collection**. [s.l: s.n.]. Disponível em: <<https://www.ren21.net/gsr-2024/>>. Acesso em: 20 dez. 2024.
- [58] NAYLOR, R. L.; HIGGINS, M. M. The rise in global biodiesel production: Implications for food security. **Global Food Security**, v. 16, p. 75–84, mar. 2018.
- [59] CONSELHO NACIONAL DE POLÍTICA ENERGÉTICA - CNPE. Resolução CNPE 08/2023. CNPE Resolução nº 8 de 2023. . 19 dez. 2023.
- [60] INTERNATIONAL RENEWABLE ENERGY AGENCY, IRENA; INTERNATIONAL LABOUR ORGANIZATION, ILO. **Renewable energy and jobs: Annual review 2024**. Abu Dhabi (IRENA), Geneve (ILO): [s.n.]. Disponível em: <<https://www.irena.org/Publications/2024/Oct/Renewable-energy-and-jobs-Annual-review-2024>>.
- [61] AGÊNCIA NACIONAL DO PETRÓLEO, GÁS NATURAL E BIOCOMBUSTÍVEIS - ANP. **Anuário Estatístico Brasileiro do Petróleo, Gás Natural e Biocombustíveis 2024**. [s.l: s.n.]. Disponível em: <<https://www.gov.br/anp/pt-br/centrais-de-conteudo/publicacoes/anuario-estatistico/anuario-estatistico-brasileiro-do-petroleo-gas-natural-e-biocombustiveis-2024#:~:text=O%20Anu%C3%A1rio%20Estat%C3%ADstico%20Brasileiro%20do,nacionais%20no%20per%C3%ADodo%202014%2D2023>>.
- [62] CAMPANELLI, P.; BANCHERO, M.; MANNA, L. Synthesis of biodiesel from edible, non-edible and waste cooking oils via supercritical methyl acetate transesterification. **Fuel**, v. 89, n. 12, p. 3675–3682, dez. 2010.
- [63] KNOTHE, G.; RAZON, L. F. Biodiesel fuels. **Progress in Energy and Combustion Science**, v. 58, p. 36–59, jan. 2017.

- [64] BEAL, C. M. et al. The Energy Return on Investment for Algal Biocrude: Results for a Research Production Facility. **BioEnergy Research**, v. 5, n. 2, p. 341–362, jun. 2012.
- [65] CHEN, J. et al. The potential of microalgae in biodiesel production. **Renewable and Sustainable Energy Reviews**, v. 90, p. 336–346, jul. 2018.
- [66] JAMIL, F. A Review on Biodiesel Production, Analysis, and Emission Characteristics from Non-Edible Feedstocks. **ChemistrySelect**, v. 8, n. 31, p. e202300800, 18 ago. 2023.
- [67] EUROPEAN PARLIAMENT AND OF THE COUNCIL; UNION. Directive (EU) 2018/2001. Renewable Energy Directive, Directive (EU) 2018/2001, (RED II) - Revised 2024. . 16 jul. 2024.
- [68] ASSOCIAÇÃO BRASILEIRA DAS INDÚSTRIAS DE ÓLEOS VEGETAIS, ABIOVE. **Biodiesel - Estatísticas 2024**. São Paulo (SP), Brazil: Associação Brasileira das Indústrias de Óleos Vegetais (ABIOVE), 2024. Disponível em: <<https://biodiesel.abiove.org.br/estatisticas-2024/>>.
- [69] EMPRESA DE PESQUISA ENERGÉTICA - EPE. **Analysis of Current Biofuels Outlook – Year 2023**. [s.l: s.n.]. Disponível em: <<https://www.epe.gov.br/en/publications/publications/analysis-of-biofuels-current-outlook-2023>>. Acesso em: 2 fev. 2025.
- [70] ARANSIOLA, E. F. et al. A review of current technology for biodiesel production: State of the art. **Biomass and Bioenergy**, v. 61, p. 276–297, fev. 2014.
- [71] SANLI, H.; CANAKCI, M. Effects of Different Alcohol and Catalyst Usage on Biodiesel Production from Different Vegetable Oils. **Energy & Fuels**, v. 22, n. 4, p. 2713–2719, 1 jul. 2008.
- [72] FREEDMAN, B.; BUTTERFIELD, R. O.; PRYDE, E. H. Transesterification kinetics of soybean oil. **Journal of the American Oil Chemists' Society**, v. 63, n. 10, p. 1375–1380, out. 1986.
- [73] DE LIMA DA SILVA, N. et al. Biodiesel Production from Integration Between Reaction and Separation System: Reactive Distillation Process. **Applied Biochemistry and Biotechnology**, v. 161, n. 1–8, p. 245–254, maio 2010.
- [74] GERPEN, J. V. Biodiesel processing and production. **Fuel Processing Technology**, v. 86, n. 10, p. 1097–1107, jun. 2005.
- [75] MOSER, B. R. Biodiesel production, properties, and feedstocks. **In Vitro Cellular & Developmental Biology - Plant**, v. 45, n. 3, p. 229–266, jun. 2009.
- [76] ZHOU, W.; KONAR, S. K.; BOOCOOCK, D. G. B. Ethyl esters from the single-phase base-catalyzed ethanolysis of vegetable oils. **Journal of the American Oil Chemists' Society**, v. 80, n. 4, p. 367–371, abr. 2003.
- [77] HOBSON, C.; MÁRQUEZ, C. **Renewable Methanol Report**. Madrid, España: Methanol Institute, 2018.

- [78] ENERKEM. **From Waste to a Sustainable Future.** , 2025. Disponível em: <<https://enerkem.com/projects-facilities>>
- [79] MA, F.; HANNA, M. A. Biodiesel production: A review. **Bioresource Technology**, v. 70, n. 1, p. 1–15, out. 1999.
- [80] SANTORI, G. et al. A review analyzing the industrial biodiesel production practice starting from vegetable oil refining. **Applied Energy**, v. 92, p. 109–132, abr. 2012.
- [81] FREEDMAN, B.; PRYDE, E. H.; MOUNTS, T. L. Variables affecting the yields of fatty esters from transesterified vegetable oils. **Journal of the American Oil Chemists' Society**, v. 61, n. 10, p. 1638–1643, out. 1984.
- [82] NOUREDDINI, H.; ZHU, D. Kinetics of transesterification of soybean oil. **Journal of the American Oil Chemists' Society**, v. 74, n. 11, p. 1457–1463, nov. 1997.
- [83] TUBINO, M.; JUNIOR, J. G. R.; BAUERFELDT, G. F. Biodiesel synthesis: A study of the triglyceride methanolysis reaction with alkaline catalysts. **Catalysis Communications**, v. 75, p. 6–12, fev. 2016.
- [84] NASREEN, S. et al. Review of Catalytic Transesterification Methods for Biodiesel Production. Em: BIERNAT, K. (Ed.). **Biofuels - State of Development**. [s.l.] InTech, 2018.
- [85] SANTACESARIA, E. et al. Main technologies in biodiesel production: State of the art and future challenges. **Catalysis Today**, v. 195, n. 1, p. 2–13, nov. 2012.
- [86] SHIMADA, Y. et al. Enzymatic alcoholysis for biodiesel fuel production and application of the reaction to oil processing. **Journal of Molecular Catalysis B: Enzymatic**, v. 17, n. 3–5, p. 133–142, jun. 2002.
- [87] BABADI, A. A. et al. Emerging technologies for biodiesel production: Processes, challenges, and opportunities. **Biomass and Bioenergy**, v. 163, p. 106521, ago. 2022.
- [88] SHARMA, Y. C.; SINGH, B.; UPADHYAY, S. N. Advancements in development and characterization of biodiesel: A review. **Fuel**, v. 87, n. 12, p. 2355–2373, set. 2008.
- [89] TREJO-ZÁRRAGA, F. et al. Kinetics of Transesterification Processes for Biodiesel Production. Em: BIERNAT, K. (Ed.). **Biofuels - State of Development**. [s.l.] InTech, 2018.
- [90] SILVA, S. P. et al. Kinetics of the biphasic liquid–liquid transesterification of vegetable oils into biodiesel. **Reaction Kinetics, Mechanisms and Catalysis**, v. 123, n. 2, p. 529–542, abr. 2018.
- [91] NARVÁEZ, P. C.; RINCÓN, S. M.; SÁNCHEZ, F. J. Kinetics of Palm Oil Methanolysis. **Journal of the American Oil Chemists' Society**, v. 84, n. 10, p. 971–977, out. 2007.

- [92] ASSMAN, G. et al. **Continuous process for the production of lower alkyl esters.**, [s.d.]. Disponível em: <<https://image-ppubs.uspto.gov/dirsearch-public/print/downloadPdf/5514820>>. Acesso em: 23 jun. 2021
- [93] LÄMSÄI, M. **Process for preparing a synthetic ester from a vegetable oil.** Finland, 23 mar. 1999. Disponível em: <<https://patents.google.com/patent/US6127560A/en>>
- [94] NAGIB KHALIL, CARLOS; FERREIRA LEITE, LUCIA CRISTINA. **Process for producing Biodiesel.**, 2005.
- [95] CADAVID ESTRADA, J. G. **Estudio del proceso de producción de biodiesel mediante extracción reactiva.** Tesis de Doctorado—Bogotá D. C.: Universidad Nacional de Colombia, 2012.
- [96] ATADASHI, I. M. Purification of crude biodiesel using dry washing and membrane technologies. **Alexandria Engineering Journal**, v. 54, n. 4, p. 1265–1272, dez. 2015.
- [97] AGÊNCIA NACIONAL DO PETRÓLEO, GÁS NATURAL E BIOCOMBUSTÍVEIS - ANP. Resolução ANP N° 920/2023.. 4 abr. 2023.
- [98] EUROPEAN COMMITTEE FOR STANDARDIZATION. **UNE EN 14214:2013 V2+A2:2019.**, 19 fev. 2019.
- [99] BASHIR, M. A. et al. Recent development of advanced processing technologies for biodiesel production: A critical review. **Fuel Processing Technology**, v. 227, p. 107120, mar. 2022.
- [100] QIU, Z.; ZHAO, L.; WEATHERLEY, L. Process intensification technologies in continuous biodiesel production. **Chemical Engineering and Processing: Process Intensification**, v. 49, n. 4, p. 323–330, abr. 2010.
- [101] CHUAH, L. F. et al. A review of cleaner intensification technologies in biodiesel production. **Journal of Cleaner Production**, v. 146, p. 181–193, mar. 2017.
- [102] NIGATU GEBREMARIAM, S.; MARIO MARCHETTI, J.; FACULTY OF SCIENCE AND TECHNOLOGY, NORWEGIAN UNIVERSITY OF LIFE SCIENCES, DRØBAKVEIEN 31, 1432, ÅS, NORWAY. Biodiesel production technologies: review. **AIMS Energy**, v. 5, n. 3, p. 425–457, 2017.
- [103] TABATABAEI, M. et al. Reactor technologies for biodiesel production and processing: A review. **Progress in Energy and Combustion Science**, v. 74, p. 239–303, set. 2019.
- [104] KUMAR PRAJAPATI, A. et al. Process intensification in biodiesel production using unconventional reactors. **Fuel**, v. 380, p. 133263, jan. 2025.
- [105] ATADASHI, I. M. et al. Membrane biodiesel production and refining technology: A critical review. **Renewable and Sustainable Energy Reviews**, v. 15, n. 9, p. 5051–5062, dez. 2011.

- [106] ATADASHI, I. M.; AROUA, M. K.; AZIZ, A. A. Biodiesel separation and purification: A review. **Renewable Energy**, v. 36, n. 2, p. 437–443, fev. 2011.
- [107] BELLO, N. et al. Characterization and evaluation of poly(ether sulfone) membranes in biodiesel production using liquid–liquid film reactors. **Chemical Engineering and Processing: Process Intensification**, v. 108, p. 226–232, out. 2016.
- [108] KANT BHATIA, S. et al. An overview on advancements in biobased transesterification methods for biodiesel production: Oil resources, extraction, biocatalysts, and process intensification technologies. **Fuel**, v. 285, p. 119117, fev. 2021.
- [109] SHUIT, S. H. et al. Membrane technology as a promising alternative in biodiesel production: A review. **Biotechnology Advances**, v. 30, n. 6, p. 1364–1380, nov. 2012.
- [110] NATARAJAN, Y. et al. An overview on the process intensification of microchannel reactors for biodiesel production. **Chemical Engineering and Processing - Process Intensification**, v. 136, p. 163–176, fev. 2019.
- [111] HUANG, S. et al. Design and development of a new static mixing bioreactor for enzymatic bioprocess: Application in biodiesel production. **Renewable Energy**, v. 197, p. 922–931, set. 2022.
- [112] TAN, S. X. et al. State of the art review on development of ultrasound-assisted catalytic transesterification process for biodiesel production. **Fuel**, v. 235, p. 886–907, jan. 2019.
- [113] HO, W. W. S.; NG, H. K.; GAN, S. Advances in ultrasound-assisted transesterification for biodiesel production. **Applied Thermal Engineering**, v. 100, p. 553–563, maio 2016.
- [114] GOLE, V. L.; GOGATE, P. R. A review on intensification of synthesis of biodiesel from sustainable feed stock using sonochemical reactors. **Chemical Engineering and Processing: Process Intensification**, v. 53, p. 1–9, mar. 2012.
- [115] PRIAMBODO, R. et al. Novel Technology for Bio-diesel Production from Cooking and Waste Cooking Oil by Microwave Irradiation. **Energy Procedia**, v. 75, p. 84–91, ago. 2015.
- [116] LEE, K. T. et al. Integration of reactive extraction with supercritical fluids for process intensification of biodiesel production: Prospects and recent advances. **Progress in Energy and Combustion Science**, v. 45, p. 54–78, dez. 2014.
- [117] NOSHADI, I.; AMIN, N. A. S.; PARNAS, R. S. Continuous production of biodiesel from waste cooking oil in a reactive distillation column catalyzed by solid heteropolyacid: Optimization using response surface methodology (RSM). **Fuel**, v. 94, p. 156–164, abr. 2012.
- [118] FARVARDIN, M. et al. Enhancement of biodiesel production from waste cooking oil: ultrasonic- hydrodynamic combined cavitation system. **Energy Sources, Part A: Recovery, Utilization, and Environmental Effects**, v. 44, n. 2, p. 5065–5079, 15 jun. 2022.

- [119] HAMIDI, R. et al. Recent developments and future outlooks of hydrodynamic cavitation as an intensification technology for renewable biofuels production. **Journal of Environmental Chemical Engineering**, v. 11, n. 5, p. 110819, out. 2023.
- [120] NARVAEZ RINCON, P. C. et al. **Reaction system for producing fatty alkyl esters using a liquid-film reactor operated countercurrentwise.** , 19 set. 2017. Disponível em: <<https://image-ppubs.uspto.gov/dirsearch-public/print/downloadPdf/9765283>>. Acesso em: 25 jun. 2021
- [121] WANG, C. Y. et al. Tube-side mass transfer for hollow fibre membrane contactors operated in the low Graetz range. **Journal of Membrane Science**, v. 523, p. 235–246, fev. 2017.
- [122] SALEH, J.; TREMBLAY, A. Y.; DUBÉ, M. A. Glycerol removal from biodiesel using membrane separation technology. **Fuel**, v. 89, n. 9, p. 2260–2266, set. 2010.
- [123] OTHMAN, R. et al. Application of polymeric solvent resistant nanofiltration membranes for biodiesel production. **Journal of Membrane Science**, v. 348, n. 1–2, p. 287–297, fev. 2010.
- [124] ALVES, M. J. et al. Biodiesel purification using micro and ultrafiltration membranes. **Renewable Energy**, v. 58, p. 15–20, out. 2013.
- [125] NORIEGA, M. A.; NARVÁEZ, P. C.; HABERT, A. C. Biodiesel separation using ultrafiltration poly(ether sulfone) hollow fiber membranes: Improving biodiesel and glycerol rich phases settling. **Chemical Engineering Research and Design**, v. 138, p. 32–42, out. 2018.
- [126] DUBÉ, M. A.; TREMBLAY, A. Y.; LIU, J. Biodiesel production using a membrane reactor. **Bioresource Technology**, v. 98, n. 3, p. 639–647, fev. 2007.
- [127] CAO, P.; DUBÉ, M. A.; TREMBLAY, A. Y. High-purity fatty acid methyl ester production from canola, soybean, palm, and yellow grease lipids by means of a membrane reactor. **Biomass and Bioenergy**, v. 32, n. 11, p. 1028–1036, nov. 2008.
- [128] MAIA FILHO, D. C.; SALIM, V. M. M.; BORGES, C. P. Membrane contactor reactor for transesterification of triglycerides heterogeneously catalyzed. **Chemical Engineering and Processing: Process Intensification**, v. 108, p. 220–225, out. 2016.
- [129] GUERREIRO, L. et al. PVA embedded hydrotalcite membranes as basic catalysts for biodiesel synthesis by soybean oil methanolysis. **Catalysis Today**, v. 156, n. 3–4, p. 191–197, 31 out. 2010.
- [130] BAROUTIAN, S. et al. A packed bed membrane reactor for production of biodiesel using activated carbon supported catalyst. **Bioresource Technology**, v. 102, n. 2, p. 1095–1102, jan. 2011.
- [131] XU, W. et al. In situ synthesis and characterization of Ca–Mg–Al hydrotalcite on ceramic membrane for biodiesel production. **Chinese Journal of Chemical Engineering**, v. 23, n. 6, p. 1035–1040, jun. 2015.

- [132] ATADASHI, I. M. et al. The effects of catalysts in biodiesel production: A review. **Journal of Industrial and Engineering Chemistry**, v. 19, n. 1, p. 14–26, jan. 2013.
- [133] MERCK S/A. **Metanol**. , 9 jul. 2024. Disponível em: <www.sigmaaldrich.com>. Acesso em: 11 jul. 2024
- [134] HAYATA. **Stainless Steel Chemical Resistance Charts**. , [s.d.]. Disponível em: <<http://hayata.com/resources/tech-info/>>. Acesso em: 22 nov. 2018
- [135] INDUSTRIAL SPECIALTIES MFG. AND IS MED SPECIALTIES. **316L Stainless Steel Chemical Compatibility Chart**. , 28 out. 2022. Disponível em: <<https://www.industrialspec.com/resources/chemical-compatibility/>>. Acesso em: 1 dez. 2022
- [136] **Bal Seal® PTFE, Filled PTFE and Polyethylene Seal Materials**. . [s.l.] Bal Seal Engineering, Inc., 12 jun. 2013. Disponível em: <www.balseal.com>. Acesso em: 20 dez. 2018.
- [137] CP LAB SAFETY. **Chemical Charts: Compatibility by Material**. , 2018. Disponível em: <<https://www.calpaclab.com/chemical-compatibility-by-resin-material/>>. Acesso em: 20 nov. 2018
- [138] TISCH SCIENTIFIC. **Membrane Filter Chemical Compatibility Chart**. , 2023. Disponível em: <<https://scientificfilters.com/membrane-filter-chemical-compatibility-chart/>>
- [139] BRASKEM S.A. **Technical Literature: Polypropylene chemical resistance**. , dez. 2005. Disponível em: <www.braskem.com.br>. Acesso em: 22 nov. 2018
- [140] KELCO ENGINEERING PTY LTD. **Nylon: Chemical Compatibility Chart**. , 15 dez. 2018. Disponível em: <<https://www.kelco.com.au/>>
- [141] BRASKEM S.A. **Technical Literature: Polyethylene chemical resistance**. , dez. 2005. Disponível em: <www.braskem.com.br>. Acesso em: 22 nov. 2018
- [142] ADVANCED SENSOR TECHNOLOGIES, INC. **KYNAR (PVDF) Chemical Compatibility & Chemical Resistance Chart**. , 9 dez. 2015. Disponível em: <<https://astisensor.com/resources/technical-documents/tech-support-docs/>>
- [143] IPEX. **Chemical Resistance Guide Kynar® Polyvinylidene Fluoride (PVDF)**. , 2021. Disponível em: <<https://ipexna.com/resources/document-repository/pvdf-chemical-resistance-guide/>>
- [144] CRANE CHEMPHARMA FLOW SOLUTIONS. **Saunders® PES Chemical Resistance**. , maio 2012. Disponível em: <www.cranechempharma.com>
- [145] FLOWCRETE UK. **Chemical Resistance Data**. , 12 jun. 2021. Disponível em: <www.flowcrete.eu>. Acesso em: 12 dez. 2022
- [146] RESOLTECH SARL. **Chemical Resistance Guide**. , 2010. Disponível em: <<https://www.resoltech.com/>>. Acesso em: 1 dez. 2022

- [147] D20 COMMITTEE. **ASTM D543-14: Practices for Evaluating the Resistance of Plastics to Chemical Reagents**. ASTM International, , 10 mar. 2020. Disponível em: <<http://www.astm.org/cgi-bin/resolver.cgi?D543-14>>. Acesso em: 19 jan. 2025
- [148] BELLO YAYA, N. **Producción continua de ésteres metílicos por extracción reactiva, empleando un módulo de membrana de fibra hueca**. Tesis de Maestría—Bogotá D. C.: Universidad Nacional de Colombia, 2015.
- [149] D02 COMMITTEE. **ASTM D6584-17: Test Method for Determination of Total Monoglycerides, Total Diglycerides, Total Triglycerides, and Free and Total Glycerin in B-100 Biodiesel Methyl Esters by Gas Chromatography**. ASTM International, , [s.d.]. Disponível em: <<http://www.astm.org/cgi-bin/resolver.cgi?D6584-17>>. Acesso em: 12 fev. 2025
- [150] CASAS, A. et al. Liquid–Liquid Phase Equilibria for Soybean Oil Methanolysis: Experimental, Modeling, and Data Prediction. **Industrial & Engineering Chemistry Research**, v. 53, n. 9, p. 3731–3736, 5 mar. 2014.
- [151] NORIEGA, M. A. et al. Liquid-liquid equilibrium for biodiesel-glycerol-methanol or ethanol systems using UNIFAC correlated parameters. **Energy**, v. 111, p. 841–849, set. 2016.
- [152] VAN GERPEN, J. et al. **Biodiesel Production Technology: August 2002–January 2004**. [s.l.: s.n.]. Disponível em: <<http://www.osti.gov/servlets/purl/15008801/>>. Acesso em: 14 abr. 2023.
- [153] FOGLER, H. S. **Elements of chemical reaction engineering**. 4th ed ed. Upper Saddle River, NJ: Prentice Hall PTR, 2006.
- [154] MIYABE, K.; ISOGAI, R. Estimation of molecular diffusivity in liquid phase systems by the Wilke–Chang equation. **Journal of Chromatography A**, v. 1218, n. 38, p. 6639–6645, set. 2011.
- [155] POLING, B. E.; PRAUSNITZ, J. M.; O’CONNELL, J. P. **Properties of Gases and Liquids, Fifth Edition**. Fifth edition ed. New York, N.Y: McGraw-Hill Education, 2020.
- [156] PINTO, J. C.; SCHWAAB, M. **Análise de Dados Experimentais: I. Fundamentos de Estatística e Estimação de Parâmetros**. [s.l.] E-Papers, 2007.
- [157] BONAMENTE, M. **Statistics and Analysis of Scientific Data**. New York, NY: Springer New York, 2017.